A MOLECULAR SNAPSHOT OF CHARGED NANOPARTICLES IN THE CELLULAR ENVIRONMENT

A Dissertation
Presented to
The Academic Faculty

by

Candace C. Fleischer

In Partial Fulfillment
of the Requirements for the Degree
Doctor of Philosophy in the
School of Chemistry and Biochemistry

Georgia Institute of Technology
May 2014

A MOLECULAR SNAPSHOT OF CHARGED NANOPARTICLES IN THE CELLULAR ENVIRONMENT

Approved by:

Professor Christine Payne, Advisor
School of Chemistry and Biochemistry
Georgia Institute of Technology

Professor Bridgette Barry
School of Chemistry and Biochemistry
Georgia Institute of Technology

Professor Mostafa El-Sayed
School of Chemistry and Biochemistry
Georgia Institute of Technology

Professor Harold Kim
School of Physics
Georgia Institute of Technology

Professor Younan Xia
School of Chemistry and Biochemistry
Georgia Institute of Technology

Date Approved: March 26, 2014

ACKNOWLEDGMENTS

The research herein has been greatly enriched by the efforts of many people. I thank my dissertation advisor, Christine Payne, for guiding the research and affording me many opportunities both in and out of the laboratory. My master's thesis advisor, Steven Emory, provided the early training towards becoming a thoughtful scientist. I thank my dissertation committee including Bridgette Barry, Mostafa El-Sayed, Younan Xia, and Harold Kim, for their insight.

I am grateful to the current and former members of the Payne lab for contributions to both research and ideas, and to Meg Mackey and Yusuf Uddin for helpful collaborations. I thank my cohorts for their solidarity and friendship, especially those from the graduate student forum and women in chemistry. I also wish to express my gratitude to the department staff for their kind assistance, especially Nicole Thompson, Marketta Powers, Wendy Harris, Cam Tyson, and Michele Yager.

Most importantly, I would like to thank my family: my parents, for their faith in my potential; and my grandparents, for lifelong inspiration. Finally, to my husband, Blake, I thank you for your tireless encouragement and support.

TABLE OF CONTENTS

LIST OF TABLES

LIST OF FIGURES

LIST OF SYMBOLS

d_h	hydrodynamic diameter
d_{TEM}	transmission electron microscopy diameter
K	equilibrium constant
λ	wavelength
g	relative centrifugal force
k	reaction rate constant
θ	ellipticity
ε	molar extinction coefficient
v/v	volume per volume
w/v	weight per volume

LIST OF ABBREVIATIONS

AF647	AlexaFluor647
BS-C-1	African green monkey kidney epithelial
BSA	bovine serum albumin
CD	circular dichroism
CHO	Chinese hamster ovary
COOH	carboxylic acid
Cy5	cyanine5 fluorescent dye
DAPI	4',6-diamidino-2-phenylindole dilactate
DiD	1,1'-dioctadecyl-3,3,3',3'-tetramethylindodicarbocyanine perchlorate
DMSO	dimethyl sulfoxide
EDTA	ethylenediaminetetraacetic acid
ef-surf	molecular surface and electrostatic potential database
EMCCD	electron multiplying charge-coupled device
EYFP	enhanced yellow fluorescent protein
FBS	fetal bovine serum
FRET	Förster resonance energy transfer
gp	glycoprotein
H_2CO	formaldehyde
$H_3C_6H_5O_7$	citric acid
HeLa	adenocarcinoma human cervical
ITC	isothermal titration calorimetry
kDa	kilodalton
LAMP1	lysosome-associated membrane protein-1
LDL	low-density lipoprotein

MEM	minimum essential medium
MPS	mononuclear phagocyte system
MRE	mean residue ellipticity
MW	molecular weight
N.A.	numerical aperture
NH_2	amine
NP	nanoparticle
PBS	phosphate buffered saline
PDB	Protein Data Bank
PDI	polydispersity index
PEG	polyethylene glycol
pI	isoelectric point
PMT	photomultiplier tube
polyA	polyadenylic acid
polyI	polyinosinic acid
PS	polystyrene
QDs	quantum dots
rpm	revolutions per minute
SDS	sodium dodecyl sulfate
TBE	Tris-Borate-EDTA
TEM	transmission electron microscopy
Tf	transferrin
UV-Vis	ultraviolet-visible
ZP	zeta potential

SUMMARY

Nanoparticles are promising platforms for biomedical applications ranging from diagnostic tools to therapeutic delivery agents. During the course of these applications, nanoparticles are exposed to a complex mixture of extracellular serum proteins that nonspecifically adsorb onto the surface. The resulting protein layer, or protein "corona," creates an interface between nanoparticles and the biological environment. Protecting the nanoparticle surface can reduce protein adsorption, but complete inhibition remains a challenge. As a result, the corona, rather than the nanoparticle itself, mediates the cellular response to the nanoparticle. The following dissertation describes the fundamental characterization of the cellular binding of charged nanoparticles, interactions of protein-nanoparticle complexes with cellular receptors, and the structural and thermodynamic properties of adsorbed corona proteins.

Cationic, amine-modified and anionic, carboxylate-modified polystyrene nanoparticles were studied as a model system. We observed that initial nanoparticle surface charge dictates cellular binding in the presence of extracellular serum proteins. The charge-dependent differences are attributed to protein-nanoparticle complexes binding to distinct cellular receptors. Similar trends were observed for a collection of nanoparticles differing in size, composition, and surface modification, demonstrating that nanoparticle surface charge determines cellular binding trends for a broad range of nanoparticles. Characterization of the protein-nanoparticle complex was extended to include structural and thermodynamic studies of adsorbed proteins. Molecular properties of adsorbed proteins were correlated with the cellular receptors used for binding establishing a molecular link between corona proteins, nanoparticles, and cellular receptors.

CHAPTER I

INTRODUCTION

1.1 Nanoparticles for Biomedical Applications

Nanoparticles (NPs) have generated broad scientific interest as platforms for biomedical applications.[1–9] Sophisticated synthetic control of the aspect ratio, surface functionalization, and size-dependent optical properties has led to a diverse collection of nanomaterials well-suited for the biological environment. The large surface area-to-volume ratio enables targeting ligands, imaging agents, and therapeutics to coexist in the same particle.[10] Intrinsic length scales allow NPs to directly probe individual cellular components and, if small enough, be cleared by the renal system.[11] Recent applications include gold NPs for drug delivery and cancer therapy,[9,12–14] quantum dots (QDs) as cellular sensors and imaging agents,[5–7] and liposomal NPs for vaccinations and delivery systems.[15–17] While the field of nanomedicine is promising, nonspecific NP interactions with biomolecules, toxicity, and unpredictable biodistribution still limit the clinical use of most NP-based platforms.[15,18] In order to advance the use of NPs in biology and medicine, fundamental characterization of NP interactions with biomolecules and cells is essential.

NPs used in biological systems are exposed to a complex mixture of extracellular proteins. The high surface energy of the NP leads to rapid adsorption of a protein layer, or "corona," on the NP surface.[19–21] The formation of a protein corona has been observed on a wide range of materials including gold,[22–24] silver,[25] and polymeric NPs.[26–28] The corona composition is dynamic and highly dependent upon NP material and surface modification. Functionalizing the NP surface with polyethylene glycol (PEG) can reduce but not completely eliminate protein adsorption. The composition

of the corona, energetics of formation, and dynamic identity all influence the response of single cells to the protein-NP complex. A complete understanding of the interface between NPs and the cellular environment requires characterization of how adsorbed proteins mediate NP interactions with cells, as well as the ways in which the NP surface induces molecular level changes to the adsorbed protein.

1.2 Protein Corona

For most biomedical applications, NPs are injected directly into the blood stream where they encounter red and white blood cells, clotting factors, inorganic salts, and extracellular proteins.[29,30] Plasma is the soluble protein component of whole blood after the red and white blood cells are removed.[30] Further purification of plasma separates the clotting factors, such as fibrinogen, from serum. Serum is a diverse mixture containing hundreds of distinct proteins.[31,32] Of particular interest has been the observation that NPs exposed to biological fluids are readily coated with a layer of proteins adsorbed to the surface.[19–21,33,34] The presence of a protein layer, or protein corona, has been observed after exposure to both plasma[35,36] and serum.[24,28,37,38]

The protein corona defines the interface between the NP and the biological surroundings and, as a result, controls NP-cell interactions.[37,39–45] Studying the formation of the corona is complicated both by the number of unique plasma proteins and the dynamic nature of the biological environment. In the presence of cells, the dynamics become even more pronounced as a continuous, localized flux of ions and biomolecules exists to maintain necessary cellular homeostasis, altering the local environment around both the NP and protein.[41] Protein corona composition is highly dependent upon NP properties such as size[23,33] and surface modification,[27,46] energetics of formation,[47] and time.[34,38]

1.2.1 Composition

The presence of a protein corona has been observed on a diverse range of NP surfaces including polymeric NPs,[26–28,37] silica NPs,[42] QDs,[24,48] iron oxide NPs,[49] silver nanoclusters,[50] silver NPs,[25] gold nanorods,[51,52] and gold NPs.[22–24,53] The corona is dominated by albumin,[19,24,28,34–36,38] the most abundant protein in serum (55%).[31,32,54] Lower abundance serum proteins such as apolipoproteins, fibrinogen, and immunoglobulins are also commonly observed,[26,35,36] and can be present in high abundance on NP surfaces despite their relatively low concentrations in plasma. This highlights the fact that the NP itself can greatly influence the composition of the corona. Recently, an 'adorbsome' was identified consisting of 125 plasma proteins that have been detected on NP surfaces.[55] Although many different proteins can bind to NP surfaces, a general trend has emerged where a few (2-6) proteins compose the majority of the corona.[55] While the focus of this dissertation is on protein interactions with NPs, it is important to note that other plasma components such as lipids and complement factors also bind and contribute to the overall cellular pathway of the NP.[44]

Several NP properties influence the composition of corona proteins including material,[26,36,46] charge,[56] surface properties,[25,27,33,46,47,49] and size.[23,26,33,57] For example, Monopoli *et al.* have observed that for sulfonated polystyrene NPs and silica NPs of similar size, serum albumin and fibrinogen are the main components of the corona.[36] However, both apolipoproteins and complement proteins are more abundant on the hydrophilic, polystyrene NP surfaces, and the composition was dependent upon the plasma concentration. NP size also influences the identity of corona proteins. For gold NPs of 5, 15, and 80 nm, protein composition and binding was investigated as a function of diameter.[23] While albumin, hemoglobin, fibrinogen, and apolipoprotein E were observed on NPs of all diameters, proteins such as myosin and apolipoproteins A2 and A4, were only detected on the 5 nm gold NPs. The 5 nm NPs also bound the most proteins per surface area, attributed to a greater radius of curvature. Generally,

differences in adsorption as a result of size are attributed to NP curvature, especially in cases where the NP and protein are of similar size.

The charge on the NP also influences protein binding, especially for proteins with several charged residues. Gessner *et al.* have demonstrated that positively charged polystyrene NPs preferentially bind proteins with an isoelectric point (pI) < 5.5, while negatively charged NPs bind proteins with a pI > 5.5.[27] The effect of pH on protein adsorption reinforces the need to characterize NPs for biological applications in an environment that best imitates the buffered, slightly basic, physiological environment.

1.2.2 Energetics of Formation

The primary forces that control protein binding to NP surfaces include hydrophobic interactions, electrostatics, and Van der Waals forces.[21,41,47,58,59] Hydrogen-bonding and π-π stacking can also contribute to the overall protein binding force.[47,58] The relative contributions from each force vary in the literature based on the NP material, functionalization, and protein characteristics.[47,59,60] Yoon *et al.* observed that adsorption of proteins to microspheres is dominated by hydrophobic interactions when the surface charge is low, but determined by electrostatics when the particle surface is completely modified with charged functional groups.[47] Kondo and Higashitani reported that adsorption isotherms of several proteins to hydrophilic, but not hydrophobic particles were dependent upon pH, concluding that both hydrophobic and electrostatic interactions control protein adsorption to particle surfaces.[60]

Hydrophobic interactions, driven by entropy, play a significant role in protein interactions with surfaces. Protein adsorption minimizes exposure of hydrophobic residues to polar solvent molecules and is usually accompanied by a loss of bound water molecules. Adsorption increases as the hydrophobicity of either the NP surface or the protein increases.[59,61] While the exact contribution of hydrophobic forces is difficult to deduce in a complex mixture of proteins, the important consequence of the

hydrophobic interaction is the potential for protein unfolding. As unfolded proteins generally contain more exposed hydrophobic residues (and potentially higher valency), unfolded proteins will have a higher affinity for hydrophobic surfaces. Structural changes to corona proteins after interaction with NP surfaces will be covered in Section 1.3.

Electrostatic interactions often contribute to the formation of the protein corona as both NPs and proteins contain some degree of surface charge. Electrostatic forces are generally long-range interactions which scale inversely with distance squared (Coulomb's law).[62] However, the high ionic strength of biological fluids (150 mM) screens the electrostatic force beyond ∼10 nm from the NP surface.[41,58,62] While most NPs become net negatively charged in biological media,[28,41,51] attractive forces are still present due to charged surface ligands on the NP surface. In addition to the NP, most proteins have regions of both positive and negative surface charge. For example, serum albumin, the most abundant serum protein,[31] is net negatively charged at physiological pH (pI ∼4.7) but contains 60 positively charged lysine groups.[63,64] Electrostatic interactions are highly dependent upon the pH of the surrounding medium as well as the accessibility of positively and negatively charged functional groups on both the NP and protein surface.

While Van der Waals forces are generally weak and decay rapidly as a function of distance, they contribute to protein-NP interactions at short range. The continuous fluctuation of electrons in both proteins and on NP surfaces creates small, localized dipole moments, both permanent and induced. The dipole moments generate attractive (or repulsive) regions of the NP surface where proteins and other macromolecules can bind. While the dipole moments for individual atoms are small, the net dipole moment across a large molecule, such as a protein or protein domain, is significant. Importantly, the localization of dipole moments means that the total interaction is maximized with a larger contact area, so NP size and the folded state of the protein

both largely influence the total Van der Waals forces.

All of these forces, among others, work in an orchestrated fashion to balance both enthalpic losses and entropic gains. While protein adsorption to surfaces is not a new area of research,[65] a full understanding of protein binding to NPs remains a challenge. The thermodynamics and energtics of binding eventually determine the protein composition, dynamics of protein adsorption over time, and molecular level changes in protein structure, all of which ultimately influence NP interactions with cells.

1.2.3 Dynamics

While the identity of the protein corona is dependent upon NP properties, ultimately, the corona composition is dynamic. Protein adsorption to surfaces is a competitive process, a phenomenon referred to as the Vroman effect.[66,67] Higher mobility proteins initially bind, forming a weakly bound "soft" corona composed primarily of albumin.[26,39] The soft corona is replaced over time with a "hard" corona composed of proteins, such as apolipoproteins, with a lower mobility but higher affinity for the surface.[26,34] Often, both an irreversible hard corona and a weakly bound soft corona in equilibrium with free proteins in solution exist simultaneously.[68] Experimentally, protein adsorption is fit biexponentially to calculate separate rate constants (k_{on} and k_{off}) for proteins forming the soft versus hard corona.[34,55] Corona formation dynamics have also been simulated numerically using population balance equations and results were consistent with experimental observations.[69] An initial metastable corona of albumin was observed and later replaced by a stable layer of high-density lipoprotein, which was used as a model particle.

The dynamic evolution of the protein corona has been observed on NPs of varied composition[26,34,44] and size,[38,44] in a range of plasma concentrations,[38] and in

both plasma and cytosolic fluid.[70] Factors such as protein association strength, diffusion constant, conformational changes, and local environment all influence the kinetics. Coarse-grained molecular dynamics simulations have modeled the contributions to the Vroman effect, concluding that protein size, affinity, diffusion constant, and conformational changes contribute to the competitive adsorption that precedes equilibrium.[71] The dynamic process by which proteins adsorb and desorb has significant cellular consequences. Competitive protein adsorption leads to NPs with a varied corona composition over time. Differences in exposed proteins and protein epitopes, changes in protein structure, and varying degrees of protein coverage all affect receptor-mediated binding, internalization pathways, and the immune response to the protein-NP complex.[39,44]

1.2.4 Inhibition

NPs for medicinal applications must interact with the biological environment predictably. Nonspecific protein adsorption and opsonization quickly direct foreign materials to the mononuclear phagocyte system (MPS). Rapid clearance reduces efficacy of nanomaterials and triggers undesirable immune responses. While many efforts have been made to prevent the formation of the corona, complete inhibition remains a challenge.[55,72–74] Protecting the NP surface with PEG is currently the most common method for reducing protein adsorption.[55,73,74] PEG can be incorporated during NP synthesis, usually with a block copolymer, or post-synthetically by chemically attaching the polymer chain to the surface.[75–77] NPs coated with PEG have an increased blood circulation time,[73,74,78] avoid uptake by the MPS,[79] and prevent activation of the complement system.[73] In general, an increased cirulation time leads to greater efficacy of nanomedicines, as greater retention affords the NP prolonged time to reach the intended biological target.

The PEG chain length and polymer configuration both significantly alter the degree of protein adsorption. Two polymer configurations, brush and mushroom, are possible for PEG terminally grafted onto a surface.[75–77] The brush configuration consists of long chain polymers densely packed on the surface, where the distance between the chains is less than the Flory radius. The Flory radius is the effective hydrodynamic radius accounting for excluded volume around the polymer.[75] The mushroom configuration arises from a less dense polymer layer where the distance between chains is larger than the Flory radius. Polymer chains are collapsed into a mushroom formation on the surface as a result of repulsion between neighboring chains. Maximum prevention of protein adsorption is achieved with a dense layer of PEG in the brush configuration.[73,74,76,77] The dense layer of the polymer reduces protein adsorption by increasing steric hindrance and introducing a high entropy cost of protein binding.[76,77] The PEG length and molecular weight necessary to prevent adsorption is dependent upon the NP material and size as well as the size and molecular weight of the protein. For example, polylactic acid NPs were coated with PEG chains with molecular weight values ranging between 2,000 to 20,000 $g \cdot mol^{-1}$.[74] The optimal PEG coating for maximum protein reduction was 5% (w/v) PEG with a molecular weight of 5,000 $g \cdot mol^{-1}$ in a brush configuration. Increase in either molecular weight or weight percent of PEG did not reduce protein adsorption further. While passivation with PEG is the most common method, drawbacks include rapid clearance of NPs over long time periods, limited interactions with cellular receptors, and the prevention of targeted uptake.[55,74,80] Alternatives to PEG, including polysaccharides[81,82] and zitterionic copolymers,[83,84] have shown recent promise in reducing protein adsorption. Preventing protein adsorption remains an active area of research for all exogenous materials introduced into the body. While the protein corona can be reduced, some degree of protein adsorption will persist. The effectiveness of antifouling must be

systematically deduced for each NP, characterizing both the reduction in protein adsorption as well as the effects on biodistribution and immune response.

1.2.5 Biological Consequences of the Corona

Arguably, the most significant consequence of the protein corona is the ability for the adsorbed proteins to control NP interactions with the biological environment. The corona can protect against NP-induced cellular toxicity and particle aggregation.[42,85] Proteins remain bound as the NP crosses biological barriers,[40] and as a result, influence cellular binding and internalization of the NP.[28,43–45] The adsorbed proteins can also mask targeting ligands on the NP surface, directing the NP away from the intended cellular target.[86] Both nonspecific physical interactions and specific recognition of the protein-NP complex are affected by corona formation, ultimately determining NP-cell interactions and the overall immune response.

Direct, nonspecific interaction of the high energy surface of NPs with cellular components can be damaging and lead to a cascade of undesirable consequences. Lesniak *et al.* have demonstrated that NPs exposed to A549 lung epithelial cells in the absence of serum proteins adhere directly to the cell membrane causing cellular damage, but the presence of serum proteins mitigated cytotoxity.[42] Similar results were observed for graphene oxide.[87] In addition to protecting cells from the high surface energy, serum proteins increase the stability of NPs in solutions with a high electrolyte content. The adsorption of serum proteins shields neighboring NPs and prevents aggregation via electrostatic and steric repulsion.[85] Increased colloidal stability in the presence of serum proteins has been observed for gold nanorods,[51] gold NPs,[88] and silver NPs.[89]

While protein adsorption protects NPs from nonspecific interactions, the corona also enables specific recognition of the NP by biological and cellular components.[39,90] Though there will always exist some degree of exchange between proteins on the NP

surface and free proteins in solution, our group previously observed that bovine serum albumin (BSA) stays bound to the surface of polystyrene NPs during both cellular binding and internalization.[37,40] These experiments have two important implications. The first is that adsorbed proteins determine the cellular transport of NPs as they are not displaced during NP interactions with cells. The second is that proteins remain bound as the NP crosses a biological membrane and into an environment with a different pH and protein concentration. These experiments used isolated BSA as a model serum protein, and it is still relatively unknown how the composition of the corona changes as NPs cross biological barriers, i.e. lipid membranes or organelles. Previous work characterizing the corona after transfer from plasma to cytosolic fluid suggests that, while the corona composition differs after transfer, the final corona contains proteins from both solutions. The potential for NPs to retain a 'memory' of proteins encountered throughout biological transport has direct implications for NP accumulation and clearance mechanisms. The challenge lies in controlling protein adsorption throughout the total circulation time until clearance, and will be unique for every NP and each local environment the NP encounters.

Since proteins remain bound to the NP during cellular binding, the corona, rather than the NP, determines the cellular receptors used by protein-NP complexes. Chapters 3 and 4 demonstrate that the presence or absence of serum proteins leads to different cellular binding trends for cationic versus anionic NPs. We have observed that protein-NP complexes formed with cationic NPs bind to scavenger receptors, a class of nonspecific receptors used to bind degradation products and a diverse range of biomacromolecules.[91–95] In comparison, protein-NP complexes formed from anionic NPs bind to native protein receptors, specifically the albumin protein receptor. We observed these trends for cationic and anionic polystyrene NPs,[28] and anionic QDs, colloidal gold nanospheres, and low-density lipoprotein (LDL).[24] The importance of the corona on the cellular binding and internalization of NPs has also been observed

in the literature for silica,[44,96] polymeric,[43–45,96–98] silver,[50] and gold NPs.[99]

Adsorbed proteins provide NPs with specific binding sites on the cell surface as many serum proteins have dedicated cellular receptors. However, the binding specificity of corona proteins has the potential to mask targeting ligands on the NP surface. A reduction in targeting capability has been observed for transferrin-conjugated silica NPs.[86] The transferrin on the NP surface can bind the native transferrin receptor *in vitro*, but the targeting capabilities are masked by the adsorption of serum proteins. A similar loss in targeting was observed for a model reaction between NPs functionalized with a cycloalkyne, bicyclonyne group and azide groups on a silicon substrate. The bicyclonyne groups conjugate to the terminal end of the azide through a copper-free click reaction in the absence of serum, but the targeting efficiency is reduced by 94% in the presence of 10% serum.[100] While loss of targeted NP binding *in vivo* remains unknown, these *in vitro* experiments demonstrate the potential for unpredictable NP-cell interactions after corona formation.

Many NP properties affect protein corona formation and subsequent cellular interactions of protein-NP complexes. However, both the composition and dynamics of the corona, along with disruption of protein structure and function upon adsorption to the NP ultimately determine the overall biological impact. Molecular level changes to protein structure and function arguably have the greatest potential for causing unwanted toxicity and immunological responses to the NP. The following section will discuss the effect of NP surfaces on protein structure and function.

1.3 Molecular Properties of Corona Proteins

Most of the research to date on the protein corona has focused on the composition as a function of NP material, size, and time. However, equally important are the structural changes to the protein upon adsorption. Conformational changes, exposure of

epitopes, and loss in protein function can all trigger cellular and immunological responses.[44,45,101] This section will focus on NP induced structural changes to adsorbed proteins and the cellular and immunological consequences of these interactions.

Protein adsorption to solid surfaces is known to alter structure and lead to partial denaturation.[61,65,102] As described in Section 1.2.2, there are many forces which contribute to protein-surface interactions. Release of free energy accompanying protein adsorption is a likely trigger of protein conformational changes.[41] Flexibility of protein structure, exposed hydrophobic or charged residues, and solvent properties, along with NP properties such as curvature, material, and surface modification all contribute to the final protein structure. The difference in studying protein adsorption to NPs versus flat surfaces is the high radius of curvature. Interactions of proteins with large NPs appear relatively flat to the protein. As the NP diameter decreases, the protein will experience the curved surface. Mandal and Kraatz observed that a helical peptide retains its secondary structure on flat surfaces and large gold NPs (20 nm diameter), but the relative number of α-helices is reduced by nearly 80% on smaller NPs (5 nm).[103] However, even on large NP surfaces, protein structure can be lost. We observe in Chapter 5 that serum albumin loses secondary structure on the surface of 58 nm cationic NPs, but the structure is retained on 60 nm anionic NPs. As many proteins can bind to a single NP upon exposure to serum, determining the effect of protein structural changes on the physiological response to the NP is a complex challenge.

Adsorption of proteins to many types of NPs has been observed to disrupt protein structure.[41,104–108] For albumin, the most abundant serum protein, disruption of secondary structure has been observed following adsorption to silver NPs,[25,46] zinc oxide NPs,[109] gold NPs,[52,110] and gold nanorods.[52] Structural changes have also been observed for lower abundance plasma proteins including fibrinogen,[22,101,111] lysozyme,[112] cytochrome c,[113,114] and chymotrypsin.[112] For lysozyme and chymotrypsin, the loss

in secondary structure was accompanied by a loss in enzymatic activity.[112] Using a model protein system, the *Streptococcal* protein GB1 binding domain, on latex NPs, Pan *et al.* observed that adsorption, accompanied by a reversible structural change, occurs via a two-step process.[108] The initial interaction of the protein with the NP is characterized by rates of adsorption and desorption, or k_{on} and k_{off}, respectively. This is followed by a conformational change with a different rate affiliated with protein unfolding, k_u, and folding, k_f. The dynamic nature of protein unfolding introduces another layer of complexity to the formation of the corona. In addition to competitive adsorption between different proteins, the binding of each protein is dynamic over time depending on the kinetics and reversibility of adsorption.

While the binding of GB1 to latex NPs undergoes a reversible conformational change, the reversibility will be protein dependent. Mahmoudi *et al.* observed that binding of the transferrin protein to superparamagnetic iron oxide NPs led to irreversible changes in transferrin conformation.[115] Characterization of protein structure for proteins bound to a NP and after desorption from the NP surface is critical for determining biological interactions. The presence of denatured proteins either bound to a NP surface or free in solution has cellular consequences. In Chapter 5, we demonstrate that a loss in secondary structure for BSA bound to polystyrene NPs directs the protein-NP complex away from the native albumin receptors and instead to scavenger receptors on the cell surface. These results are consistent with previous research that demonstrates chemically or structurally modified albumin on the surface of gold NPs bind to a class of scavenger receptors specific to modified albumins.[91–93]

Misfolded proteins and aggregates in solution lead to an enhanced immune response and are linked to a number of disease states.[116,117] Polymeric NPs, cerium oxide NPs, QDs, and carbon nanotubes were all observed to induce the nucleation and fibrillation of human β2-microglobulin.[118] However, not all proteins are disrupted by adsorption onto NPs. A comparison of chymotrypsin and cytochrome c adsorbed

onto 7 nm gold NPs showed that while the structure of chymotrypsin was disrupted, cytochrome c retained its secondary structure.[119] Mahmoudi *et al.* demonstrated that silica NPs, polystyrene NPs, and carbon nanotubes coated with a protein corona all slow the formation of amyloid-β fibrillation, with applications for protein misfolding diseases.[120]

Both uncoated NP surfaces and protein structural changes trigger immune responses. Yan *et al.* observed that changes in BSA structure on the surface of polymeric NPs accompanied an increase in NP uptake by human monocytic cells compared to bare NPs.[45] In comparison, similar uptake was observed in macrophage cells for NPs with and without a corona. While the differences in uptake in monocytes was attributed to protein structure, it is difficult to separate the effect of the presence of a corona from the effect of a change in protein structure on cellular uptake. Deng *et al.* reported that unfolding of fibrinogen on gold NPs activates the Mac-1 receptor promoting the NF-κB pathway.[101] This led to a triggered immune response and the subsequent release of cytokines in THP-1 cells. These studies demonstrate that both the NP and the protein adsorbed to the NP can activate the immune system. A holistic examination of the role of the pristine NP surface, free proteins, and protein-NP complexes is required for a complete physiological understanding.

As disruption of protein structure induces protein aggregation, accompanies a loss in function, and exposes new peptide sequences, or epitopes,[106,121] fundamental studies of protein structure on NP surfaces will need to be extended *in vivo* to understand the full biological effect of NP-induced conformational changes. For most nanomedicines, the mechanism of how protein structure on a NP surface alters NP interactions with cellular components and triggers the immune system remains unknown.

1.4 Dissertation Overview

The use of NPs in biology and medicine requires a fundamental characterization of the interactions between NPs and proteins in a physiologically relevant environment, as well as precise control over NP interactions with the surrounding biological milieu. This dissertation focuses on the former with the ultimate goal of understanding the molecular characteristics of the protein-NP complex and the cellular consequences of formation. Protein-NP interactions in the cellular environment are complex and dynamic as the protein controls the NP interactions with cells, yet the NP surface alters the structure and molecular properties of the adsorbed protein. Our initial observations that the presence of serum proteins enhanced the cellular binding of cationic, polystyrene NPs led to an investigation of the role of serum proteins in charged NP interactions with cells. Interestingly, we observed the opposite trend for anionic polystyrene NPs as the presence of serum proteins inhibited cellular binding. In Chapter 3, we demonstrate that initial NP surface charge dictates the cellular binding of NPs when proteins are present. We determined that the differences are due to protein-NP complexes binding to distinct cellular receptors. Complexes formed with cationic NPs bind to scavenger receptors, whereas complexes formed with anionic NPs bind to native protein receptors. We determined that these trends are not dependent upon NP diameter or cell type. Chapter 4 demonstrates that the trends we observed for polystyrene NP binding are consistent for anionic QDs, colloidal gold nanospheres, and LDL. These biomedically relevant NPs differ in size, composition, and surface modification, suggesting that initial NP surface charge is a dominating factor in the cellular binding of NPs.

Chapter 5 extends the cellular binding results to include structural and thermodynamic studies of adsorbed proteins. We used NP surface charge to modulate protein secondary structure using BSA as a model protein. We observe that protein secondary structure is retained on anionic NPs and disrupted on cationic NPs. By

correlating the secondary structure of proteins adsorbed to a NP surface with the cellular receptors used to bind the protein-NP complex, we determined a molecular level relationship between adsorbed proteins, NPs, and cellular receptors. The loss of secondary structure on cationic NPs redirects the protein-NP complex away from native protein receptors and instead to scavenger receptors which commonly bind modified proteins. In comparison, the native protein structure on anionic NPs allows these complexes to be recognized by the native albumin receptor. Future work will extend the structural and thermodynamic studies to other NP and protein systems, probe the relationship between structure and cellular internalization, and direct NP binding to specific cellular receptors using our understanding of the role of both NP surface charge and protein structure.

1.5 References

[1] De, M., Ghosh, P. S., and Rotello, V. M., "Applications of nanoparticles in biology." *Adv. Mater.*, **2008**, *20*, 4225–4241.

[2] Giljohann, D., Seferos, D., Daniel, W., Massich, M., Patel, P., and Mirkin, C., "Gold nanoparticles for biology and medicine." *Angew. Chem., Int. Ed.*, **2010**, *49*, 3280–3294.

[3] Dreaden, E. C., Alkilany, A. M., Huang, X., Murphy, C. J., and El-Sayed, M. A., "The golden age: Gold nanoparticles for biomedicine." *Chem. Soc. Rev.*, **2012**, *41*, 2740–2779.

[4] Pelaz, B., Jaber, S., de Aberasturi, D. J., Wulf, V., Aida, T., de la Fuente, J. M., Feldmann, J., Gaub, H. E., Josephson, L., Kagan, C. R., Kotov, N. A., Liz-Marzán, L. M., Mattoussi, H., Mulvaney, P., Murray, C. B., Rogach, A. L., Weiss, P. S., Willner, I., and Parak, W. J., "The state of nanoparticle-based nanoscience and biotechnology: Progress, promises, and challenges." *ACS Nano*, **2012**, *6*, 8468–8483.

[5] Alivisatos, A. P., Gu, W., and Larabell, C., "Quantum dots as cellular probes." *Annu. Rev. Biomed. Eng.*, **2005**, *7*, 55–76.

[6] Michalet, X., Pinaud, F. F., Bentolila, L. A., Tsay, J. M., Doose, S., Li, J. J., Sundaresan, G., Wu, A. M., Gambhir, S. S., and Weiss, S., "Quantum dots for live cells, *in vivo* imaging, and diagnostics." *Science*, **2005**, *307*, 538–544.

[7] Mattoussi, H., Palui, G., and Na, H. B., "Luminescent quantum dots as platforms for probing *in vitro* and *in vivo* biological processes." *Adv. Drug Delivery Rev.*, **2012**, *64*, 138–166.

[8] Medintz, I. L., Uyeda, H. T., Goldman, E. R., and Mattoussi, H., "Quantum dot bioconjugates for imaging, labelling and sensing." *Nat. Mater.*, **2005**, *4*, 435–446.

[9] Ghosh, P., Han, G., De, M., Kim, C. K., and Rotello, V. M., "Gold nanoparticles in delivery applications." *Adv. Drug Delivery Rev.*, **2008**, *60*, 1307–1315.

[10] Kircher, M. F., de la Zerda, A., Jokerst, J. V., Zavaleta, C. L., Kempen, P. J., Mittra, E., Pitter, K., Huang, R., Campos, C., Habte, F., Sinclair, R., Brennan, C. W., Mellinghoff, I. K., Holland, E. C., and Gambhir, S. S., "A brain tumor molecular imaging strategy using a new triple-modality MRI-photoacoustic-raman nanoparticle." *Nat. Med.*, **2012**, *18*, 829–834.

[11] Choi, H. S., Liu, W., Misra, P., Tanaka, E., Zimmer, J. P., Ipe, B. I., Bawendi, M. G., and Frangioni, J. V., "Renal clearance of quantum dots." *Nat. Biotechnol.*, **2007**, *25*, 1165–1170.

[12] Dreaden, E. C., Mackey, M. A., Huang, X., Kang, B., and El-Sayed, M. A., "Beating cancer in multiple ways using nanogold." *Chem. Soc. Rev.*, **2011**, *40*, 3391–3404.

[13] Jain, P. K., El-Sayed, I. H., and El-Sayed, M. A., "Au nanoparticles target cancer." *Nano Today*, **2007**, *2*, 18–29.

[14] Liu, Y., Miyoshi, H., and Nakamura, M., "Nanomedicine for drug delivery and imaging: A promising avenue for cancer therapy and diagnosis using targeted functional nanoparticles." *Int. J. Cancer*, **2007**, *120*, 2527–2537.

[15] Duncan, R. and Gaspar, R., "Nanomedicine(s) under the microscope." *Mol. Pharmaceutics*, **2011**, *8*, 2101–2141.

[16] Zhang, L., Gu, F. X., Chan, J. M., Wang, A. Z., Langer, R. S., and Farokhzad, O. C., "Nanoparticles in medicine: Therapeutic applications and developments." *Clin. Pharmacol. Ther.*, **2008**, *83*, 761–769.

[17] Allen, T. M. and Cullis, P. R., "Liposomal drug delivery systems: From concept to clinical applications." *Adv. Drug Delivery Rev.*, **2013**, *65*, 36–48.

[18] Wei, A., Mehtala, J. G., and Patri, A. K., "Challenges and opportunities in the advancement of nanomedicines." *J. Controlled Release*, **2012**, *164*, 236–246.

[19] Walczyk, D., Bombelli, F. B., Monopoli, M. P., Lynch, I., and Dawson, K. A., "What the cell "sees" in bionanoscience." *J. Am. Chem. Soc.*, **2010**, *132*, 5761–5768.

[20] Lynch, I., Cedervall, T., Lundqvist, M., Cabaleiro-Lago, C., Linse, S., and Dawson, K. A., "The nanoparticle-protein complex as a biological entity; A complex fluids and surface science challenge for the 21st century." *Adv. Colloid Interface Sci.*, **2007**, *134-135*, 167–174.

[21] Treuel, L. and Nienhaus, G. U., "Toward a molecular understanding of nanoparticle-protein interactions." *Biophys. Rev.*, **2012**, *4*, 137–147.

[22] Lacerda, S. H. D., Park, J. J., Meuse, C., Pristinski, D., Becker, M. L., Karim, A., and Douglas, J. F., "Interaction of gold nanoparticles with common human blood proteins." *ACS Nano*, **2010**, *4*, 365–379.

[23] Schäffler, M., Semmler-Behnke, M., Sarioglu, H., Takenaka, S., Wenk, A., Schleh, C., Hauck, S. M., Johnston, B. D., and Kreyling, W. G., "Serum protein identification and quantification of the corona of 5, 15 and 80 nm gold nanoparticles." *Nanotechnology*, **2013**, *24*, 265103.

[24] Fleischer, C. C., Kumar, U., and Payne, C. K., "Cellular binding of anionic nanoparticles is inhibited by serum proteins independent of nanoparticle composition." *Biomater. Sci.*, **2013**, *1*, 975–982.

[25] Podila, R., Chen, R., Ke, P. C., Brown, J. M., and Rao, A. M., "Effects of surface functional groups on the formation of nanoparticle-protein corona." *Appl. Phys. Lett.*, **2012**, *101*, 263701.

[26] Cedervall, T., Lynch, I., Foy, M., Berggård, T., Donnelly, S. C., Cagney, G., Linse, S., and Dawson, K. A., "Detailed identification of plasma proteins adsorbed on copolymer nanoparticles." *Angew. Chem., Int. Ed.*, **2007**, *46*, 5754–5756.

[27] Gessner, A., Lieske, A., Paulke, B.-R., and Müller, R. H., "Functional groups on polystyrene model nanoparticles: Influence on protein adsorption." *J. Biomed. Mater. Res., Part A*, **2003**, *65A*, 319–326.

[28] Fleischer, C. C. and Payne, C. K., "Nanoparticle surface charge mediates the cellular receptors used by protein-nanoparticle complexes." *J. Phys. Chem. B*, **2012**, *116*, 8901–8907.

[29] Alberts, B., Bray, D., Lewis, J., Raff, M., Roberts, K., and Watson, J. D., *Molecular Biology of the Cell*. Garland Publishing Inc., New York, 3rd edn., **1994**.

[30] Voet, D. and Voet, J. G., *Biochemistry*, vol. 1. John Wiley and Sons, Inc., Hoboken, 3rd edn., **2004**.

[31] Anderson, N. L. and Anderson, N. G., "The human plasma proteome: History, character, and diagnostic prospects." *Mol. Cell. Proteomics*, **2002**, *1*, 845–867.

[32] Pieper, R., Gatlin, C. L., Makusky, A. J., Russo, P. S., Schatz, C. R., Miller, S. S., Su, Q., McGrath, A. M., Estock, M. A., Parmar, P. P., Zhao, M., Huang, S. T., Zhou, J., Wang, F., Esquer-Blasco, R., Anderson, N. L., Taylor, J., and Steiner, S., "The human serum proteome: Display of nearly 3700 chromatographically separated protein spots on two-dimensional electrophoresis gels and identification of 325 distinct proteins." *Proteomics*, **2003**, *3*, 1345–1364.

[33] Lundqvist, M., Stigler, J., Elia, G., Lynch, I., Cedervall, T., and Dawson, K. A., "Nanoparticle size and surface properties determine the protein corona with possible implications for biological impacts." *Proc. Natl. Acad. Sci. U. S. A.*, **2008**, *105*, 14265–14270.

[34] Cedervall, T., Lynch, I., Lindman, S., Berggård, T., Thulin, E., Nilsson, H., Dawson, K. A., and Linse, S., "Understanding the nanoparticle-protein corona using methods to quantify exchange rates and affinities of proteins for nanoparticles." *Proc. Natl. Acad. Sci. U. S. A.*, **2007**, *104*, 2050–2055.

[35] Barrán-Berdón, A. L., Pozzi, D., Caracciolo, G., Capriotti, A. L., Caruso, G., Cavaliere, C., Riccioli, A., Palchetti, S., and Laganá, A., "Time evolution of nanoparticle-protein corona in human plasma: Relevance for targeted drug delivery." *Langmuir*, **2013**, *29*, 6485–6494.

[36] Monopoli, M. P., Walczyk, D., Campbell, A., Elia, G., Lynch, I., Bombelli, F. B., and Dawson, K. A., "Physical-chemical aspects of protein corona: Relevance to *in vitro* and *in vivo* biological impacts of nanoparticles." *J. Am. Chem. Soc.*, **2011**, *133*, 2525–2534.

[37] Doorley, G. W. and Payne, C. K., "Cellular binding of nanoparticles in the presence of serum proteins." *Chem. Commun.*, **2011**, *47*, 466–468.

[38] Casals, E., Pfaller, T., Duschl, A., Oostingh, G. J., and Puntes, V., "Time evolution of the nanoparticle protein corona." *ACS Nano*, **2010**, *4*, 3623–3632.

[39] Monopoli, M. P., Åberg, C., Salvati, A., and Dawson, K. A., "Biomolecular coronas provide the biological identity of nanosized materials." *Nat. Nanotechnol.*, **2012**, *7*, 779–786.

[40] Doorley, G. W. and Payne, C. K., "Nanoparticles act as protein carriers during cellular internalization." *Chem. Commun.*, **2012**, *48*, 2961–2963.

[41] Nel, A. E., Madler, L., Velegol, D., Xia, T., Hoek, E. M. V., Somasundaran, P., Klaessig, F., Castranova, V., and Thompson, M., "Understanding biophysicochemical interactions at the nano-bio interface." *Nat. Mater.*, **2009**, *8*, 543–557.

[42] Lesniak, A., Fenaroli, F., Monopoli, M. P., Åberg, C., Dawson, K. A., and Salvati, A., "Effects of the presence or absence of a protein corona on silica nanoparticle uptake and impact on cells." *ACS Nano*, **2012**, *6*, 5845–5857.

[43] Lunov, O., Syrovets, T., Loos, C., Beil, J., Delecher, M., Tron, K., Nienhaus, G. U., Musyanovych, A., Mailaender, V., Landfester, K., and Simmet, T., "Differential uptake of functionalized polystyrene nanoparticles by human macrophages and a monocytic cell line." *ACS Nano*, **2011**, *5*, 1657–1669.

[44] Tenzer, S., Docter, D., Kuharev, J., Musyanovych, A., Fetz, V., Hecht, R., Schlenk, F., Fischer, D., Kiouptsi, K., Reinhardt, C., Landfester, K., Schild, H., Maskos, M., Knauer, S. K., and Stauber, R. H., "Rapid formation of plasma protein corona critically affects nanoparticle pathophysiology." *Nat. Nanotechnol.*, **2013**, *8*, 772–781.

[45] Yan, Y., Gause, K. T., Kamphuis, M. M. J., Ang, C.-S., O'Brien-Simpson, N. M., Lenzo, J. C., Reynolds, E. C., Nice, E. C., and Caruso, F., "Differential roles of the protein corona in the cellular uptake of nanoporous polymer particles by monocyte and macrophage cell lines." *ACS Nano*, **2013**, *7*, 10960–10970.

[46] Treuel, L., Malissek, M., Grass, S., Diendorf, J., Mahl, D., Meyer-Zaika, W., and Epple, M., "Quantifying the influence of polymer coatings on the serum albumin corona formation around silver and gold nanoparticles." *J. Nanopart. Res.*, **2012**, *14*, 1–12.

[47] Yoon, J.-Y., Kim, J.-H., and Kim, W.-S., "Interpretation of protein adsorption phenomena onto functional microspheres." *Colloids Surf., B*, **1998**, *12*, 15 – 22.

[48] Röcker, C., Potzl, M., Zhang, F., Parak, W. J., and Nienhaus, G. U., "A quantitative fluorescence study of protein monolayer formation on colloidal nanoparticles." *Nat. Nanotechnol.*, **2009**, *4*, 577–580.

[49] Jedlovszky-Hajdú, A., Bombelli, F. B., Monopoli, M. P., Tombácz, E., and Dawson, K. A., "Surface coatings shape the protein corona of SPIONs with relevance to their application *in vivo*." *Langmuir*, **2012**, *28*, 14983–14991.

[50] Shang, L., Dörlich, R. M., Trouillet, V., Bruns, M., and Nienhaus, G. U., "Ultrasmall fluorescent silver nanoclusters: Protein adsorption and its effects on cellular responses." *Nano Res.*, **2012**, *5*, 531–542.

[51] Alkilany, A. M., Nagaria, P. K., Hexel, C. R., Shaw, T. J., Murphy, C. J., and Wyatt, M. D., "Cellular uptake and cytotoxicity of gold nanorods: Molecular origin of cytotoxicity and surface effects." *Small*, **2009**, *5*, 701–708.

[52] Chakraborty, S., Joshi, P., Shanker, V., Ansari, Z. A., Singh, S. P., and Chakrabarti, P., "Contrasting effect of gold nanoparticles and nanorods with different surface modifications on the structure and activity of bovine serum albumin." *Langmuir*, **2011**, *27*, 7722–7731.

[53] Brewer, S. H., Glomm, W. R., Johnson, M. C., Knag, M. K., and Franzen, S., "Probing BSA binding to citrate-coated gold nanoparticles and surfaces." *Langmuir*, **2005**, *21*, 9303–9307.

[54] Adkins, J. N., Varnum, S. M., Auberry, K. J., Moore, R. J., Angell, N. H., Smith, R. D., Springer, D. L., and Pounds, J. G., "Toward a human blood serum proteome: Analysis by multidimensional separation coupled with mass spectrometry." *Mol. Cell. Proteomics*, **2002**, *1*, 947–955.

[55] Walkey, C. D. and Chan, W. C. W., "Understanding and controlling the interaction of nanomaterials with proteins in a physiological environment." *Chem. Soc. Rev.*, **2012**, *41*, 2780–2799.

[56] Hühn, D., Kantner, K., Geidel, C., Brandholt, S., De Cock, I., Soenen, S. J. H., Rivera Gil, P., Montenegro, J.-M., Braeckmans, K., Müllen, K., Nienhaus, G. U., Klapper, M., and Parak, W. J., "Polymer-coated nanoparticles interacting with proteins and cells: Focusing on the sign of the net charge." *ACS Nano*, **2013**, *7*, 3253–3263.

[57] Liu, W., Rose, J., Plantevin, S., Auffan, M., Bottero, J.-Y., and Vidaud, C., "Protein corona formation for nanomaterials and proteins of a similar size: Hard or soft corona?" *Nanoscale*, **2013**, *5*, 1658–1668.

[58] Yang, S.-T., Liu, Y., Wang, Y.-W., and Cao, A., "Biosafety and bioapplication of nanomaterials by designing protein-nanoparticle interactions." *Small*, **2013**, *9*, 1635–1653.

[59] Andrade, J. and Hlady, V., "Protein adsorption and materials biocompatibility: A tutorial review and suggested hypotheses." *In* "Biopolymers/Non-Exclusion HPLC," Springer-Verlag, vol. 79 of *Advances in Polymer Science*, **1986**, 1–63.

[60] Kondo, A. and Higashitani, K., "Adsorption of model proteins with wide variation in molecular properties on colloidal particles." *J. Colloid Interface Sci.*, **1992**, *150*, 344 – 351.

[61] Hlady, V. and Buijs, J., "Protein adsorption on solid surfaces." *Curr. Opin. Biotechnol.*, **1996**, *7*, 72–77.

[62] Phillips, R., Kondev, J., and Theriot, J., *Physical Biology of the Cell*. Garland Science, New York, **2009**.

[63] Carter, D. C. and Ho, J. X., "Structure of serum albumin." *In* "Advances in Protein Chemistry," Academic Press, vol. 45, **1994**, 153–203.

[64] Hirayama, K., Akashi, S., Furuya, M., and Fukuhara, K.-I., "Rapid confirmation and revision of the primary structure of bovine serum albumin by ESIMS and Frit-FAB LC/MS." *Biochem. Biophys. Res. Commun.*, **1990**, *173*, 639–646.

[65] Rabe, M., Verdes, D., and Seeger, S., "Understanding protein adsorption phenomena at solid surfaces." *Adv. Colloid Interface Sci.*, **2011**, *162*, 87–106.

[66] Vroman, L., "Effect of adsorbed proteins on the wettability of hydrophilic and hydrophobic solids." *Nature*, **1962**, *196*, 476–477.

[67] Vroman, L., Adams, A., Fischer, G., and Munoz, P., "Interaction of high molecular weight kininogen, factor XII, and fibrinogen in plasma at interfaces." *Blood*, **1980**, *55*, 156–159.

[68] Kaufman, E. D., Belyea, J., Johnson, M. C., Nicholson, Z. M., Ricks, J. L., Shah, P. K., Bayless, M., Pettersson, T., Feldoto, Z., Blomberg, E., Claesson, P., and Franzen, S., "Probing protein adsorption onto mercaptoundecanoic acid stabilized gold nanoparticles and surfaces by quartz crystal microbalance and zeta-potential measurements." *Langmuir*, **2007**, *23*, 6053–6062.

[69] Sahneh, F. D., Scoglio, C., and Riviere, J., "Dynamics of nanoparticle-protein corona complex formation: Analytical results from population balance equations." *PLoS One*, **2013**, *8*, e64690.

[70] Lundqvist, M., Stigler, J., Cedervall, T., Berggård, T., Flanagan, M. B., Lynch, I., Elia, G., and Dawson, K., "The evolution of the protein corona around nanoparticles: A test study." *ACS Nano*, **2011**, *5*, 7503–7509.

[71] Vilaseca, P., Dawson, K. A., and Franzese, G., "Understanding and modulating the competitive surface-adsorption of proteins through coarse-grained molecular dynamics simulations." *Soft Matter*, **2013**, *9*, 6978–6985.

[72] Tonga, G. Y., Saha, K., and Rotello, V. M., "25th Anniversary Article: Interfacing nanoparticles and biology: New strategies for biomedicine." *Adv. Mater.*, **2014**, *26*, 359–370.

[73] Gref, R., Domb, A., Quellec, P., Blunk, T., Müller, R. H., Verbavatz, J. M., and Langer, R., "The controlled intravenous delivery of drugs using PEG-coated sterically stabilized nanospheres." *Adv. Drug Delivery Rev.*, **1995**, *16*, 215–233.

[74] Gref, R., Lück, M., Quellec, P., Marchand, M., Dellacherie, E., Harnisch, S., Blunk, T., and Müller, R. H., "'Stealth' corona-core nanoparticles surface modified by polyethylene glycol (PEG): Influences of the corona (PEG chain length and surface density) and of the core composition on phagocytic uptake and plasma protein adsorption." *Colloids Surf., B*, **2000**, *18*, 301–313.

[75] de Gennes, P. G., "Polymers at an interface; A simplified view." *Adv. Colloid Interface Sci.*, **1987**, *27*, 189–209.

[76] Jeon, S., Lee, J., Andrade, J., and Gennes, P. D., "Protein-surface interactions in the presence of polyethylene oxide: I. Simplified theory." *J. Colloid Interface Sci.*, **1991**, *142*, 149–158.

[77] Jeon, S. and Andrade, J., "Protein-surface interactions in the presence of polyethylene oxide: II. Effect of protein size." *J. Colloid Interface Sci.*, **1991**, *142*, 159–166.

[78] Gref, R., Minamitake, Y., Peracchia, M., Trubetskoy, V., Torchilin, V., and Langer, R., "Biodegradable long-circulating polymeric nanospheres." *Science*, **1994**, *263*, 1600–1603.

[79] Bazile, D., Prud'homme, C., Bassoullet, M.-T., Marlard, M., Spenlehauer, G., and Veillard, M., "Stealth Me.PEG-PLA nanoparticles avoid uptake by the mononuclear phagocytes system." *J. Pharm. Sci.*, **1995**, *84*, 493–498.

[80] Wang, M. and Thanou, M., "Targeting nanoparticles to cancer." *Pharmacol. Res.*, **2010**, *62*, 90–99.

[81] Lemarchand, C., Gref, R., and Couvreur, P., "Polysaccharide-decorated nanoparticles." *Eur. J. Pharm. Biopharm.*, **2004**, *58*, 327–341.

[82] Lemarchand, C., Gref, R., Passirani, C., Garcion, E., Petri, B., Müller, R., Costantini, D., and Couvreur, P., "Influence of polysaccharide coating on the interactions of nanoparticles with biological systems." *Biomaterials*, **2006**, *27*, 108–118.

[83] Chang, Y., Chen, S., Zhang, Z., and Jiang, S., "Highly protein-resistant coatings from well-defined diblock copolymers containing sulfobetaines." *Langmuir*, **2006**, *22*, 2222–2226.

[84] Murthy, A. K., Stover, R. J., Hardin, W. G., Schramm, R., Nie, G. D., Gourisankar, S., Truskett, T. M., Sokolov, K. V., and Johnston, K. P., "Charged gold nanoparticles with essentially zero serum protein adsorption in undiluted fetal bovine serum." *J. Am. Chem. Soc.*, **2013**, *135*, 7799–7802.

[85] Segets, D., Marczak, R., Schäfer, S., Paula, C., Gnichwitz, J.-F., Hirsch, A., and Peukert, W., "Experimental and theoretical studies of the colloidal stability of nanoparticles - A general interpretation based on stability maps." *ACS Nano*, **2011**, *5*, 4658–4669.

[86] Salvati, A., Pitek, A. S., Monopoli, M. P., Prapainop, K., Bombelli, F. B., Hristov, D. R., Kelly, P. M., Åberg, C., Mahon, E., and Dawson, K. A., "Transferrin-functionalized nanoparticles lose their targeting capabilities when a biomolecule corona adsorbs on the surface." *Nat. Nanotechnol.*, **2013**, *8*, 137–143.

[87] Hu, W., Peng, C., Lv, M., Li, X., Zhang, Y., Chen, N., Fan, C., and Huang, Q., "Protein corona-mediated mitigation of cytotoxicity of graphene oxide." *ACS Nano*, **2011**, *5*, 3693–3700.

[88] Dominguez-Medina, S., Blankenburg, J., Olson, J., Landes, C. F., and Link, S., "Adsorption of a protein monolayer via hydrophobic interactions prevents nanoparticle aggregation under harsh environmental conditions." *ACS Sustainable Chem. Eng.*, **2013**, *1*, 833–842.

[89] Gebauer, J. S., Malissek, M., Simon, S., Knauer, S. K., Maskos, M., Stauber, R. H., Peukert, W., and Treuel, L., "Impact of the nanoparticle-protein corona on colloidal stability and protein structure." *Langmuir*, **2012**, *28*, 9673–9679.

[90] Mao, Z., Zhou, X., and Gao, C., "Influence of structure and properties of colloidal biomaterials on cellular uptake and cell functions." *Biomater. Sci.*, **2013**, *1*, 896–911.

[91] Schnitzer, J. E., Sung, A., Horvat, R., and Bravo, J., "Preferential interaction of albumin-binding proteins, gp30 and gp18, with conformationally modified albumins. Presence in many cells and tissues with a possible role in catabolism." *J. Biol. Chem.*, **1992**, *267*, 24544–24553.

[92] Schnitzer, J. E. and Bravo, J., "High affinity binding, endocytosis, and degradation of conformationally modified albumins. Potential role of gp30 and gp18 as novel scavenger receptors." *J. Biol. Chem.*, **1993**, *268*, 7562–7570.

[93] Schnitzer, J. E. and Oh, P., "Albondin-mediated capillary permeability to albumin. Differential role of receptors in endothelial transcytosis and endocytosis of native and modified albumins." *J. Biol. Chem.*, **1994**, *269*, 6072–6082.

[94] Krieger, M., Acton, S., Ashkenas, J., Pearson, A., Penman, M., and Resnick, D., "Molecular flypaper, host defense, and atherosclerosis. Structure, binding properties, and functions of macrophage scavenger receptors." *J. Biol. Chem.*, **1993**, *268*, 4569–4572.

[95] Brown, M. S., Basu, S. K., Falck, J. R., Ho, Y. K., and Goldstein, J. L., "The scavenger cell pathway for lipoprotein degradation: Specificity of the binding site that mediates the uptake of negatively-charged LDL by macrophages." *J. Supramol. Struct.*, **1980**, *13*, 67–81.

[96] Lesniak, A., Salvati, A., Santos-Martinez, M. J., Radomski, M. W., Dawson, K. A., and Åberg, C., "Nanoparticle adhesion to the cell membrane and its effect on nanoparticle uptake efficiency." *J. Am. Chem. Soc.*, **2013**, *135*, 1438–1444.

[97] Ehrenberg, M. S., Friedman, A. E., Finkelstein, J. N., Oberdörster, G., and McGrath, J. L., "The influence of protein adsorption on nanoparticle association with cultured endothelial cells." *Biomaterials*, **2009**, *30*, 603–610.

[98] Baier, G., Costa, C., Zeller, A., Baumann, D., Sayer, C., Araujo, P. H. H., Mailaender, V., Musyanovych, A., and Landfester, K., "BSA adsorption on differently charged polystyrene nanoparticles using isothermal titration calorimetry and the influence on cellular uptake." *Macromol. Biosci.*, **2011**, *11*, 628–638.

[99] Liu, X., Huang, N., Li, H., Jin, Q., and Ji, J., "Surface and size effects on cell interaction of gold nanoparticles with both phagocytic and nonphagocytic cells." *Langmuir*, **2013**, *29*, 9138–9148.

[100] Mirshafiee, V., Mahmoudi, M., Lou, K., Cheng, J., and Kraft, M. L., "Protein corona significantly reduces active targeting yield." *Chem. Commun.*, **2013**, *49*, 2557–2559.

[101] Deng, Z. J., Liang, M., Monteiro, M., Toth, I., and Minchin, R. F., "Nanoparticle-induced unfolding of fibrinogen promotes Mac-1 receptor activation and inflammation." *Nat. Nanotechnol.*, **2011**, *6*, 39–44.

[102] Gray, J. J., "The interaction of proteins with solid surfaces." *Curr. Opin. Struct. Biol.*, **2004**, *14*, 110–115.

[103] Mandal, H. S. and Kraatz, H.-B., "Effect of the surface curvature on the secondary structure of peptides adsorbed on nanoparticles." *J. Am. Chem. Soc.*, **2007**, *129*, 6356–6357.

[104] You, C.-C., Verma, A., and Rotello, V. M., "Engineering the nanoparticle-biomacromolecule interface." *Soft Matter*, **2006**, *2*, 190–204.

[105] Slocik, J. M. and Naik, R. R., "Probing peptide-nanomaterial interactions." *Chem. Soc. Rev.*, **2010**, *39*, 3454–3463.

[106] Shemetov, A. A., Nabiev, I., and Sukhanova, A., "Molecular interaction of proteins and peptides with nanoparticles." *ACS Nano*, **2012**, *6*, 4585–4602.

[107] Roach, P., Farrar, D., and Perry, C. C., "Interpretation of protein adsorption: Surface-induced conformational changes." *J. Am. Chem. Soc.*, **2005**, *127*, 8168–8173.

[108] Pan, H., Qin, M., Meng, W., Cao, Y., and Wang, W., "How do proteins unfold upon adsorption on nanoparticle surfaces?" *Langmuir*, **2012**, *28*, 12779–12787.

[109] Chakraborti, S., Joshi, P., Chakravarty, D., Shanker, V., Ansari, Z. A., Singh, S. P., and Chakrabarti, P., "Interaction of polyethyleneimine-functionalized ZnO nanoparticles with bovine serum albumin." *Langmuir*, **2012**, *28*, 11142–11152.

[110] Wangoo, N., Suri, C. R., and Shekhawat, G., "Interaction of gold nanoparticles with protein: A spectroscopic study to monitor protein conformational changes." *Appl. Phys. Lett.*, **2008**, *92*, 133104.

[111] Deng, Z. J., Liang, M., Toth, I., Monteiro, M. J., and Minchin, R. F., "Molecular interaction of poly(acrylic acid) gold nanoparticles with human fibrinogen." *ACS Nano*, **2012**, *6*, 8962–8969.

[112] Gagner, J. E., Lopez, M. D., Dordick, J. S., and Siegel, R. W., "Effect of gold nanoparticle morphology on adsorbed protein structure and function." *Biomaterials*, **2011**, *32*, 7241–7252.

[113] Aubin-Tam, M. E., Zhou, H., and Hamad-Schifferli, K., "Structure of cytochrome c at the interface with magnetic $CoFe_2O_4$ nanoparticles." *Soft Matter*, **2008**, *4*, 554–559.

[114] Gong, J., Yao, P., Duan, H., Jiang, M., Gu, S., and Chunyu, L., "Structural transformation of cytochrome c and apo cytochrome c induced by sulfonated polystyrene." *Biomacromolecules*, **2003**, *4*, 1293–1300.

[115] Mahmoudi, M., Shokrgozar, M. A., Sardari, S., Moghadam, M. K., Vali, H., Laurent, S., and Stroeve, P., "Irreversible changes in protein conformation due to interaction with superparamagnetic iron oxide nanoparticles." *Nanoscale*, **2011**, *3*, 1127–1138.

[116] Rosenberg, A., "Effects of protein aggregates: An immunologic perspective." *AAPS J.*, **2006**, *8*, E501–E507.

[117] Goldberg, A. L., "Protein degradation and protection against misfolded or damaged proteins." *Nature*, **2003**, *426*, 895–899.

[118] Linse, S., Cabaleiro-Lago, C., Xue, W. F., Lynch, I., Lindman, S., Thulin, E., Radford, S. E., and Dawson, K. A., "Nucleation of protein fibrillation by nanoparticles." *Proc. Natl. Acad. Sci. U. S. A.*, **2007**, *104*, 8691–8696.

[119] Srivastava, S., Verma, A., Frankamp, B. L., and Rotello, V. M., "Controlled assembly of protein-nanoparticle composites through protein surface recognition." *Adv. Mater.*, **2005**, *17*, 617–621.

[120] Mahmoudi, M., Monopoli, M. P., Rezaei, M., Lynch, I., Bertoli, F., McManus, J. J., and Dawson, K. A., "The protein corona mediates the impact of nanomaterials and slows amyloid beta fibrillation." *ChemBioChem*, **2013**, *14*, 568–572.

[121] Gagner, J. E., Shrivastava, S., Qian, X., Dordick, J. S., and Siegel, R. W., "Engineering nanomaterials for biomedical applications requires understanding the nano-bio interface: A perspective." *J. Phys. Chem. Lett.*, **2012**, *3*, 3149–3158.

CHAPTER II

MATERIALS AND METHODS

Experiments were performed in water at room temperature unless otherwise specified. Aqueous solutions were prepared with nanopure water (18 MΩ). Concentrations reported are the final concentration in solution. Experiments were repeated, at minimum, with triplicate samples prepared independently. Cell experiments were performed with cells from multiple passage numbers unless a uniform passage number was required. Concentrations of biological molecules are reported in $mg \cdot mL^{-1}$. Chemicals were used without further purification unless otherwise noted.

2.1 Nanoparticle Characterization

The diameter provided by the manufacturer is used to denote the NPs throughout the text. The following fluorescent polystyrene nanoparticles (NPs) were used in experiments: 87 nm amine-modified (Invitrogen, C29029), 200 nm amine-modified (Invitrogen, F8764), 40 nm carboxylate-modified (Invitrogen, F8795), 93 nm carboxylate-modified (Bangs Laboratories, FC02F), and 200 nm carboxylate-modified (Invitrogen, F8811). The reported maximum excitation and emission wavelengths are 505 and 515 nm, respectively, and were verified with fluorescence spectroscopy in our laboratory prior to experiments. The exception was the 87 nm NPs which have reported excitation and emission maxima at 490 and 515 nm, respectively. The maximum excitation was measured to be 480 nm with maximum emission peaks at 490 and 525 nm. Dark, non-fluorescent 60 nm carboxylate-modified (Bangs Laboratories, PC02N) and 58 nm amine-modified (Bangs Laboratories, PA02N) polystyrene NPs were used in experiments where the fluorescence interfered with the measurement. NP solutions were sonicated for 10-20 minutes prior to use.

Carboxylate-modified CdSe/ZnS quantum dots (QDs, Invitrogen, Q21341MP, emission maximum: 525 nm) were used after sonication for 10 minutes. Citrate-modified gold NPs (Sigma-Aldrich, 753629), with a measured absorbance maximum at 524 nm, were concentrated via centrifugation (10,000g, 10 minutes, 4 °C) from an initial concentration of 0.3 nM to a final concentration between 10 and 20 nM. The gold NPs were sonicated for 20 minutes prior to spectroscopy and cellular binding experiments. The concentration of gold NPs was calculated using a molar extinction coefficient (ε) of 3.36 x 10^9 $M^{-1}{\cdot}cm^{-1}$. Low-density lipoprotein (LDL, Biomedical Technologies, BT-903, 5 $mg{\cdot}mL^{-1}$ stock solution) was fluorescently labeled with 1,1'-dioctadecyl-3,3,3',3'-tetramethylindodicarbocyanine perchlorate (DiD, Invitrogen, D-307; excitation maximum: 644 nm, emission maximum: 664 nm) as previously reported.[1] Briefly, DiD (25 mM in DMSO) was added to LDL (stock) at a ratio of 200:4 (v/v) LDL to DiD under sterile conditions. The LDL was minimally exposed to the air to avoid oxidation. The LDL-DiD solution was mixed by gently pipetting the solution every 10 minutes for 1 hour at room temperature. The DiD-labeled LDL was separated from free DiD with a NAP5 size exclusion column (GE Healthcare, 17-0853) pre-equilibrated with phosphate buffered saline without calcium and magnesium (PBS, Invitrogen, 14190250). A single fraction was collected from the column and filtered with a 0.22 μm syringe filter (Fisher Scientific, 09-720-3) immediately prior to use. The final concentration of LDL was approximated by accounting for dilution of the LDL stock after both addition of DiD and filtration through the NAP5 column. A final volume of between 450 and 500 μL of labeled LDL was collected, and a 90% yield from the column was assumed using the manufacturer's specification.

2.1.1 Protein-Nanoparticle Complexes

2.1.1.1 Washed NPs

NPs were incubated in minimum essential medium (MEM, Invitrogen, 61100061) supplemented with 10% (v/v) fetal bovine serum (FBS, Invitrogen, 10437028) or

10 mg·mL^{-1} bovine serum albumin (BSA, Fisher, BP1600) at 4 °C for 10 minutes. The gold NPs were incubated at 4 °C for 30 minutes to match the conditions used for cellular binding experiments. Most NPs could not be pelleted in MEM alone. Incubation was followed by wash steps consisting of centrifugation, removal of the supernatant, and resuspension in water. The NP concentration and number of wash steps were optimized based on the solubility and stability of each NP (Table 1).

Table 1: Experimental conditions for washed polystyrene (PS) and gold NPs

NP	Material	Initial [NP]	Speed (g)	Time (minutes)	Wash steps
200 nm NH_2	PS	15 nM	16,000	10	6
200 nm COOH	PS	13 nM	16,000	10	6
87 nm NH_2	PS	173 pM	16,000	10	4
58 nm NH_2	PS	0.4 nM	16,000	10	4
60 nm COOH	PS	14 nM	16,000	10	4
30 nm $H_3C_6H_5O_7$	gold	1 nM	10,000	10	5

2.1.1.2 Protein-Gold NP Complexes

Characterization of protein-gold NP complexes was measured using absorption spectroscopy. FBS (0.075 - 300 μM) was titrated into an aqueous solution of gold NPs (0.17 nM), keeping the total volume constant between samples. The λ at the maximum absorbance of gold NPs in the presence of protein was determined from absorption spectra measured on a SpectraMax plate reader (Molecular Devices, M2e) and averaged for triplicate measurements. Changes in λ ($\Delta\lambda$) relative to gold NPs in the absence of protein (524 nm) were used with the Langmuir adsorption isotherm model (Equation 1) to quantify surface coverage. The $\Delta\lambda_{max}$ is the maximum wavelength shift corresponding to maximum protein adsorption, K is the equilibrium association

constant (M^{-1}), and $[protein]$ is the molar FBS concentration. The Langmuir equation was fit linearly using a Lineweaver-Burk plot (Equation 2). The inverse of the y-intercept is equal to $\Delta\lambda_{max}$. K is calculated from the ratio of the y-intercept and the slope.

$$\frac{\Delta\lambda}{\Delta\lambda_{max}} = \frac{K[protein]}{1 + K[protein]} \tag{1}$$

$$\frac{1}{\Delta\lambda} = \frac{1}{\Delta\lambda_{max}} + \frac{1}{\Delta\lambda_{max} K[protein]} \tag{2}$$

2.1.2 Dynamic Light Scattering and Zeta Potential Measurements

The hydrodynamic diameter and zeta potential of the NPs was measured with a Malvern Zetasizer (Malvern Instruments, Nano-ZS). NPs were measured in water at the following concentrations: 87 nm amine-modified (173 pM), 200 nm amine-modified (15 pM), 40 nm carboxylate-modified (3.3 nM), 200 nm carboxylate-modified (13 pM), 93 nm carboxylate-modified (37 pM), 60 nm carboxylate-modified (1.4 nM), and 58 nm amine-modified (1.4 nM) polystyrene NPs, QDs (80 nM), and gold NPs (0.75 pM). The hydrodynamic diameter of the QDs could not be measured reliably with dynamic light scattering due to strong absorption and fluorescence of the scattering laser. From a previous literature report, the diameter in water is ~10 nm.[2] LDL was incubated in MEM and diluted in water to a working concentration of 1 $\mu g \cdot mL^{-1}$; a buffered solution was required to obtain a reliable measurement. NP concentrations were optimized based on the stock NP solution. For washed NPs, the protein-NP pellet collected after the final wash step was resuspended in water for dynamic light scattering measurements. The 60 nm carboxylate-modified and 58 nm amine-modified NPs were also measured in colorless MEM (Invitrogen, 51200038) and MEM supplemented with either 10% (v/v) FBS or 10 $mg \cdot mL^{-1}$ BSA. Solutions

prepared with MEM were diluted by 10% (v/v) for zeta potential measurements to reduce the conductivity. For the 58 nm amine-modified NPs, solutions in MEM supplemented with 10% (v/v) FBS were filtered with a 0.2 μm syringe filter to remove aggregates formed in the presence of protein. Triplicate measurements were acquired for each sample. All experiments were carried out with three samples prepared independently and measurements were acquired in general purpose mode. Hydrodynamic diameter measurements were acquired from 12 runs per measurement. Zeta potential measurements were acquired from 30 runs per measurement. The Smoluchowski approximation was used to calculate zeta potential from electrophoretic mobility.

2.1.3 Transmission Electron Microscopy

The NP diameter of fluorescent polystyrene NPs measured by the manufacturer with transmission electron microscopy (TEM) was provided with the certificate of analysis. For the dark, 60 nm carboxylate-modified and 58 nm amine-modified NPs, the TEM diameter was measured in the lab of Professor Ingeborg Schmidt-Krey with graduate student Yusuf Uddin. NP solutions (2 μL; 140 nM unwashed or 14 nM washed) were spread onto a carbon-coated copper grid (SPI, 2040C, 400 mesh), incubated for one minute, and blotted with filter paper (Whatman-4). The grids were stained with 2% (w/v) uranyl acetate (Ted Pella Inc., 19481) for 30 seconds and the uranyl acetate was removed by blotting. Grids were screened with a TEM (JEOL, JEM-1400) operated at an acceleration voltage of 120 kV. Images were acquired using both a Gatan Orius SC1000 CCD camera and an Ultrascan 1000 CCD camera at between 60,000x to 150,000x magnification. The mean diameter was determined using the ImageJ measure tool on >100 NPs for unwashed NPs in MEM, between 37-41 NPs for washed NPs after incubation in MEM, and between 66-84 NPs for washed NPs after incubation in MEM supplemented with BSA. The feret diameter, or diameter along the longest axis, is reported. A histogram of NP diameters was plotted with 2

nm binning for the unwashed NPs in MEM and fit to a Gaussian distribution.

2.2 Gel Electrophoresis

2.2.1 Polyacrylamide

Washed NPs were used for all polyacrylamide gels. For the fluorescent polystyrene and gold NPs, the supernatant was collected after each wash. After the final wash, the sample was suspended in either buffer containing 6% (w/v) SDS, (New England Biolabs, B7703S) to remove the protein from the NP surface, or in water. Supernatant solutions were diluted by 50% (v/v) in Laemmli buffer (Boston Bioproducts, BP-110R), boiled for 5 min, and loaded onto the gel. The supernatant from the first wash was diluted to 10% (v/v) for polystyrene and 1% (v/v) for gold NPs. The second supernatant was diluted to 10% (v/v) for the gold NPs due to the high protein concentration. Proteins were separated, along with a 5-225 kDa molecular weight marker (Lonza, 50547), on a 4-20% gradient gel (polystyrene NPs, Bio-Rad 456-1094) or a 12% mini-protean gel (gold NPs, Bio-Rad, 456-8044) run for 1-2 hours at 40 mA and 130 V. For better separation, the gel was run at a lower voltage (60-90 V) for the first 20 minutes to allow the protein solution to load evenly into the stacking gel. Proteins were stained with Simply Blue Safe Stain (Invitrogen, LC6060) for one hour and destained in water overnight. Polyacrylamide gels were imaged with either a Canon scanner (CanoScan LiDE 200, 1200 dpi) or an Odyssey imaging system (Li-Cor Classic 9120, 0.5 mm depth, 700 nm excitation).

2.2.2 Agarose

QDs (0.8 μM) were incubated with water, MEM, or MEM supplemented with 10% FBS for 10 minutes before loading onto a 1% (w/v) agarose gel. A 5X Tris-Borate-EDTA (TBE) buffer stock was prepared with 0.45 M tris(hydroxymethyl)aminomethane, 0.45 M boric acid, and 10 mM ethylenediaminetetraacetic acid, pH 8.3. The agarose gel was cast with a 1X TBE buffer using microwave heating to dissolve the

solid agarose. Glycerol was added to the QD solutions to aid in well loading. QDs were separated on the gel in 0.5X TBE buffer for 1 hour and 30 minutes at 90 V with constant voltage, and a handheld UV light was used to image migration of the QDs during separation. The gel was imaged on a GE Healthcare Typhoon Trio scanner (Model 9410, excitation: 488 nm; emission: 520/40 nm bandpass filter; 25 μm resolution).

2.3 Cell Culture

African green monkey kidney epithelial cells (BS-C-1, ATCC), human cervical carcinoma cells (HeLa, ATCC), and Chinese hamster ovary cells (CHO, ATCC) were maintained in a 95% humidity, 5% carbon dioxide atmosphere at 37 °C in MEM (Invitrogen, 61100061) with 10% (v/v) FBS. CHO cells were maintained in Ham's F-12 (F-12, Invitrogen). Cells were passaged every 2-4 days using trypsin (Invitrogen, 25200072) to detach adherent cells. From the absorption spectrum of FBS, using the extinction coefficient of BSA (43,824 $M^{-1}{\cdot}cm^{-1}$), the total protein concentration in 10% (v/v) FBS is approximately 10 $mg{\cdot}mL^{-1}$. For fluorescence microscopy and flow cytometry, cells were grown in 35 mm glass-bottom cell culture dishes (MatTek).

Cells used for gold NP experiments were seeded in 12-well plates (Falcon, 353043) 24 hours prior to cellular binding studies. For dark field imaging, cells were grown on circular glass cover slips (Fisher Scientific, 12-545-100) in 12-well plates. Cover slips were pre-treated with collagen (Roche, 11179179001) to aid in cellular adhesion. A stock solution was prepared with 10 mg collagen dissolved in 0.2% (v/v) sterile acetic acid. The collagen stock solution was diluted in a ratio of 1:50 (v/v) in PBS with calcium and magnesium and $\sim$500 μL was incubated with the cover slip for between 30 minutes to 2 hours at 37 °C. After incubation, the collagen solution was removed from the well plate and the cover slip was allowed to air dry under sterile conditions.

For transport studies, BS-C-1 cells stably expressing the lysosome-associated membrane protein-1 (LAMP1) fluorescently labeled with enhanced yellow fluorescent protein (EYFP) were used. The LAMP1-EYFP plasmid (Addgene, 1816) contains G418 resistance and was initially transfected with Fugene6 (Roche, 11805091001). The BS-C-1 cells expressing LAMP1-EYFP were cultured in medium supplemented with 400 μg·mL^{-1} G418 sulfate (CalBioChem, 345810).

2.4 Fluorescent Labeling

2.4.1 Protein Labeling

BSA was fluorescently labeled with AlexaFluor647 (AF647, Invitrogen, A2006) according to previous protocols and consistent with the manufacturers guidelines.[3] Briefly, an aqueous BSA solution (10 mg·mL^{-1} stock) was combined with AF647 (10 mg·mL^{-1} stock, DMSO) in a 10:1 (v/v) ratio of BSA to AF647 in a sodium bicarbonate buffer (0.1 M, pH 8.3-9.0). The solution was gently shaken via vortex for 1 hour at room temperature, and the reaction was quenched with 1.5 M hydroxylamine (pH 8.5). Immediately after quenching, the final product was filtered on a NAP5 size exclusion column to remove unbound AF647. The final concentrations were determined with UV-Vis absorption spectroscopy (ε_{BSA} = 43,824 M^{-1}·cm^{-1} at 275 nm; ε_{AF647} = 239,000 M^{-1}·cm^{-1} at 647 nm. The final ratio of AF647 dyes per protein was between 2-3. A correction factor of 0.03 was used to subtract the AF647 absorbance contribution at 275 nm. The AF647 λ_{max} value was used to discriminate between AF647-protein conjugates and free AF647. The λ_{max} value of free AF647 is 647 nm, while AF647 conjugated to protein is between 650-652 nm.

2.4.2 Immunofluorescence

For transport studies, the LAMP1 protein was immunofluorescently labeled with Cy5. The BS-C-1 cells stably expressing LAMP1-EYFP could not be used for NP transport experiments due to overlap of the EYFP and NP emission. After NP incubation, cells

were washed twice with PBS with calcium and magnesium (Invitrogen, 14040182) and fixed for 30 minutes in 4% (v/v) H_2CO (Thermo Scientific, 28908, 16% (v/v) stock solution) in PBS. The cells were then rinsed twice with PBS, and immunostained to fluorescently label the LAMP1 protein and identify lysosomal vesicles. All immunostaining steps were performed in a 1 mL solution volume while gently rocking, and cells were rinsed twice in wash buffer (0.3% w/v BSA and 0.1% v/v octyl phenol ethoxylate (Triton-X, JT Baker, X198-05) in PBS) between permeabilization and after incubation of primary and secondary antibodies. Cells were permeabilized for 15 minutes (3% (w/v) BSA, 10% (v/v) FBS, 0.5% (v/v) Triton-X in PBS) and incubated for 1 hour in blocking buffer (3% (w/v) BSA, 10% (v/v) FBS in PBS). To fresh blocking buffer, the LAMP1 primary antibody (mouse, Abcam, ab25630) was added to a final antibody concentration of 1 μg/mL and incubated overnight (minimum of 12 hours) at 4 °C. After a second blocking step, secondary antibody (rabbit anti-mouse-Cy5, Chemicon, AP160S) was added to a final concentration of 2.5 μg/mL and incubated for 2 hours at room temperature. The final wash step prior to imaging was done in PBS and imaging was done in 1 mL PBS. Control experiments were completed in parallel for every immunostaining experiment consisting of cells incubated with primary antibody alone and secondary antibody alone. All other steps were kept constant, and these control plates were imaged with the immunostained plates to determine laser power and detector voltage thresholds.

2.5 Microscopy

2.5.1 Wide Field Fluorescence

For cellular binding experiments, cells were cooled to 4 °C on ice for 10 minutes. NPs and QDs were incubated with cells for 10 minutes, and LDL-DiD was incubated with cells for 30 minutes at 4 °C by adding the NPs directly to 1 mL of MEM, MEM supplemented with 10% (v/v) FBS, or MEM supplemented with 10 $mg{\cdot}mL^{-1}$ BSA.

Cells were rinsed twice with PBS with calcium and magnesium to remove unbound NPs. Cells were either imaged in 1 mL PBS immediately or after fixing with 4% (v/v) H_2CO in PBS. NP binding to cells was imaged with a fluorescence microscope (Olympus, IX71) using a 60x, 1.20 numerical aperture (N.A.), water immersion objective (Olympus). Fluorescence emission was collected with an electron multiplying charge-coupled device (EMCCD) camera (Andor, DU-897). Multiple fluorophores in the same spatial location were imaged by acquiring multiple images at the same focus but with different filter sets. Images for comparison were collected with the same exposure time and EM gain. Both were optimized for each experiment but were usually in the range of a 100 - 200 ms exposure time and an EM gain of 2. Nuclei were stained with 27 μM 4,6-diamidino-2-phenylindole dilactate (DAPI, Invitrogen, D35671) at 37 °C for 30 minutes to 1 hour. The following bandpass and dichroic filters were used for imaging: nuclear staining with DAPI (excitation: 387/11; emission: 447/60; Semrock, DAPI-1160A), NPs and QDs (excitation: 480/40, Chroma; dichroic: FF506-Di02, Semrock; emission: 536/40, Semrock), and LDL-DiD (excitation: 620/60, Chroma; dichroic: FF660-Di01, Semrock; emission: 692/40, Semrock).

2.5.2 Confocal Fluorescence

Cellular transport experiments were imaged with a laser scanning confocal microscope (Olympus, Fluoview 1000) and a 60x, 1.42 N.A., oil immersion objective (Olympus). Vesicles positive for LAMP1 were used as the endpoint for endocytic cellular transport. BS-C-1 cells were incubated with BSA-AF647 (final BSA concentration: 2.2 μM) or BSA-NP complexes (final BSA concentration: 0.12 μM; final NP concentration: 0.034 nM) at 37 °C for between 10 minutes and 18 hours. To form the BSA-NP complexes, unlabeled BSA was incubated with the NPs for 20 minutes before adding to cells. BSA-AF647 transport was imaged in the LAMP1-EYFP BS-C-1 cells, and BSA-NP transport was imaged in BS-C-1 cells with immunofluorescently

labeled LAMP1-Cy5. A 150 μm confocal aperture and 12.5 μs dwell time was used to acquire all fluorescence images. Fluorescence was recorded on photomultiplier tubes (PMTs) and final images were acquired with Kalman averaging on 10 successive images. NPs and EYFP were excited with the 488 and 515 nm lines of an argon ion laser, respectively. Both AF647 and Cy5 were excited with a 635 nm diode laser. NP emission was collected with a 505-605 nm bandpass filter, YFP with a 535-565 nm bandpass filter, and both Cy5 and AF647 emission were collected with a 655-755 nm bandpass filter. Shorter wavelength emission was separated from longer wavelengths with a 640 nm dichroic mirror. Comparative images in a series were imaged with the same respective laser power and PMT voltages. Quantification of colocalization between BSA-AF647 and BSA-NP with LAMP1 positive vesicles was done using the ImageJ Image5D plugin. A 100 μm^2 grid was placed over the image and $\sim$1 vesicle per grid square was analyzed, avoiding the perinuclear region where vesicle aggregation is common. Vesicles positive for LAMP1 were identified in the single channel images to avoid bias for vesicles colocalized with BSA-AF647 or BSA-NP. Final colocalization numbers were acquired by analyzing 20 vesicles per cell on $\geq$6 cells from $\geq$2 unique cell passage numbers. Mean and standard deviation values per cell are reported.

2.5.3 Dark Field

Cellular binding of gold NPs used the same protocol as fluorescent NPs, except that the NPs were incubated for 30 minutes with cells grown on circular cover slips. After rinsing with PBS, cells were fixed with 4% (v/v) H_2CO. Images were acquired from cells sealed between the circular cover slip and a second clean cover slip. A small amount of glycerol was added between the cover slips to prevent drying. Dark field images were acquired using both an inverted microscope (Olympus, IX70) in the lab of Professor Mostafa El-Sayed[4] and an upright microscope (Olympus, BX51) on a setup built in our lab (Chapter 7.2.3). A 100x, 0.5 - 1.35 variable N.A., oil immersion

iris objective (Olympus, UPlanApo) and a 1.2 N.A. dark field condenser (Olympus, U-DCW) were used for imaging and a Nikon digital camera (D200) attached to either the front port (inverted) or top port (upright) of the microscope was used to image scattered light.

2.6 Binding Competition Assays

2.6.1 Flow Cytometry

Binding competition studies used FBS and BSA as competitors for serum protein receptors. Fucoidan (Sigma-Aldrich, F5631) and polyinosinic acid (Sigma-Aldrich, P4154) were used as competitors for scavenger receptors. Polyadenylic acid (Sigma-Aldrich, P9403) was used as a control. The competitor or control molecule was incubated with cells for 20 minutes at 4 °C in MEM for carboxylate-modified polystyrene NPs, QDs, and LDL, or in MEM supplemented with either 10% (v/v) FBS or 10 mg·mL^{-1} BSA for amine-modified NPs. The NPs were then incubated with cells in the presence of the competitor molecule for 10 minutes. Cells were rinsed twice with PBS with calcium and magnesium to remove unbound NPs, twice with PBS without calcium and magnesium, and incubated in 10 mM ethylenediaminetetraacetic acid (Mallinckrodt, 49310-04) for 30 minutes at 37 °C to remove adherent cells from the culture dishes. The solution in the cell culture dish was pipetted across the bottom of the dish several times to detach the cells completely, and the cell suspension was transferred to a microcentrifuge tube. Cells were rinsed twice with Leibovitz's L-15 buffer (Invitrogen, 21083027) via centrifugation at 10,000g for 10 minutes, filtered with a 40 μm cell strainer (BD Falcon, 352340), and kept on ice for one hour prior to analysis with flow cytometry (BD Biosciences, LSR-II). Data was collected for 10,000 live cells in each sample. The dead cell population was distinguished with propidium iodide staining. Cells alone in the absence of NPs, using the same conditions and

PMT voltages used in competition studies, were also measured to determine the contribution from cellular autofluorescence. A 488 nm laser was used to excite the NPs and QDs, and fluorescence emission was collected on a 530/30 nm bandpass filter. LDL and BSA-AF647 fluorescence was excited with a 633 nm laser, and emission was collected on a 660/20 nm bandpass filter. Scatter plots and fluorescence histograms were analyzed with the Weasel software (Walter and Eliza Hall Institute of Medical Research, Victoria, Australia, version 3.0.1). The mean fluorescence intensity calculated from the histograms was used to quantify fluorescence.

2.6.2 Differential Absorbance

Cellular binding competition studies of gold NPs used the same conditions as for dark field microscopy, except that cells were grown in 12-well plates rather than on glass cover slips. To prevent gold NP aggregation, 0.17 nM gold NPs were incubated with 0.5% (v/v) FBS for 20 minutes to form protein-gold NP complexes before adding to MEM. Competitors, including 10% (v/v) FBS and 10 mg·mL^{-1} BSA, were incubated with cells at 4 °C in colorless MEM for 10 minutes prior to addition of protein-gold NP complexes and were present during NP incubation. After incubation, the supernatant solution above the cell monolayer was transferred to a 96-well plate and absorption spectra were recorded between 300 and 700 nm with a SpectraMax plate reader (Molecular Devices, M2e). The maximum absorbance at 524 nm due to absorption by the gold NP localized surface plasmon resonance was baseline corrected and subtracted from the absorbance value of gold NPs in the absence of cells. The difference in absorbance is attributed to the gold NPs that remain bound to the cell surface.

2.7 Spectroscopy

2.7.1 UV-Vis Absorption

UV-Vis absorption spectra were measured on a spectrophotometer (Beckman-Coulter, DU-800) with a scan speed of 1200 nm·minute^{-1} and 1.0 nm wavelength interval. Spectra were acquired between 200 and 800 nm with a 1 cm path length, UV silica cuvette (Beckman Coulter, 523450).

2.7.2 Fluorescence

Fluorescence spectra were acquired on a spectrofluorophotometer (Shimadzu, RF-5301) with a 3 x 3 mm light path cuvette (Hellma, 105.254-QS) and a 1 nm sampling interval. Samples were excited at 280 nm and emission was collected between 250 and 500 nm using 5 nm slit widths for both the excitation and emission monochromaters. All solutions were prepared in 10% (v/v) PBS without calcium and magnesium. BSA (9.8 μg·mL^{-1}) was measured in the presence of non-fluorescent 60 nm carboxylate-modified and 58 nm amine-modified NPs. Working NP concentration ranged from 0.067 nM to 0.53 nM. Experiments were repeated in triplicate. Corrected spectra are the raw spectra with the NP scatter peak and buffer contribution subtracted out, and the initial emission value at 250 nm set to zero. The Stern-Volmer relationship was used to determine the equilibrium constant (Equation 3).

$$\frac{F_o}{F} = 1 + K_{SV}[NP] \tag{3}$$

The fluorescence intensity ratio of BSA at λ_{max} in the absence (F_o) and presence (F) of a quencher was calculated and plotted versus the NP quencher concentration (*[NP]*). The first four points were used in a linear fit of the data, and the slope of the line is equal to an effective Stern-Volmer equilibrium constant (K_{SV}, M^{-1}). The K_{SV} is equal to the effective equilibrium association constant.[5]

2.7.3 Circular Dichroism

Circular dichroism (CD) spectra were acquired on an Olis CD spectrophotometer with the sample chamber maintained at 20 °C. Measurements were made using a 0.5 mm path length quartz cell (Starna, 20/O-Q-0.5). The bandwidth was set to 2 nm and the integration time was a function of the PMT voltage. Samples were measured in 10% (v/v) PBS without calcium and magnesium. Buffer alone without protein was used as a blank. BSA (0.098 mg·mL^{-1}) and holo-transferrin (0.049 mg·mL^{-1}, Sigma, T1283) were measured alone and in the presence of 60 nm carboxylate-modified NPs (0.4 nM) and 58 nm amine-modified NPs (0.4 nM). BSA was also measured in the presence of 200 nm carboxylate-modified NPs (13 pM) and 200 nm amine-modified NPs (13 pM). The NP concentration was optimized to reduce scatter and absorbance from the NPs. Samples with BSA were incubated for 10 minutes prior to acquisition and all spectra are an average of 10 consecutive scans. All measurements were repeated in triplicate. Spectra were smoothed with a Savitzy-Golay least-squares fitting[6] (digital filter = 13) and the value at 260 nm was set to zero to account for spectral drift. Spectra were acquired in millidegrees and converted to mean residue ellipticity using Equation 4.

$$[\theta] = \frac{[\theta]_{obs} MW}{10lCn} \tag{4}$$

The mean residue ellipticity ($[\theta]$), in units of degrees·cm^2·dmol^{-1}, is a function of the observed signal in millidegrees, $[\theta]_{obs}$, the average molecular weight of the protein (MW), path length in cm (l), protein concentration in g·L^{-1} (C), and the total number of amino acids (n). BSA has a molecular weight of 66,430 g·mol^{-1} and 583 total amino acids.[7] The approximate molecular weight and total number of amino acids in bovine holo-transferrin are 79,000 and 660, respectively (Sigma-Aldrich). The percentage of α-helices was calculated from Equation 5.

$$\%\alpha - helix = \frac{-[\theta]_{MRE} - 4,000}{33,000 - 4,000} \quad (5)$$

The α-helicity of a protein is a function of the mean residue ellipticity at 208 nm ($[\theta]_{MRE}$), minus the contribution from the β-form and random coil conformations at 208 nm (4,000). The observed value is compared to the mean residue ellipticity of a pure α-helix protein (33,000).

2.8 Isothermal Titration Calorimetry

Isothermal Titration Calorimetry (ITC) measurements were made on a Nano ITC (TA Instruments, low volume) at 25 °C with a constant stirring speed of 250 rpm. For all titrations, sixteen 3 μL injections were made with a 300 second equilibration time before and after each injection. All solutions were prepared in a 20 mM HEPES buffer (pH 7.4). Titration of BSA (75 μM) alone into buffer was subtracted injection-by-injection from BSA titrations into NP solutions. The 60 nm carboxylate-modified NPs (0.005 nM) or 58 nm amine-modified NPs (1.4 nM) were loaded into the sample cell. NP and protein concentrations, along with the buffer, were optimized such that BSA saturation and equilibrium was achieved. The baseline between peaks was selected manually. Integration of differential power plots as a function of time gave binding curves, and the raw data was fit with the one independent site model using the NanoAnalyze software (TA Instruments, version 2.4.1).[8] The first injection was excluded from the fit. Each titration curve was repeated 3-4 times. The theoretical monolayer coverage of BSA molecules per NP was calculated using the assumption that BSA binds end-on to the NP surface with a footprint of 3.3 x 10^{12} BSA molecules per cm^2.[9,10]

2.9 Data Analysis

All experiments were repeated, at minimum, in triplicate. Mean and standard deviation are reported for all numerical values. Error bars represent the standard deviation. Significance and p-values were determined using a two-tailed, two-sample independent t-test. Numerical analysis and quantification (e.g. colocalization methods) are described in the respective subsection. All images were analyzed with ImageJ software version 1.43u (http://rsb.info.nih.gov/ij/). Images for comparison were set to equal brightness and contrast.

2.9.1 Modeling

Protein structures were rendered using the visual molecular dynamics modeling program developed with NIH support by the Theoretical and Computation Biophysics group at the Beckman Institute, University of Illinois at Urbana-Champaign. Electrostatic surface maps of proteins were created using eF-surf (http://ef-site.hgc.jp/eF-surf/top.do) for BSA (PDB: 4F5S) and transferrin (PDB: 3QYT).

2.10 References

[1] Humphries, W. H., Fay, N. C., and Payne, C. K., "Intracellular degradation of low-density lipoprotein probed with two-color fluorescence microscopy." *Integr. Biol.*, **2010**, *2*, 536–544.

[2] Cady, N. C., Strickland, A. D., and Batt, C. A., "Optimized linkage and quenching strategies for quantum dot molecular beacons." *Mol. Cell. Probes*, **2007**, *21*, 116–124.

[3] Doorley, G. W. and Payne, C. K., "Cellular binding of nanoparticles in the presence of serum proteins." *Chem. Commun.*, **2011**, *47*, 466–468.

[4] Kang, B., Mackey, M. A., and El-Sayed, M. A., "Nuclear targeting of gold nanoparticles in cancer cells induces DNA damage, causing cytokinesis arrest and apoptosis." *J. Am. Chem. Soc.*, **2010**, *132*, 1517–1519.

[5] Lakowicz, J. R., *Principles of Fluorescence Spectroscopy*. Springer, New York, 3rd edn., **2006**.

[6] Gorry, P. A., "General least-squares smoothing and differentiation by the convolution (Savitzky-Golay) method." *Anal. Chem.*, **1990**, *62*, 570–573.

[7] Hirayama, K., Akashi, S., Furuya, M., and Fukuhara, K.-I., "Rapid confirmation and revision of the primary structure of bovine serum albumin by ESIMS and Frit-FAB LC/MS." *Biochem. Biophys. Res. Commun.*, **1990**, *173*, 639–646.

[8] Freire, E., Mayorga, O. L., and Straume, M., "Isothermal titration calorimetry." *Anal. Chem.*, **1990**, *62*, 950A–959A.

[9] Brewer, S. H., Glomm, W. R., Johnson, M. C., Knag, M. K., and Franzen, S., "Probing BSA binding to citrate-coated gold nanoparticles and surfaces." *Langmuir*, **2005**, *21*, 9303–9307.

[10] Rezwan, K., Meier, L. P., Rezwan, M., Voros, J., Textor, M., and Gauckler, L. J., "Bovine serum albumin adsorption onto colloidal Al_2O_3 particles: A new model based on zeta potential and UV-Vis measurements." *Langmuir*, **2004**, *20*, 10055–10061.

CHAPTER III

CELLULAR BINDING OF CHARGED NANOPARTICLES

3.1 Introduction

Nanoparticles (NPs) used in biomedical applications will be exposed to the complex biological milieu containing a diverse mixture of extracellular proteins. For example, NPs injected directly into the blood stream will encounter thousands of unique proteins present in serum.[1–3] These proteins rapidly adsorb onto the NP surface forming a protein "corona."[4–6] We have previously observed that serum proteins remain bound to the NP surface during both cellular binding and internalization[7,8]. Importantly, it is the proteins adsorbed on the NP surface, rather than the NP, that mediate NP interactions with cells. Many serum proteins have dedicated cellular binding sites,[9–12] suggesting that serum proteins can influence cellular binding of NPs both by the formation of a protein-NP complex and subsequently by competing with the NPs for cellular receptors. NPs designed for use in biological systems require characterization in a realistic environment, representative of what the NP will encounter through the course of application.

While many NP properties can alter the composition and dynamics of protein adsorption to the NP surface, of specific interest has been the role of NP surface charge. NPs used in biology and medicine often have a charged surface, either as a result of the NP synthesis or from the intentional addition of surface ligands. Charged functional groups screen the high energy surface of the NP from other NPs or cells in proximity, and aid in the direct interaction of NPs with cells and cellular receptors.[13] A general picture has emerged suggesting that neutral or negatively charged NPs help to shield NPs from adsorption of negatively charged serum proteins, but have a low

affinity for the negatively charged binding sites on the plasma membrane.[13,14] In comparison, positively charged NPs risk adsorption of anionic serum proteins, but readily bind and are internalized by anionic proteoglycans on the cell surface.[15] The physical reality is much more complex as anionic polystyrene,[4,16,17] citrate-modified gold NPs,[18] and polyacrylic acid-modified gold nanorods[19] have all been shown to form complexes with serum proteins. Many proteins contain both positive and negative residues at physiological pH, regardless of their net charge, allowing for electrostatic adsorption to both cationic and anionic surfaces. Surface plasmon resonance studies of gold surfaces show that albumin, a highly abundant serum protein,[1–3] binds more readily to anionic carboxylate-modified surfaces than cationic amine-modified surfaces, likely due to the presence of multiple positively charged lysine residues.[20]

Cellular binding is the first step in the interaction of NPs with cells. Binding mediates NP entry into cells and can subsequently determine the cellular transport pathway. Our goal was to determine how the cellular binding of cationic and anionic NPs is affected by extracellular serum proteins. We studied cellular binding independent of internalization to isolate the effect of serum proteins on NP binding to the cell surface. To address this question, we carried out a side-by-side comparison of the cellular binding of NPs in the presence of serum proteins using NPs of the same composition but with opposite initial surface charge.[21] Using gel electrophoresis and dynamic light scattering measurements, we observed that both cationic and anionic NPs formed protein-NP complexes when exposed to serum proteins. While the presence of serum proteins enhanced the cellular binding of cationic NPs, serum proteins inhibited the binding of anionic NPs. We determined that this difference in cellular binding is due to the cellular receptors used by the protein-NP complexes. Fluorescence microscopy and flow cytometry were used to characterize and quantify cellular binding trends. Protein-NP complexes formed from cationic NPs bind to scavenger receptors on the cell surface. In comparison, the protein-NP complexes formed from

anionic NPs compete with serum proteins in solution for native protein receptors. As NPs are increasingly important for *in vivo* applications, we anticipate these results will inform the design of NPs with improved cellular binding.

3.2 Results and Discussion

In the course of experiments we used cationic, amine-modified polystyrene NPs and anionic, carboxylate-modified polystyrene NPs (Fluospheres, Invitrogen). Within our lab, the hydrodynamic diameter (d_h) and zeta potential (ZP) of the NPs was measured using a Malvern Zetasizer (Table 2). NPs were diluted in water and measurements were carried out in triplicate. The NP diameter measured with TEM (d_{TEM}) was supplied by Invitrogen and is also provided in Table 1. Throughout the text we use the diameter provided in the catalog to refer to the NP. For example, carboxylate-modified NPs with a d_{TEM} of 45 nm and a d_h of 60 nm are described as 40 nm NPs.

Table 2: TEM diameter (d_{TEM}), hydrodynamic diameter (d_h), and zeta potential (ZP) of the NPs used in the course of experiments

NPs	d_{TEM} (nm)[a]	d_h (nm)	ZP (mV)
87 nm NH_2	87 ± 6	152.7 ± 3.2	39.2 ± 3.6
200 nm NH_2	200 ± 11	270.1 ± 9.3	19.9 ± 3.4
40 nm COOH	45 ± 6	60.04 ± 0.91	-43.3 ± 1.5
200 nm COOH	210 ± 10	236.2 ± 3.3	-31.0 ± 1.6

[a]TEM data provided with certificate of analysis from Invitrogen.

3.2.1 Cationic and Anionic NPs Form Protein-NP Complexes

We first determined whether both cationic and anionic NPs would form protein-NP complexes when exposed to extracellular serum proteins. Cells are typically cultured in an aqueous solution of amino acids, vitamins, inorganic salts, and glucose, described as the medium, which is generally supplemented with serum.[22] Minimum Essential Medium (MEM) supplemented with 10% (v/v) fetal bovine serum (FBS) is commonly used for cell culture, and we used this mixture as a representative biological environment. A combination of gel electrophoresis, zeta potential, and hydrodynamic diameter measurements were used to characterize the NPs after incubation in MEM supplemented with 10% (v/v) FBS. The cationic NPs are expected to bind to net anionic serum proteins as previously observed with zeta potential measurements and fluorescently-labeled serum proteins.[7,8] This was confirmed by incubating the 200 nm amine-modified NPs (15 pM) with MEM supplemented with 10% (v/v) FBS for 10 minutes at 4 °C, identical to the conditions used in cellular experiments. The solution of NPs and serum proteins was then centrifuged (16,000g, 10 minutes) and resuspended in water 6 times. After each wash the supernatant was collected, run on an polyacrylamide gel (4-20% gradient), and stained with Simply Blue Safe Stain for 1 hr. The first supernatant contained the highest protein concentration and was diluted to 10% (v/v) to avoid overloading the gel. A gel run under similar conditions but without dilution of the supernatant is shown in Figure 2 for comparison. After 5 washes, no protein was detected in the supernatant demonstrating that unbound protein had been removed from the NP-protein mixture. The NPs were then resuspended in a solution of 6% (w/v) sodium dodecyl sulfate (SDS), a detergent that is expected to remove any proteins that remain bound to the NP. Following resuspension in SDS, a protein band at ∼66 kDa is visible in the gel (Figure 1A, NP + SDS). In the absence of SDS, no protein is visible (NP + H_2O). This demonstrates that incubation in MEM supplemented with 10% (v/v) FBS results in the adsorption of

proteins on the 200 nm cationic NPs.

The protein-NP complex that remained following the final wash, in the absence of SDS, was used for zeta potential and hydrodynamic diameter measurements (Figures 1B and 1C). These measurements show that the protein-NP complex formed with the cationic NPs becomes anionic (-19.4 mV ± 1.8 mV) and increases in diameter (365.1 nm ± 39.8 nm). Similar results were obtained for the 87 nm amine-modified NPs although these NPs were more difficult to pellet resulting in greater conductivity and polydispersity (Figure 3).

We next determined whether the 200 nm anionic NPs formed a protein-NP complex, similar to the cationic NPs, or if they were resistant to protein adsorption and remained bare NPs in the presence of FBS. The adsorption of serum proteins on the anionic NPs was investigated using gel electrophoresis, zeta potential, and hydrodynamic diameter measurements as described for the cationic NPs. Like the cationic NPs, protein was detected on "washed" anionic NPs following gel electrophoresis and SDS treatment (Figure 1D, NP + SDS). The first supernatant (S1) was again diluted by 10% (v/v). The charge of the anionic NPs increased to -26.5 mV ± 2.5 mV (Figure 1B), more similar to the zeta potential of BSA (-22 mV, data not shown), and the diameter of the NP increased (410.2 nm ± 38.8 nm, Figure 1C). This demonstrates that exposure to FBS results in the adsorption of proteins on the 200 nm anionic NPs, in good agreement with previous results showing the adsorption of serum proteins on 100 nm carboxylate-modified polystyrene NPs.[16] The 40 nm carboxylate-modified NPs were too small to pellet and could not be analyzed after washing.

Using three different methods, we have shown that serum proteins remain bound to both cationic and anionic NPs following multiple wash steps that remove free and weakly bound proteins. Based on the molecular weight of the protein removed in the SDS wash (Figures 1A and 1D), it is likely that BSA is the main protein adsorbed on the NPs although lower abundance proteins would not be detected using this

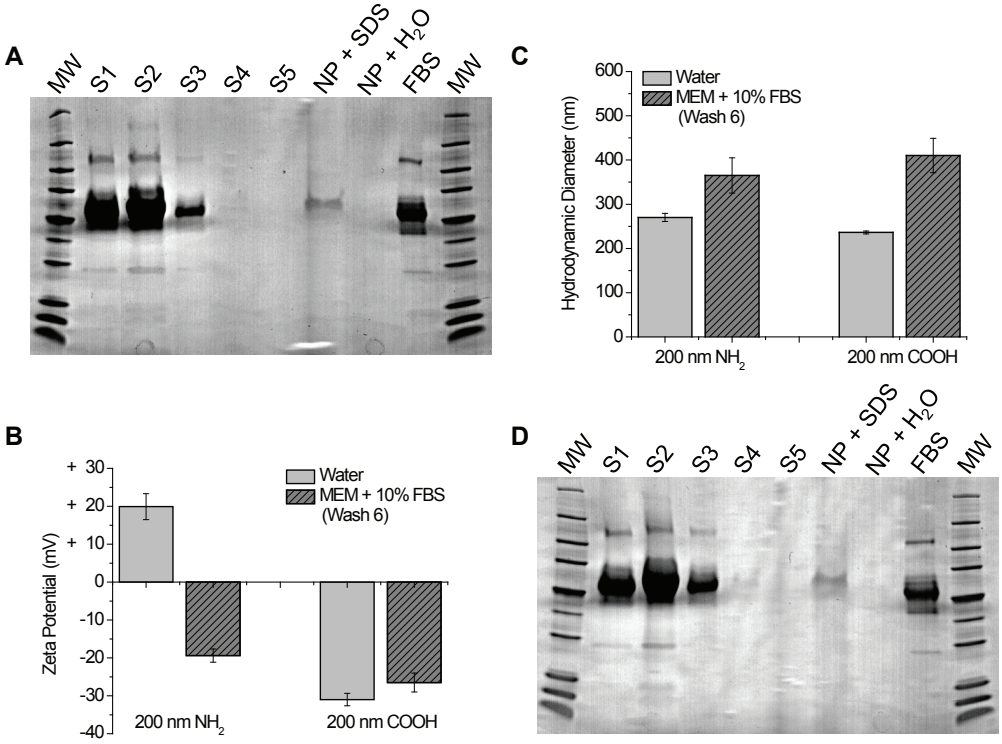

Figure 1: Formation of a protein-NP complex confirmed with gel electrophoresis, zeta potential, and hydrodynamic diameter. (A) Gel electrophoresis of supernatants (S) following repeated centrifugation and wash steps of the 200 nm amine-modified NPs. NPs were incubated in either SDS (NP + SDS), to remove the protein corona, or water (NP + H_2O). Molecular weight (MW) marker shows 225, 150, 100, 75, 50, 35, 25, 15, 10, and 5 kDa. FBS, in the absence of NPs, is shown for comparison. (B) Zeta potential of NPs incubated in MEM supplemented with FBS after six wash steps. (C) Hydrodynamic diameter after six wash steps. (D) Gel electrophoresis of the 200 nm carboxylate-modified NPs using the same procedure as in (A).

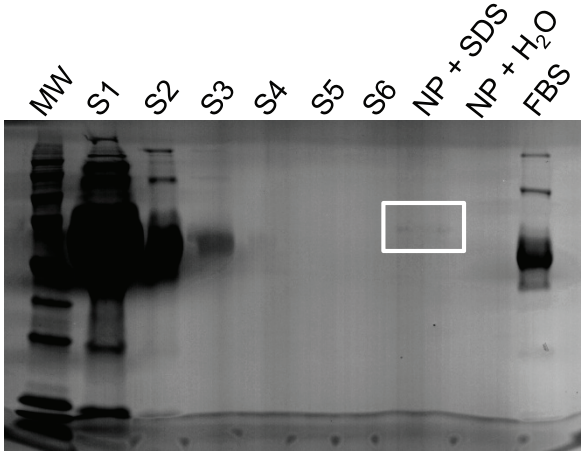

Figure 2: Gel electrophoresis of undiluted supernatants (S) of 200 nm carboxylate-modified NPs incubated in MEM supplemented with FBS following each wash step. SDS removes bound protein from the NP (NP + SDS, white box) whereas water does not (NP + H_2O). Molecular weight (MW) marker shows 225, 150, 100, 75, 50, 35, 25, 15, 10, and 5 kDa.

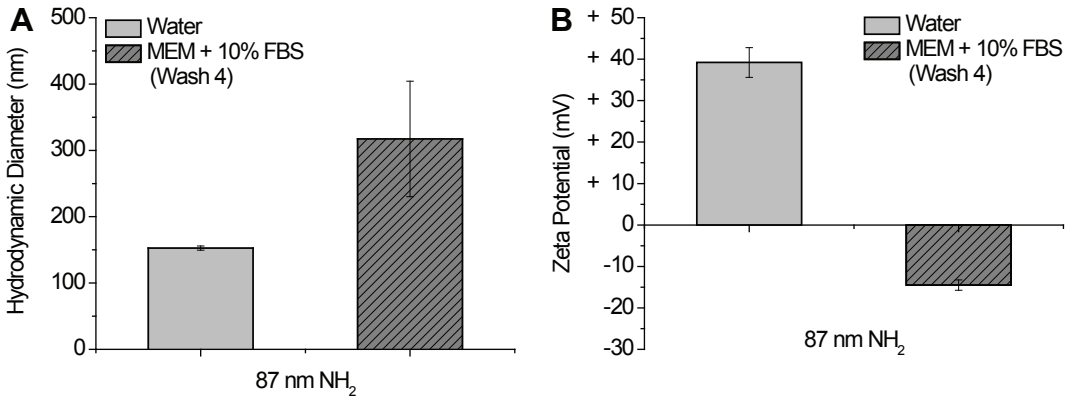

Figure 3: Formation of a protein-NP complex on 87 nm amine-modified NPs after four wash steps via centrifugation and resupension in water. (A) Hydrodynamic diameter. (B) Zeta potential.

approach. This is an interesting result as it shows both cationic and anionic NPs form a protein-NP complex. The protein-NP complex formed from both cationic and anionic NPs appears to be similar: both types of NPs are net anionic following exposure to 10% (v/v) FBS and both form a corona of mainly BSA.

3.2.2 Cationic NP Binding is Enhanced by Serum Proteins

To compare the cellular binding of the protein-NP complexes formed from the cationic and anionic NPs, we examined the cellular binding of the NPs in the presence and absence of excess serum proteins. We first compared the cellular binding of NPs in MEM, which lacks proteins, to MEM supplemented with 10% (v/v) FBS. Cells were cooled to 4 °C for 20 minutes before the addition of NPs and were maintained at 4 °C during 10 minutes of incubation with the NPs. At 4 °C NP internalization is blocked, allowing us to image cellular binding independent of internalization.[23–28] After 10 minutes at 4 °C, cells were rinsed twice with phosphate buffered saline (PBS) and then imaged using fluorescence microscopy. The concentration of NPs incubated with the cells is provided. We find that the 87 nm cationic NPs (34 pM) have minimal binding to cells in the absence of FBS and significant binding in the presence of FBS (Figure 4A). A similar increase in binding was observed for 200 nm cationic NPs (15 pM) in the presence of FBS (Figure 4B). We propose that the lower zeta potential of the 200 nm NPs results in greater direct interaction with the plasma membrane, possibly via hydrophobic interactions, in the absence of FBS. These results demonstrate that the formation of a protein-NP complex enhances the cellular binding of cationic NPs. Enhanced binding in excess FBS suggests that the protein adsorbed on the NP is responsible for cellular binding and that this protein-NP complex does not compete with free proteins in solution for cellular binding sites.

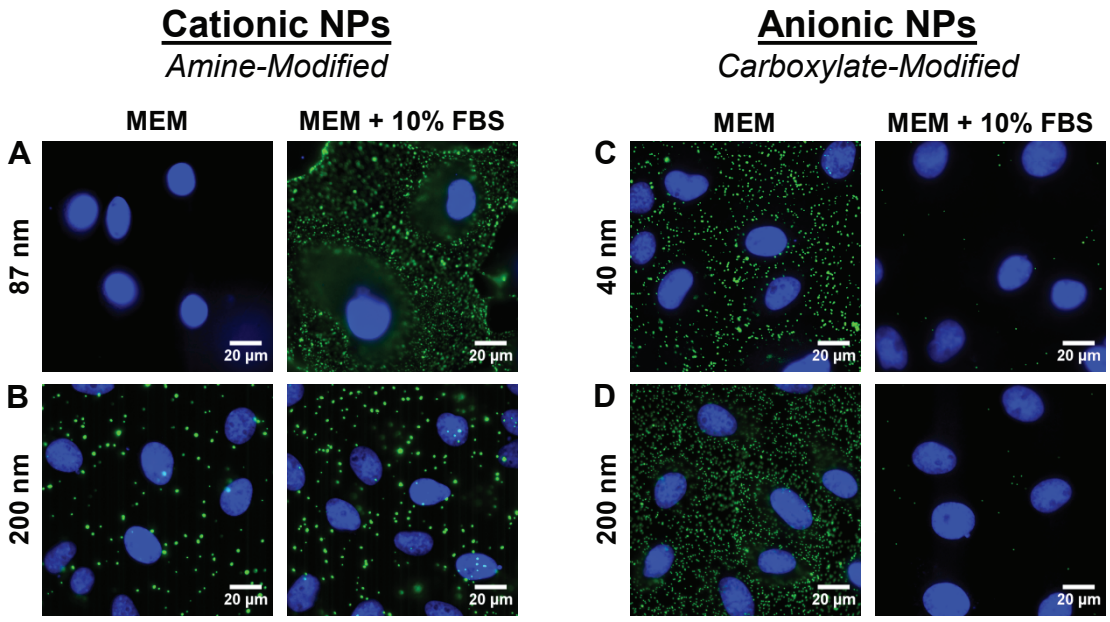

Figure 4: Fluorescence microscopy images of NPs (green) bound to BS-C-1 cells at 4 °C in MEM and MEM supplemented with FBS. Nuclei are stained with DAPI (blue). Cationic NPs are amine-modified and anionic NPs are carboxylate-modified.

3.2.3 Anionic NP Binding is Inhibited by Serum Proteins

Unlike the cationic NPs, the cellular binding of both the 40 nm (26 pM) and 200 nm (13 pM) anionic NPs was inhibited by the addition of serum proteins (Figures 4C and 4D). As the anionic NPs form a protein-NP complex when exposed to FBS (Figure 1), it is the cellular binding of this protein-NP complex that is inhibited by the excess serum proteins in solution. This suggests that the protein-NP complex formed from the anionic NPs competes with the free proteins in solution for cellular binding sites. Our results are in good agreement with recent experiments that showed the cellular uptake of 49 nm and 100 nm anionic polystyrene NPs is inhibited by the presence of serum proteins.[29] Based on our results, which distinguish cellular binding from uptake, it is likely that decreased binding of anionic NPs in the presence of serum proteins led to the observed decrease in uptake. In addition, the results for polystyrene NPs are in good agreement with previous work showing that the cellular

uptake of gold NPs functionalized with DNA or siRNA is inhibited by the presence of serum proteins.[30] Like the carboxylate-modified polystyrene NPs, the DNA- and siRNA-modified gold NPs are anionic suggesting the reduced binding in the presence of serum proteins may be due to NP charge rather than composition.

While the conventional view has been that anionic NPs have fewer cellular binding sites and limited uptake compared to cationic NPs,[13] previous reports of the cellular binding of NPs as function of charge provide a conflicting picture. For example, 18 nm gold NPs modified with a cationic polymer were found to enter adenocarcinoma breast cells (SK-BR-3) to a much greater extent than the same NPs with a negative surface charge.[14] Similar results were obtained for ∼100 nm polymer NPs in adenocarcinoma human cervical cells (HeLa).[31] In comparison, the uptake of cerium oxide NPs by adenocarcinoma lung cells (A549) was found to be much greater for anionic NPs.[32] Similarly, high uptake of anionic 35 nm iron oxide NPs was observed for HeLa cells.[33] While some variation may be due to differences in cell type, similar trends are expected for non-phagocytic cells. Based on our results (Figure 4), it is clear that differences in NP binding are highly dependent on the presence or absence of serum proteins: serum proteins enhance the binding of cationic NPs and inhibit the binding of anionic NPs. Interpretation of previous results examining cellular binding and uptake as a function of charge is often difficult because it is not clear from publications if FBS or other serum proteins were present. In addition to the presence of serum proteins, the concentration of NPs is an important factor for cellular binding. Repeating the experiments described above using much higher concentrations of NPs, we find that the observed trends no longer hold (Figure 5). When the NP concentration reaches a high enough threshold, cationic NPs can bind to cells in the absence of FBS and anionic NPs can bind in the presence of FBS. It is important to note that NP concentration may be one factor responsible for seemingly conflicting results in the literature.

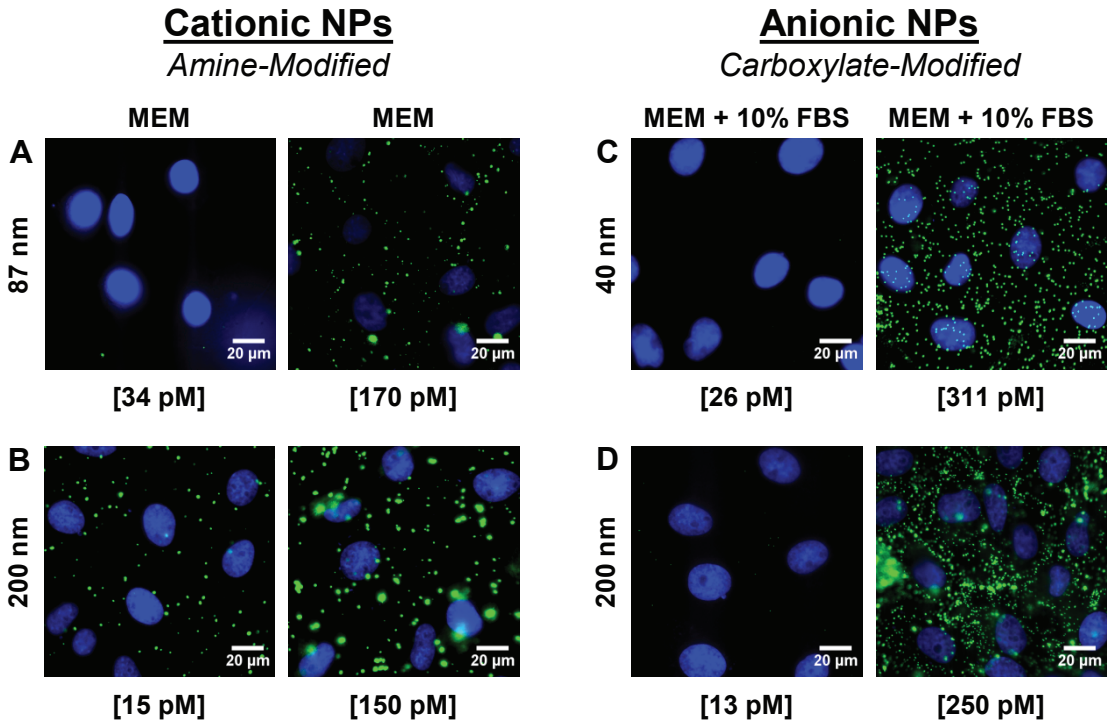

Figure 5: Effect of NP concentration on cellular binding to BS-C-1 cells in MEM (cationic NPs) and MEM supplemented with FBS (anionic NPs).

3.2.4 Cellular Binding Trends are Independent of Cell Type

As cellular binding studies have been reported in the literature for several cell types, it is important to consider the variable of the cell surface. To determine if the trends we observe are dependent upon cell type, we repeated cellular binding experiments with polystyrene NPs in multiple cell lines. Initial experiments were performed with green African monkey kidney epithelial (BS-C-1) cells. Cellular binding experiments with polystyrene NPs were repeated in HeLa cells. Cationic, 87 nm (84 pM) and 200 nm (150 pM) amine-modified polystyrene NPs, and anionic, 40 nm (26 pM) and 200 nm (26 pM) carboxylate-modified polystyrene NPs were incubated with HeLa cells for 10 minutes at 4 °C in MEM and MEM supplemented with 10% (v/v) FBS. The 87 nm amine-modified NPs did not bind to cells in MEM alone, but binding was enhanced in the presence of FBS (Figure 6A). The 200 nm amine-modified NPs did not bind to HeLa cells at any concentration between 15 and 150 pM (Figure 6B). The lack of binding may be due to differences in available cell surface receptors between HeLa and BS-C-1 cells in culture.

We observe that both the 40 nm and 200 nm, carboxylate-modified polystyrene NPs bind to HeLa cells in MEM alone (Figures 6C and 6D). This is consistent to what was observed with BS-C-1 cells. The cellular binding for both diameters of anionic NPs is inhibited in the presence of serum proteins. We also repeated the same cellular binding experiments using Chinese hamster ovary (CHO) cells (Figure 7), an epithelial-like cell line. Hams F-12 nutrient mixture, the native cell culture medium for CHO cells, was used instead of MEM for cellular binding experiments. In CHO cells, the binding of 87 nm amine-modified NPs (17 pM) was enhanced by serum proteins (Figure 7A), where the 200 nm amine-modified NPs (75 pM) did not bind to CHO cells (Figure 7B). Both the 200 nm (64 pM) and 40 nm (52 pM) carboxylate-modified NPs bound to cells in the presence of Ham's F-12 without serum proteins (Figures 7C and 7D), and the presence of serum proteins inhibited binding.

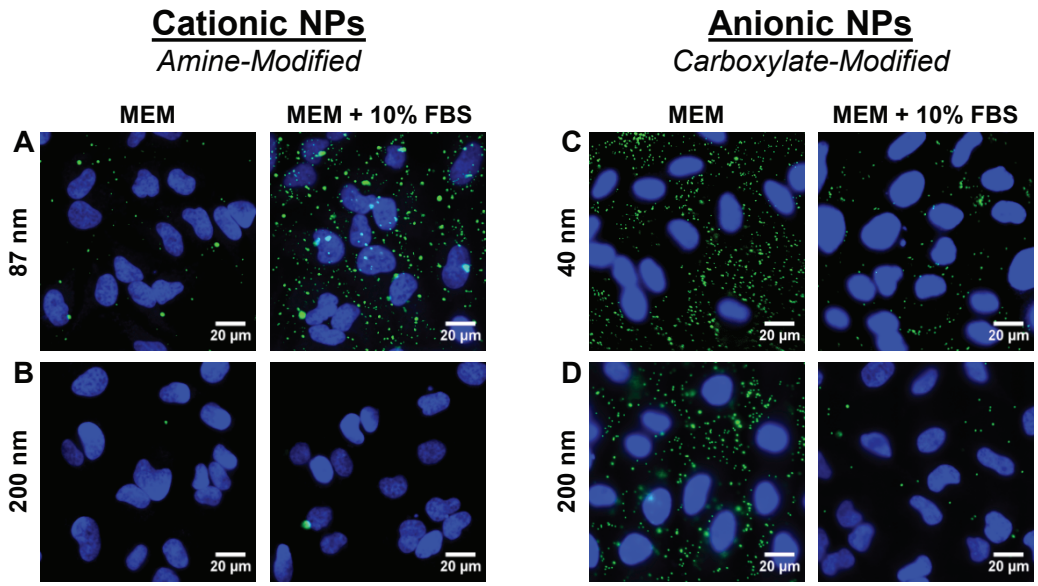

Figure 6: Fluorescence microscopy images of NPs (green) bound to HeLa cells at 4 °C in MEM and MEM supplemented with FBS. Nuclei are stained with DAPI (blue). Cationic NPs are amine-modified and anionic NPs are carboxylate-modified.

The binding trends are similar to those observed with both HeLa and BS-C-1 cells, suggesting that the binding of charged NPs in the presence of serum proteins is not dependent on cell type or the specific formulation of the cell culture medium.

3.2.5 Protein-NP Complexes Formed from Cationic NPs Bind to Scavenger Receptors

Although both cationic and anionic NPs form protein-NP complexes, these protein-NP complexes have very different cellular binding behavior. In the case of the cationic NPs, the formation of the protein-NP complex enhances binding. In comparison, the cellular binding of the protein-NP complex formed with the anionic NPs is inhibited by the presence of serum proteins in solution. This suggests that the protein-NP complex formed from anionic NPs competes with a protein present in FBS for the same binding site, while the protein-NP complex formed from cationic NPs is able to access a different set of cellular receptors.

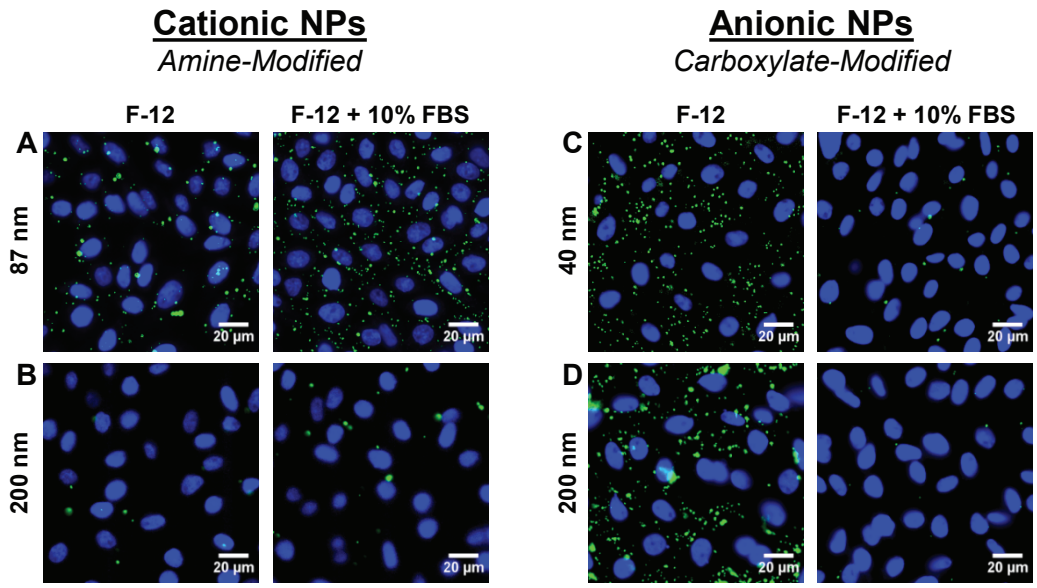

Figure 7: Fluorescence microscopy images of NPs (green) bound to CHO cells at 4 °C in F-12 medium and F-12 medium supplemented with FBS. Nuclei are stained with DAPI (blue). Cationic NPs are amine-modified and anionic NPs are carboxylate-modified.

Blood plasma is a complex mixture of hundreds of distinct proteins, the most abundant of which is albumin (55%).[1–3] Lower abundance proteins exist but are harder to detect. The protein composition of serum is similar to plasma with the removal of clotting factors such as fibrinogen. In the case of FBS, the relevant albumin is bovine serum albumin (BSA). Albumin has well-characterized cellular receptors responsible for binding and internalization.[9–11] However, it has been shown that chemical modifications to albumin, including adsorption on the surface of 5 nm gold NPs, alters the binding site of albumin.[34–36] Instead of the cell surface receptors used by albumin, modified albumin binds to glycoprotein(gp)30 and gp18, which act as scavenger receptors.

To determine if scavenger receptors are responsible for the serum protein-dependent binding of the cationic NPs, we carried out a series of competition assays. Confluent

monolayers of BS-C-1 cells were incubated with polyinosinic acid in MEM supplemented with 10% (v/v) FBS for 20 minutes. This polyanionic molecule is a known competitor for scavenger receptors.[16,30,35] If the NPs, complexed with serum proteins, bind to scavenger receptors, we expect the addition of polyinosinic acid to compete with the protein-NP complex for binding sites on the cell surface thereby inhibiting cellular binding of the NPs.

Flow cytometry was used to measure the NP fluorescence from individual cells. A representative scatter plot and fluorescence histograms are shown in Figure 8. The live cell population used in analysis is circled in the scatter plot (Figure 8A). The choice of this population was based on a propidium iodide assay used to distinguish live from dead cells. We observed that polyinosinic acid inhibits the binding of the 87 nm cationic NPs in the presence of FBS (Figures 8B and 9A). NP binding is normalized to 100% in the absence of polyinosinic acid. Fluorescence from cellular background, in the absence of NPs, is 11%. A control experiment with polyadenylic acid, a molecule similar in structure that does not compete for binding with scavenger receptors,[30] shows no competition with the 87 nm NPs (Figure 9B). Similar results were obtained for the 200 nm cationic NPs (Figure 10A). These results demonstrate that scavenger receptors are important for the cellular binding of the protein-NP complex formed from cationic NPs.

3.2.6 Protein-NP Complexes Formed from Anionic NPs Bind to Native Protein Receptors

Unlike the protein-NP complexes formed from cationic NPs, the cellular binding of the protein-NP complexes formed from anionic NPs is inhibited by the presence of excess serum proteins (Figures 4C and 4D). This suggests that these protein-NP complexes compete with proteins present in FBS for cellular binding sites. A competition assay using the 40 nm anionic NPs in MEM with increasing concentrations of FBS results in decreased binding (Figure 9C). At 10% (v/v) FBS, the amount of FBS used in the

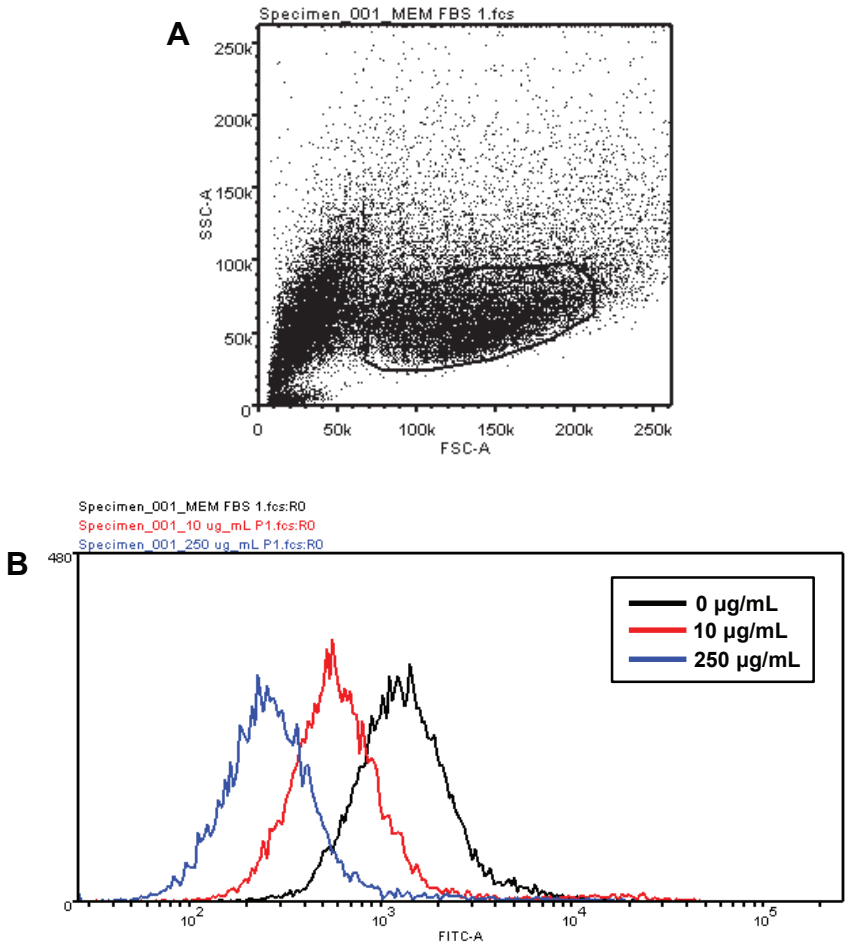

Figure 8: Representative flow cytometry data used to generate bar graphs for competition assays. (A) Forward and side scatter plot showing the cell population used for analysis (circled). (B) Fluorescence histograms demonstrating that the presence of increasing concentrations of polyinosinic acid (0 to 250 μg·mL^{-1}) leads to decreased fluorescence from 87 nm cationic NPs bound to the surface of BS-C-1 cells.

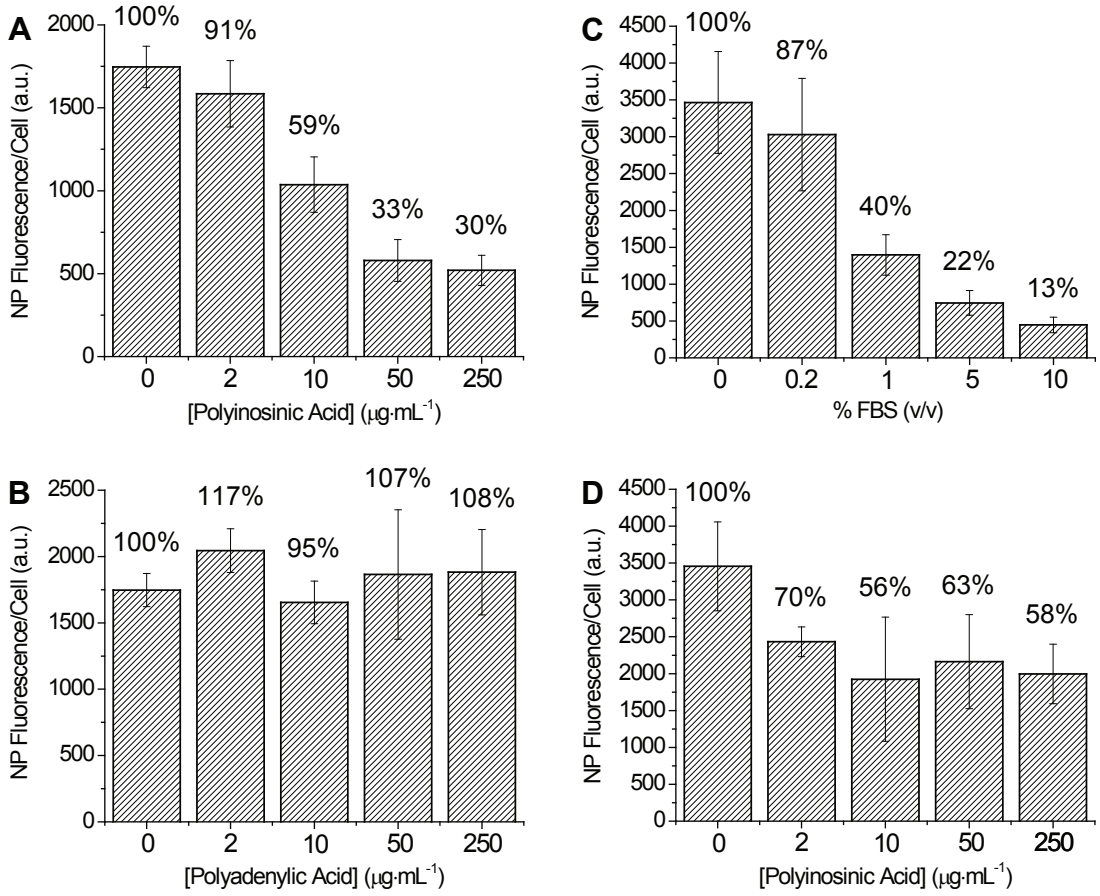

Figure 9: Cellular binding competition studies of protein-NP complexes. (A) Cellular binding of 87 nm amine-modified NPs in MEM supplemented with FBS in the presence of increasing concentrations of polyinosinic acid and (B) polyadenylic acid. (C) Cellular binding of 40 nm carboxylate-modified NPs in the presence of increasing concentrations of FBS and (D) polyinosinic acid.

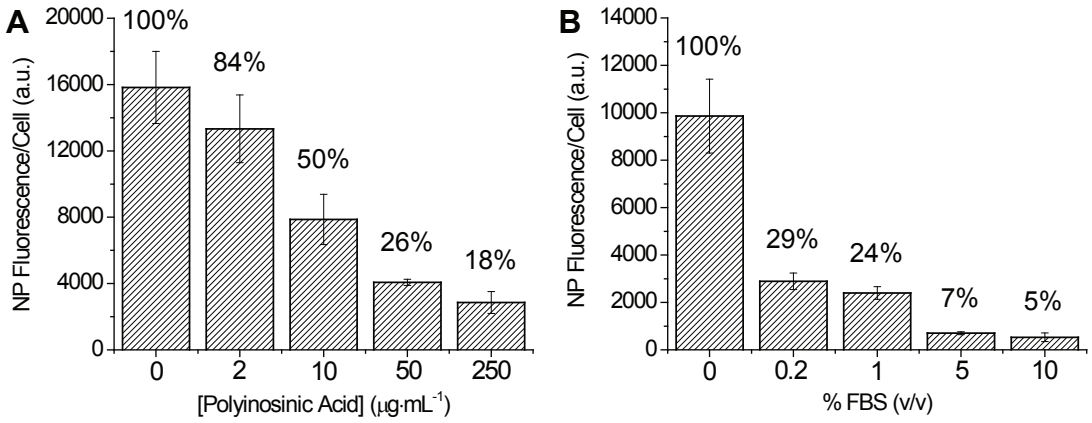

Figure 10: Cellular binding competition studies of 200 nm NPs. (A) 200 nm amine-modified NPs in MEM supplemented with FBS in the presence of increasing concentrations of polyinosinic acid. (B) 200 nm carboxylate-modified NPs in the presence of increasing concentrations of FBS.

cellular imaging experiments, only minimal binding is observed. Cellular background in the absence of NPs is 8%. Similar results were obtained for the 200 nm anionic NPs (Figure 10B). These results indicate that the protein-NP complex formed from the 40 nm anionic NPs does not bind to scavenger receptors, but instead binds to a native protein receptor.

To determine if the scavenger receptors play any role in the binding of the bare anionic NPs, we carried out a competition assay in MEM, in the absence of FBS, using polyinosinic acid as the competitor (Figure 9D). Compared to the 87 nm protein-NP complex (Figure 9A), cellular binding of the bare 40 nm anionic NPs was minimally inhibited by the presence of polyinosinic acid and lacked any concentration dependence. These results demonstrate that the bare 40 nm anionic NPs do not require binding to scavenger receptors. The specific cellular receptor for the bare 40 nm carboxylate-modified NPs remains unidentified.

3.3 Conclusions

We have determined that the binding of NPs to the cell surface in the presence of extracellular serum proteins is highly dependent on the charge of the NP. Although serum proteins adsorb onto the surface of both cationic and anionic NPs in solution forming a protein-NP complex (Figure 1), these protein-NP complexes display opposite cellular binding trends. The cellular binding of cationic NPs is enhanced by the presence of serum proteins while the binding of anionic NPs is inhibited (Figure 4). We have determined that these differences in cellular binding are due to the cellular receptors used by the protein-NP complexes. The protein-NP complex formed from cationic NPs binds to scavenger receptors on the cell surface (Figure 9A). In comparison, the protein-NP complex formed from anionic NPs competes with proteins present in FBS for cellular binding sites (Figure 9C). It is possible that the use of different cellular receptors is due to adsorption of a low abundance protein not detected with gel electrophoresis or differences in the conformation of the adsorbed protein on the NP surface. Differences in protein conformation as a function of charge have been observed previously for gold surfaces.[37] In Chapter 5, we explore the role of protein conformation on the cellular receptors used by protein-NP complexes.

Our studies focused on polystyrene NPs, modified with chemical groups to control the effective surface charge. While these NPs provide a good model system, it is also worth considering how these results may relate to NPs of other compositions. Binding of serum proteins to NPs appears to be quite general and has been carefully characterized for aluminum oxide NPs,[38] gold NPs and nanorods,[18,19] poly(amidoamine) dendrimers,[39] and quantum dots.[40] The addition of a neutral polymer such as polyethylene glycol can reduce this nonspecific binding, but the complete inhibition of nonspecific binding remains a challenge.[41–43] This suggests that a wide variety of NPs will be affected by the nonspecific adsorption of serum proteins and that the interaction of these protein-NP complexes will be highly dependent on the

initial NP surface charge. The dependence on scavenger receptors for cellular binding of the protein-NP complexes formed from the cationic polystyrene NPs is similar to that observed for 13 nm gold NPs functionalized with DNA or siRNA[30] as well as 5 nm gold NPs complexed with albumin.[34–36] These results from the literature demonstrate that scavenger receptors are binding sites for NPs of diverse compositions. In Chapter 4, our results are extended beyond polystyrene to multiple anionic NPs with biomedical relevance: quantum dots, gold nanospheres, and low-density lipoprotein particles.

NP-cell interactions are governed by a number of factors including NP size, composition, and charge. These interactions are complicated by the presence of extracellular serum proteins that adsorb on the surface of the NP. We anticipate that a direct comparison of the cellular binding of cationic and anionic NPs in the presence of serum proteins will help reconcile previous results and inform the design of NPs for *in vivo* applications.

This chapter was adapted with permission from Reference [21]. Copyright 2012 American Chemical Society.

3.4 References

[1] Anderson, N. L. and Anderson, N. G., "The human plasma proteome: History, character, and diagnostic prospects." *Mol. Cell. Proteomics*, **2002**, *1*, 845–867.

[2] Pieper, R., Gatlin, C. L., Makusky, A. J., Russo, P. S., Schatz, C. R., Miller, S. S., Su, Q., McGrath, A. M., Estock, M. A., Parmar, P. P., Zhao, M., Huang, S. T., Zhou, J., Wang, F., Esquer-Blasco, R., Anderson, N. L., Taylor, J., and Steiner, S., "The human serum proteome: Display of nearly 3700 chromatographically separated protein spots on two-dimensional electrophoresis gels and identification of 325 distinct proteins." *Proteomics*, **2003**, *3*, 1345–1364.

[3] Adkins, J. N., Varnum, S. M., Auberry, K. J., Moore, R. J., Angell, N. H., Smith, R. D., Springer, D. L., and Pounds, J. G., "Toward a human blood serum proteome: Analysis by multidimensional separation coupled with mass spectrometry." *Mol. Cell. Proteomics*, **2002**, *1*, 947–955.

[4] Walczyk, D., Bombelli, F. B., Monopoli, M. P., Lynch, I., and Dawson, K. A., "What the cell "sees" in bionanoscience." *J. Am. Chem. Soc.*, **2010**, *132*, 5761–5768.

[5] Lynch, I., Cedervall, T., Lundqvist, M., Cabaleiro-Lago, C., Linse, S., and Dawson, K. A., "The nanoparticle-protein complex as a biological entity; A complex fluids and surface science challenge for the 21st century." *Adv. Colloid Interface Sci.*, **2007**, *134-135*, 167–174.

[6] Treuel, L. and Nienhaus, G. U., "Toward a molecular understanding of nanoparticle-protein interactions." *Biophys. Rev.*, **2012**, *4*, 137–147.

[7] Doorley, G. W. and Payne, C. K., "Cellular binding of nanoparticles in the presence of serum proteins." *Chem. Commun.*, **2011**, *47*, 466–468.

[8] Doorley, G. W. and Payne, C. K., "Nanoparticles act as protein carriers during cellular internalization." *Chem. Commun.*, **2012**, *48*, 2961–2963.

[9] Schnitzer, J. E., "gp60 is an albumin-binding glycoprotein expressed by continuous endothelium involved in albumin transcytosis." *Am. J. Physiol.-Heart C.*, **1992**, *262*, H246–H254.

[10] Schnitzer, J. E., Carley, W. W., and Palade, G. E., "Albumin interacts specifically with a 60-kDa microvascular endothelial glycoprotein." *Proc. Natl. Acad. Sci.*, **1988**, *85*, 6773–6777.

[11] Schnitzer, J. E., Carley, W. W., and Palade, G. E., "Specific albumin binding to microvascular endothelium in culture." *Am. J. Physiol.-Heart C.*, **1988**, *254*, H425–H437.

[12] Hopkins, C. R. and Trowbridge, I. S., "Internalization and processing of transferrin and the transferrin receptor in human carcinoma A431 cells." *J. Cell. Biol.*, **1983**, *97*, 508–521.

[13] Verma, A. and Stellacci, F., "Effect of surface properties on nanoparticle-cell interactions." *Small*, **2010**, *6*, 12–21.

[14] Cho, E. C., Xie, J., Wurm, P. A., and Xia, Y., "Understanding the role of surface charges in cellular adsorption versus internalization by selectively removing gold nanoparticles on the cell surface with a I_2/KI etchant." *Nano Lett.*, **2009**, *9*, 1080–1084.

[15] Payne, C. K., Jones, S. A., Chen, C., and Zhuang, X., "Internalization and trafficking of cell surface proteoglycans and proteoglycan-binding ligands." *Traffic*, **2007**, *8*, 389–401.

[16] Lunov, O., Syrovets, T., Loos, C., Beil, J., Delecher, M., Tron, K., Nienhaus, G. U., Musyanovych, A., Mailaender, V., Landfester, K., and Simmet, T., "Differential uptake of functionalized polystyrene nanoparticles by human macrophages and a monocytic cell line." *ACS Nano*, **2011**, *5*, 1657–1669.

[17] Gessner, A., Lieske, A., Paulke, B.-R., and Müller, R. H., "Functional groups on polystyrene model nanoparticles: Influence on protein adsorption." *J. Biomed. Mater. Res., Part A*, **2003**, *65A*, 319–326.

[18] Brewer, S. H., Glomm, W. R., Johnson, M. C., Knag, M. K., and Franzen, S., "Probing BSA binding to citrate-coated gold nanoparticles and surfaces." *Langmuir*, **2005**, *21*, 9303–9307.

[19] Alkilany, A. M., Nagaria, P. K., Hexel, C. R., Shaw, T. J., Murphy, C. J., and Wyatt, M. D., "Cellular uptake and cytotoxicity of gold nanorods: Molecular origin of cytotoxicity and surface effects." *Small*, **2009**, *5*, 701–708.

[20] Silin, V., Weetall, H., and Vanderah, D. J., "SPR studies of the nonspecific adsorption kinetics of human IgG and BSA on gold surfaces modified by self-assembled monolayers (SAMs)." *J. Colloid Interface Sci.*, **1997**, *185*, 94–103.

[21] Fleischer, C. C. and Payne, C. K., "Nanoparticle surface charge mediates the cellular receptors used by protein-nanoparticle complexes." *J. Phys. Chem. B*, **2012**, *116*, 8901–8907.

[22] Freshney, R. I., *Culture of Animal Cells*. John Wiley and Sons, Inc., Hoboken, 5th edn., **2005**.

[23] Pastan, I. and Willingham, M., "Journey to the center of the cell: Role of the receptosome." *Science*, **1981**, *214*, 504–509.

[24] Szymanski, C. J., Yi, H., Liu, J. T., Wright, E. R., and Payne, C. K., "Imaging intracellular quantum dots: Fluorescence microscopy and transmission electron microscopy." *In* Rosenthal, S. J. and Wright, D. X., eds., "Nanobiotechnology Protocols," Humana Press, **2012**.

[25] Callaini, G., Dallai, R., and Riparbelli, M. G., "Microfilament distribution in cold-treated Drosophila embryos." *Exp. Cell Res.*, **1991**, *194*, 316–321.

[26] Watts, R. G. and Howard, T. H., "Evidence for a gelsolin-rich, labile F-actin pool in human polymorphonuclear leukocytes." *Cell Motil. Cytoskel.*, **1992**, *21*, 25–37.

[27] Goldenthal, K. L., Pastan, I., and Willingham, M. C., "Initial steps in receptor-mediated endocytosis - The influence of temperature on the shape and distribution of plasma-membrane clathrin-coated pits in cultured mammalian-cells." *Exp. Cell Res.*, **1984**, *152*, 558–564.

[28] Harding, C., Heuser, J., and Stahl, P., "Receptor-mediated endocytosis of transferrin and recycling of the transferrin receptor in rat reticulocytes." *J. Cell Biol.*, **1983**, *97*, 329–339.

[29] Guarnieri, D., Guaccio, A., Fusco, S., and Netti, P., "Effect of serum proteins on polystyrene nanoparticle uptake and intracellular trafficking in endothelial cells." *J. Nanopart. Res.*, **2011**, *13*, 4295–4309.

[30] Patel, P. C., Giljohann, D. A., Daniel, W. L., Zheng, D., Prigodich, A. E., and Mirkin, C. A., "Scavenger receptors mediate cellular uptake of polyvalent oligonucleotide-functionalized gold nanoparticles." *Bioconjugate Chem.*, **2010**, *21*, 2250–2256.

[31] Harush-Frenkel, O., Debotton, N., Benita, S., and Altschuler, Y., "Targeting of nanoparticles to the clathrin-mediated endocytic pathway." *Biochem. Biophys. Res. Commun.*, **2007**, *353*, 26–32.

[32] Patil, S., Sandberg, A., Heckert, E., Self, W., and Seal, S., "Protein adsorption and cellular uptake of cerium oxide nanoparticles as a function of zeta potential." *Biomaterials*, **2007**, *28*, 4600–4607.

[33] Wilhelm, C., Billotey, C., Roger, J., Pons, J. N., Bacri, J. C., and Gazeau, F., "Intracellular uptake of anionic superparamagnetic nanoparticles as a function of their surface coating." *Biomaterials*, **2003**, *24*, 1001–1011.

[34] Schnitzer, J. E., Sung, A., Horvat, R., and Bravo, J., "Preferential interaction of albumin-binding proteins, gp30 and gp18, with conformationally modified albumins. Presence in many cells and tissues with a possible role in catabolism." *J. Biol. Chem.*, **1992**, *267*, 24544–24553.

[35] Schnitzer, J. E. and Bravo, J., "High affinity binding, endocytosis, and degradation of conformationally modified albumins. Potential role of gp30 and gp18 as novel scavenger receptors." *J. Biol. Chem.*, **1993**, *268*, 7562–7570.

[36] Schnitzer, J. E. and Oh, P., "Albondin-mediated capillary permeability to albumin. Differential role of receptors in endothelial transcytosis and endocytosis of native and modified albumins." *J. Biol. Chem.*, **1994**, *269*, 6072–6082.

[37] Nakata, S., Kido, N., Hayashi, M., Hara, M., Sasabe, H., Sugawara, T., and Matsuda, T., "Chemisorption of proteins and their thiol derivatives onto gold surfaces: Characterization based on electrochemical nonlinearity." *Biophys. Chem.*, **1996**, *62*, 63–72.

[38] Rezwan, K., Meier, L. P., Rezwan, M., Voros, J., Textor, M., and Gauckler, L. J., "Bovine serum albumin adsorption onto colloidal Al_2O_3 particles: A new model based on zeta potential and UV-Vis measurements." *Langmuir*, **2004**, *20*, 10055–10061.

[39] Giri, J., Diallo, M. S., Simpson, A. J., Liu, Y., Goddard, I., William A., Kumar, R., and Woods, G. C., "Interactions of poly(amidoamine) dendrimers with human serum albumin: Binding constants and mechanisms." *ACS Nano*, **2011**, *5*, 3456–3468.

[40] Hanaki, K.-I., Momo, A., Oku, T., Komoto, A., Maenosono, S., Yamaguchi, Y., and Yamamoto, K., "Semiconductor quantum dot/albumin complex is a long-life and highly photostable endosome marker." *Biochem. Biophys. Res. Commun.*, **2003**, *302*, 496–501.

[41] Gref, R., Domb, A., Quellec, P., Blunk, T., Müller, R. H., Verbavatz, J. M., and Langer, R., "The controlled intravenous delivery of drugs using PEG-coated sterically stabilized nanospheres." *Adv. Drug Delivery Rev.*, **1995**, *16*, 215–233.

[42] Gref, R., Lück, M., Quellec, P., Marchand, M., Dellacherie, E., Harnisch, S., Blunk, T., and Müller, R. H., "'Stealth' corona-core nanoparticles surface modified by polyethylene glycol (PEG): Influences of the corona (PEG chain length and surface density) and of the core composition on phagocytic uptake and plasma protein adsorption." *Colloids Surf., B*, **2000**, *18*, 301–313.

[43] Walkey, C. D. and Chan, W. C. W., "Understanding and controlling the interaction of nanomaterials with proteins in a physiological environment." *Chem. Soc. Rev.*, **2012**, *41*, 2780–2799.

CHAPTER IV

CELLULAR BINDING TRENDS OF BIOMEDICALLY RELEVANT NANOPARTICLES

4.1 Introduction

The use of nanoparticles (NPs) for biological and medical applications is predicated on a fundamental understanding of NP interactions with cells. In the course of these applications, the NP will inevitably encounter extracellular proteins, such as serum proteins, which readily adsorb onto the NP surface.[1,2] The underlying mechanisms that dictate the interactions of protein-NP complexes with cells is a critical question. In Chapter 3, using a model system of polystyrene, we observed that the receptors used by protein-NP complexes are determined by the initial NP surface charge.[3] Chapter 4 extends these results to determine if the trends we observed for polystyrene hold true for NPs with biomedical applications. We examined the cellular binding of a collection of anionic NPs including quantum dots (QDs), colloidal gold NPs, and low-density lipoprotein (LDL).[4] NPs with different surface modifications and compositions were used to determine the interactions of a diverse range of NPs with cells in the presence of serum proteins. We focused solely on anionic NPs for these studies as commercially available NPs, as well as those used in cellular applications, are more commonly anionic.

Previously, we determined that anionic, carboxylate-modified polystyrene NPs are inhibited by the presence of free serum proteins in solution. These free serum proteins compete with the protein-anionic NP complex for binding sites on the cell surface. We first measured the cellular binding of carboxylate-modified CdSe/ZnS QDs using fluorescence microscopy and flow cytometry. Our goal was to determine if NPs with

the same surface modification, but different composition, follow the same binding trend as the carboxylate-modified polystyrene NPs. QDs are used as cellular sensors and probes due to their bright photoluminescence and size-tunable emission properties.[5–7] We then repeated cellular binding studies using citrate-modified gold NPs as an example of NPs with a different surface modification and composition. Gold NPs have biomedical applications in drug delivery, cellular and tissue imaging, and cancer therapy.[8,9] Cellular binding was characterized with dark field microscopy and UV-Vis spectroscopy. As a point of comparison for synthetic QDs and gold NPs, we also measured the cellular binding of LDL using fluorescence microscopy and flow cytometry. LDL is a <100 nm particle that serves as a lipid transporter in the blood stream.[10] LDL particles are composed of cholesteryl ester, cholesterol, phospholipids, and a single molecule of apolipoprotein B-100.[11] The use of LDL allowed us to determine if NP surface charge plays a similiar role for biological NPs.

We observed that binding of anionic carboxylate-modified semiconductor QDs, citrate-modified colloidal gold NPs, and LDL to the cell surface is inhibited by the presence of serum proteins. These results are identical to the trends observed for carboxylate-modified polystyrene NPs. As these NPs vary in surface modification and composition, our results suggest that the initial charge of the NP may be the determining factor in whether NPs will bind to cells in a physiological environment where serum proteins are present.

4.2 Results and Discussion

The zeta potential (ZP), hydrodynamic diameter (D_h), and biomedical applications of the NPs used in cellular binding experiments are presented in Table 3. The hydrodynamic diameter of the QDs could not be measured reliably due to strong absorption and fluorescence by the QDs. From a previous literature report, the hydrodynamic diameter is ∼10 nm.[12] To determine the effect of serum proteins on cellular binding,

NPs were incubated with cells in minimum essential medium (MEM) without protein and MEM supplemented with 10% (v/v) fetal bovine serum (FBS). MEM supplemented with 10% (v/v) FBS is commonly used as a cell culture medium.[13] The total protein concentration present in a 10% (v/v) FBS solution is approximately 10 mg·mL^{-1} based on the UV-Vis absorption spectrum. In comparison, physiological serum protein levels are approximately 70 mg·mL^{-1}.[14–16]

Table 3: Properties of anionic NPs used in cellular binding experiments

NP	Surface Modification	ZP (mV)	D_h (nm)	Applications
QD	carboxylate	-45.2 ± 1.0	N/A[a]	Cellular imaging and sensing, FRET probes
Gold	citrate	-17.7 ± 2.9	39.3 ± 2.2	Drug delivery, *in vivo* imaging, photothermal therapy
LDL[b]	N/A	-15.8 ± 2.1	68.0 ± 20.6	Lipid transport

[a]D_h ∼10 nm (Chapter 2.1.2). [b]Measurements carried out in Minimum Essential Medium. ZP, zeta potential; D_h, hydrodynamic diameter; QD, quantum dot; FRET, Förster resonance energy transfer; LDL, low-density lipoprotein.

The mixture of proteins present in FBS represents the complex biological environment that NPs used for biomedical applications will encounter. As FBS is a mixture of many different proteins, experiments were repeated using just bovine serum albumin, (BSA, 10 mg·mL^{-1}) the protein of greatest abundance in the FBS mixture.[14–16] This concentration of BSA is equivalent to the total protein concentration present in the 10% (v/v) FBS experiments. For all NP binding experiments, cells were kept at 4 °C to block cellular internalization and only allow NP binding to the cell surface.[17–22]

4.2.1 Carboxylate-Modified Quantum Dots

We first confirmed that a protein corona formed on the surface of the anionic QDs, resulting in a protein-QD complex. Previous fluorescence correlation spectroscopy

experiments have shown that human serum albumin, the main protein present in human serum,[14–16] adsorbs onto the surface of carboxylate-modified QDs.[23] To confirm that a protein corona forms with FBS under the same conditions used in our cellular binding experiments, we carried out a similar analysis using gel electrophoresis. QDs (0.8 μM) were incubated for 10 minutes at room temperature in a solution of MEM supplemented with 10% (v/v) FBS, similar to conditions used in cell culture experiments. Protein-QD complexes were run on a 1% (w/v) agarose gel. As a control, QDs incubated in both water and MEM in the absence of protein were run on the same gel. The differing mobilities of QDs in the presence and absence of FBS confirms that QDs exposed to serum proteins will form a protein-QD complex (Figure 11). In the absence of protein, QDs show high mobility on the gel (QD + H_2O and QD + MEM). In comparison, the addition of FBS significantly reduces the mobility of the QDs (QD + FBS). The formation of a protein corona on anionic NPs has also been observed for polystyrene NPs,[3,24] gold nanorods,[25] and gold NPs.[26] We expect that the positive residues of the serum proteins interact with the anionic NP surface.[27]

To study the effect of serum proteins on the cellular binding of QDs, carboxylate-modified QDs (8 nM) were incubated with BS-C-1 monkey kidney epithelial cells in MEM, MEM supplemented with 10% (v/v) FBS, and MEM supplemented with 10 mg·mL^{-1} BSA for 10 minutes at 4 °C. The cells were rinsed twice with PBS prior to imaging to remove QDs that did not bind to the cell surface. In the absence of serum proteins, anionic QDs readily bind to BS-C-1 cells (Figure 12A). In comparison, cellular binding of anionic QDs is blocked by the addition of FBS (Figure 12B). As with FBS, the presence of BSA blocked the cellular binding of QDs (Figure 12C), suggesting that the protein-QD complex competes with free BSA in solution for cellular receptors. Flow cytometry, which provides a high-throughput measurement of cellular fluorescence, was used to quantify the cellular binding of QDs in the presence of serum proteins (Figure 13). Flow cytometry measurements demonstrate that the

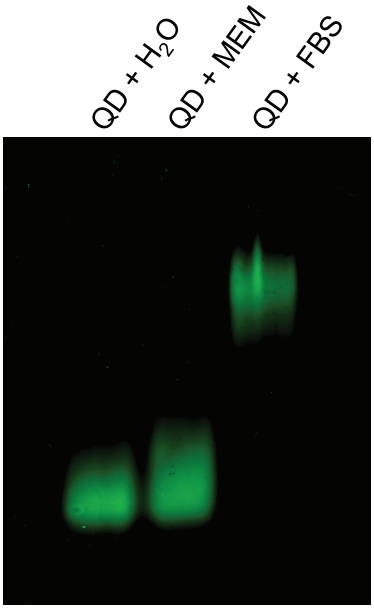

Figure 11: Formation of a protein corona on carboxylate-modified QDs confirmed with gel electrophoresis. QDs (green) were incubated in water (QD + H_2O), MEM (QD + MEM), and MEM supplemented with FBS (QD + FBS).

addition of either 10% (v/v) FBS or 10 mg·mL^{-1} BSA, protein concentrations used in cell culture, completely inhibits the cellular binding of QDs. Cellular binding is normalized to 100% QD binding in MEM. The baseline autofluorescence of cells in the absence of QDs is shown for comparison. Quantitative measurements obtained with flow cytometry (Figure 13) are in good agreement with the fluorescence microscopy images (Figure 12).

These results for carboxylate-modified QDs follow the same trend observed for anionic carboxylate-modified polystyrene NPs with hydrodynamic diameters of 60 nm and 236 nm.[3] This suggests that the inhibition of cellular binding of anionic NPs in the presence of serum proteins is independent of NP composition or diameter. In addition, previous work with carbon NPs[28] and anionic silver nanoclusters[29] has shown decreased cellular uptake of NPs in the presence of serum proteins. This may indicate a broader trend, although it is important to note that our experiments

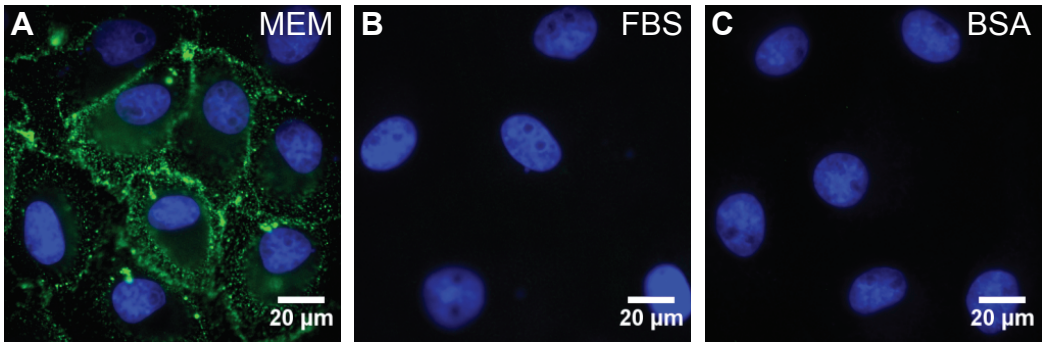

Figure 12: Fluorescence microscopy images of carboxylate-modified QDs (green) bound to BS-C-1 cells at 4 °C. Nuclei are stained with DAPI (blue). QDs were incubated with cells in (A) MEM, (B) MEM supplemented with FBS, and (C) MEM supplemented with BSA.

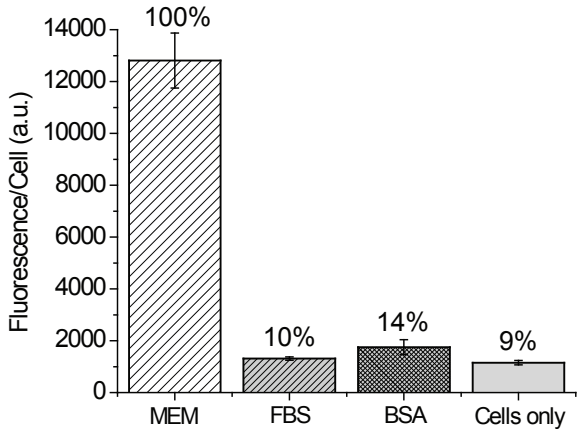

Figure 13: Cellular binding of QDs in MEM, MEM supplemented with FBS (FBS), and MEM supplemented with BSA (BSA) quantified with flow cytometry. Autofluorescence from cells in the absence of QDs (cells only) is shown for comparison.

measure cellular binding rather than uptake.

4.2.2 Citrate-Modified Gold NPs

As with the QDs, we first confirmed that a protein corona forms on the surface of the citrate-modified gold NPs. Previous research has shown that a protein corona forms on the surface of citrate-modified gold NPs after incubation with a mixture of plasma proteins,[30] as well as with BSA alone.[27,31] The formation of a protein corona on the anionic citrate-modified gold NPs was confirmed by incubating gold NPs (1 nM) with MEM supplemented with 10% (v/v) FBS for 30 minutes at 4 °C. The NPs were then washed with repeated centrifugation and resuspension in H_2O. The supernatant collected after each wash step was run on a polyacrylamide gel (12%). The final NP pellet was resuspended in a solution containing 6% (w/v) sodium dodecyl sulfate (SDS), a detergent that will remove adsorbed proteins from the NP surface. The first two wash steps result in a high concentration of protein in the supernatant (S1, diluted to 1% (v/v), and S2, diluted to 10% (v/v), Figure 14). After 4 washes, no protein is detected in the supernatant. The addition of SDS to the gold NP pellet solubilizes any proteins adsorbed on the NP surface resulting in a band at ∼66 kDa (NP + SDS). As a control, the addition of water, rather than SDS, does not result in a protein band (NP + H_2O). Based on the molecular weight, it is likely that BSA (66 kDa) is the main protein adsorbed on the gold NPs. As BSA is the major component of serum (∼55%),[14–16] this is unsurprising. These results are in agreement with previous reports that BSA adsorbs onto the surface of both citrate-modified[26,27] and borohydride-modified gold NPs.[32]

To image cellular binding, gold NPs (0.34 nM) were incubated with BS-C-1 cells, grown on glass cover slips, for 30 minutes at 4 °C in MEM or MEM supplemented with 10% (v/v) FBS. Cells were washed twice with PBS prior to dark field imaging. Cells were then fixed to cover slips with 4% (v/v) formaldehyde and sandwiched between

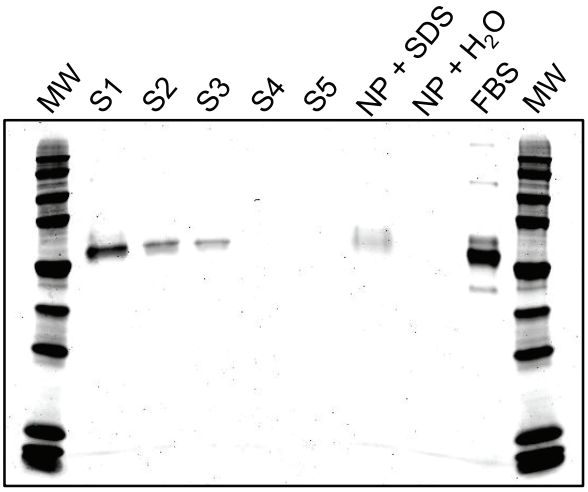

Figure 14: Formation of a protein corona on the surface of citrate-modified gold NPs after incubation in MEM supplemented with FBS. NPs were washed via centrifugation five times and the supernatants (S) were analyzed with gel electrophoresis. NP pellets were resuspended in either SDS (NP + SDS) or water (NP + H_2O). FBS alone is shown for comparison. Molecular weight (MW) marker shows 225, 150, 100, 75, 50, 35, 25, 15, 10, and 5 kDa.

a second glass cover slip for imaging. Using dark field microscopy, we observed that gold NPs bind to cells in the absence of serum proteins and that binding is inhibited in the presence of serum proteins (Figures 15A and 15B). The decreased binding of citrate-modified gold NPs in the presence of serum proteins is consistent with what we have observed for carboxylate-modified QDs (Figure 12) and carboxylate-modified polystyrene NPs.[3] Control images acquired in the absence of NPs show the scatter from cells in MEM (Figure 15C) and MEM supplemented with 10% (v/v) FBS (Figure 15D). We also acquired a dark field image and bright field image of the same cell in MEM supplemented with 10% (v/v) FBS (Figure 16) to show the localized cellular regions from which the scattering is observed.

However, substantial gold NP aggregation is observed in medium without serum, consistent with previous studies.[26] This allows for the possibility that aggregated gold NPs are able to access a different cellular receptor than individual gold NPs.

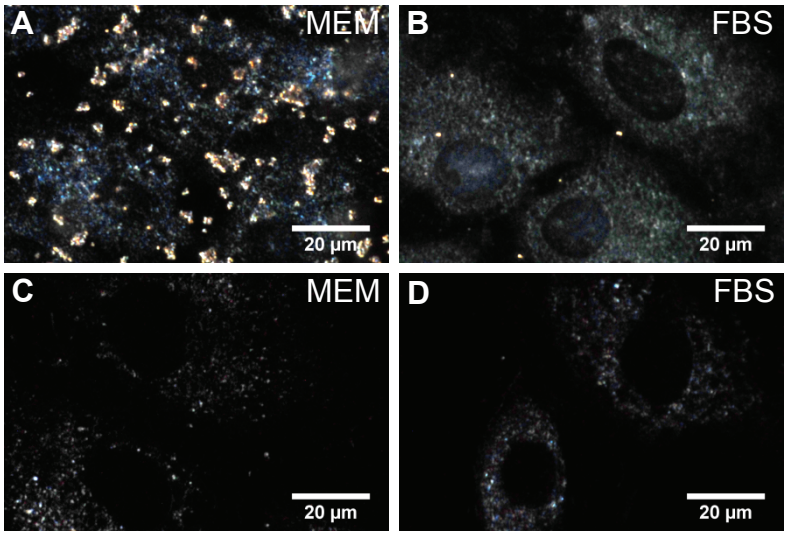

Figure 15: Dark-field microscopy images of citrate-modified gold NPs (yellow) bound to BS-C-1 cells at 4 °C after incubation in (A) MEM and (B) MEM supplemented with FBS. Control images show cells in the absence of NPs in (C) MEM and (D) MEM supplemented with FBS.

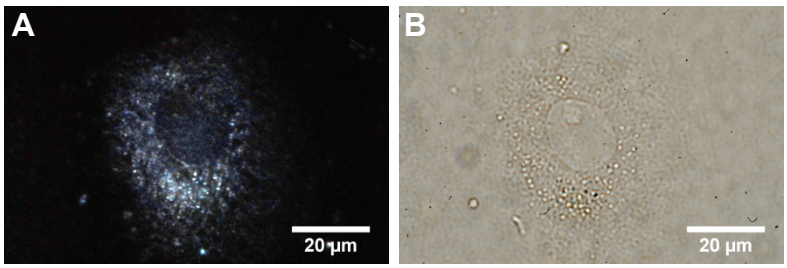

Figure 16: Microscopy images of a BS-C-1 cell in MEM supplemented with FBS in the absence of NPs. (A) Dark field. (B) Bright field.

To ensure that aggregation was not responsible for the difference in cellular binding, we compared the cellular binding of protein-gold NP complexes in the presence and absence of excess FBS. If cellular binding of protein-gold NPs is inhibited by excess FBS, it suggests that the protein-gold NP complexes compete for the same cellular receptors as the free serum proteins in solution.

We first characterized the formation of protein-gold NP complexes in solution using absorption spectroscopy. FBS was titrated into a solution of gold NPs (0.17 nM), and the λ_{max} values were monitored as a function of the protein to NP ratio (Figure 17A). Changes in the λ_{max} values for the protein-NP complexes relative to the λ_{max} value of gold NPs in the absence of protein (524 nm) were used with the Langmuir equation to quantify protein adsorption (Chapter 2.1.1.2). We calculated a maximum shift in wavelength of $\sim$5 nm, corresponding to an FBS concentration of 7.5 μM, or 0.5% (v/v). This concentration is the approximate saturation point of protein adsorption to 30 nm gold NPs, and was used in binding competition studies to create a protein-NP complex without excess protein in solution. Interestingly, we observed a shift in wavelength of 3 nm for the washed NPs, attributed primarily to loss of the "soft" protein corona during wash steps. From a linear fit of the Langmuir adsorption isotherm data using a Lineweaver-Burk plot (Figure 17B), we report an equilibrium association constant of 8.1 x $10^6 \pm$ 1.4 x 10^6 M^{-1}. Error bars are present for all data points but are too small to see on the respective scale.

To measure the cellular binding of non-aggregated protein-gold NP complexes, we used UV-Vis absorption spectroscopy. Flow cytometry cannot be used to directly probe binding as gold NPs are not intrinsically fluorescent. Absorption spectra of gold NP solutions were acquired before and after incubation with cells. The difference in absorbance values at $\sim$520 nm was used as a relative measure of gold NPs bound to the cell surface. Representative UV-Vis difference spectra of gold NPs after incubation with MEM or MEM supplemented with 10% (v/v) FBS are presented in Figure 18A.

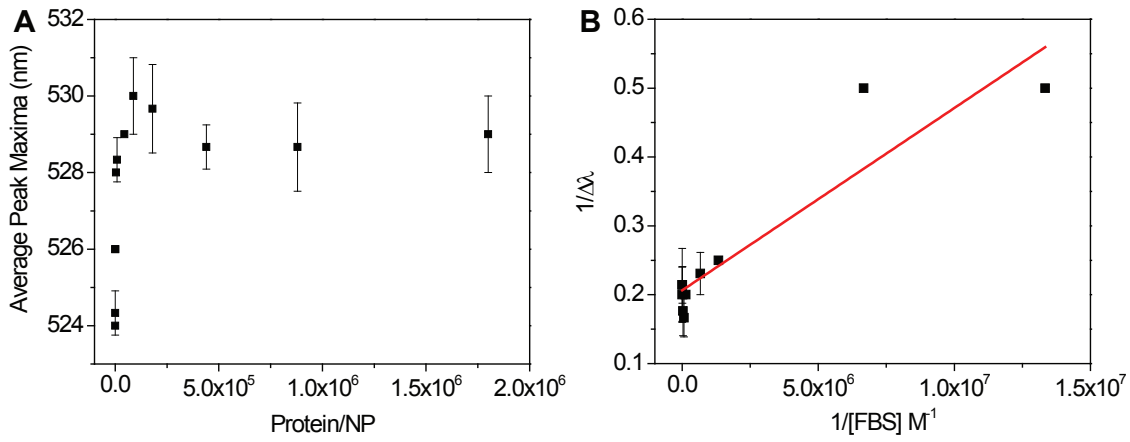

Figure 17: Langmuir plots of FBS adsorption to gold NPs. (A) Average λ_{max} as a function of protein coverage. (B) Lineweaver-Burk plot of inverse shift in wavelength versus inverse FBS concentration.

Protein-gold NP complexes were formed by incubating gold NPs (0.17 nM) in 0.5% (v/v) FBS for 20 minutes. Complexes were then incubated with cells for 30 minutes. Relative differences in absorbance after incubation in MEM, MEM supplemented with 10% (v/v) FBS, or MEM supplemented with 10 mg·mL^{-1} BSA were normalized to gold NPs incubated with MEM (Figure 18B). Absorption by MEM incubated with cells, but without NPs, was negligible. These measurements show that 10% (v/v) FBS inhibits the cellular binding of gold NPs, similar to the aggregated gold NPs (Figure 15), carboxylate-modified QDs (Figure 12), and carboxylate-modified polystyrene NPs,[3] although the inhibition is less extensive. BSA alone also inhibits the cellular binding of the gold NPs. We did not observe a statistically significant difference between the gold NP binding measured for FBS and BSA. Cellular binding of the single protein-gold NP complexes was also imaged with dark field microscopy (Figure 19). While binding of the complexes to cells is observed, quantification is difficult due to decreased scattering by individual gold NPs.

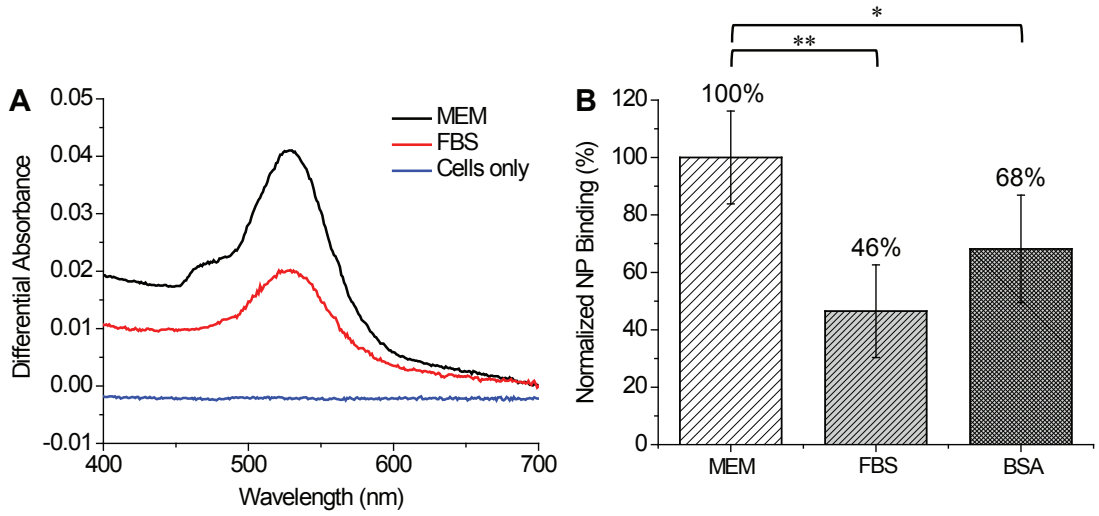

Figure 18: Cellular binding of protein-gold NP complexes was measured using the absorption spectra of gold NPs before and after incubation with the cells. (A) Representative difference spectra of gold NPs after incubation with cells in MEM (black), MEM supplemented with FBS (red), or cells in the absence of NPs (cells only, blue). (B) Binding of protein-gold NP complexes in MEM, MEM supplemented with FBS (FBS), and MEM supplemented with BSA (BSA). (Statistical p-values: *$p < 0.05$; **$p < 0.01$; there was no statistically significant difference between FBS and BSA.)

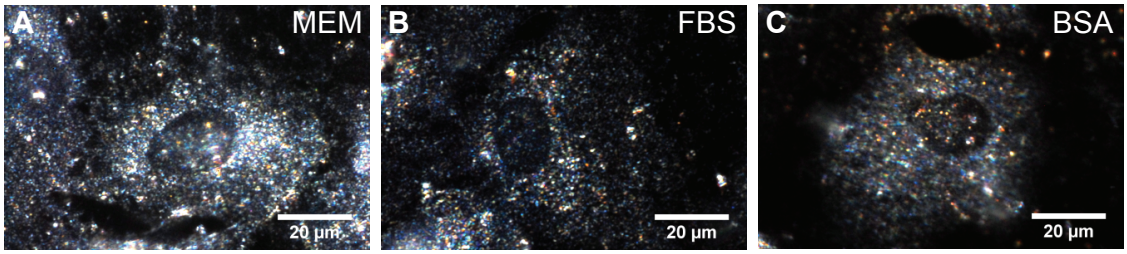

Figure 19: Dark-field microscopy images of citrate-modified protein-gold NP complexes (yellow) bound to BS-C-1 cells in (A) MEM, (B) MEM supplemented with FBS, and (C) MEM supplemented with BSA.

4.2.3 Low-Density Lipoprotein

Low-density lipoprotein (LDL) was used as a representative anionic biological NP. Unlike QDs and gold NPs, LDL has a dedicated cellular receptor.[10] The cellular binding of LDL was observed by fluorescently labeling LDL with DiD, a red lipophilic dye. DiD-labeled LDL (100 μg·mL^{-1}) was then incubated with BS-C-1 cells at 4 °C for 20 minutes in MEM and MEM supplemented with 10% (v/v) FBS. In the absence of serum proteins, significant binding of LDL to cells was observed (Figure 20A). In the presence of serum proteins, cellular binding of anionic LDL decreases (Figure 20B). These results demonstrate that the cellular binding of anionic LDL follows the same trends as carboxylate-modified QDs (Figure 12), citrate-modified gold NPs (Figure 15), and carboxylate-modified polystyrene NPs.[3] BSA alone does not inhibit the cellular binding of LDL (Figure 20C). This suggests that lower abundance proteins in FBS, most likely lipoproteins, are responsible for inhibiting LDL binding to the cell surface. These results were quantified with flow cytometry using the same methods as for the carboxylate-modified QDs (Figure 13). The quantitative flow cytometry data is in agreement with the qualitative results from fluorescence microscopy (Figure 20). The presence of 10% (v/v) FBS inhibits the binding of LDL relative to MEM alone (Figure 21, 66% binding), while the addition of 10 mg·mL^{-1} BSA actually increases binding (Figure 21, 171% binding). Fluorescence microscopy experiments were repeated in HeLa cells yielding similar trends (data not shown).

4.3 Conclusions

The common theme that emerges from these experiments is that a broad range of anionic NPs can form protein-NP complexes and that the cellular binding of these complexes is inhibited by free serum proteins in solution. The cellular binding of carboxylate-modified QDs, citrate-modified colloidal gold NPs, and LDL is inhibited by extracellular serum proteins, similar to previous results for carboxylate-modified

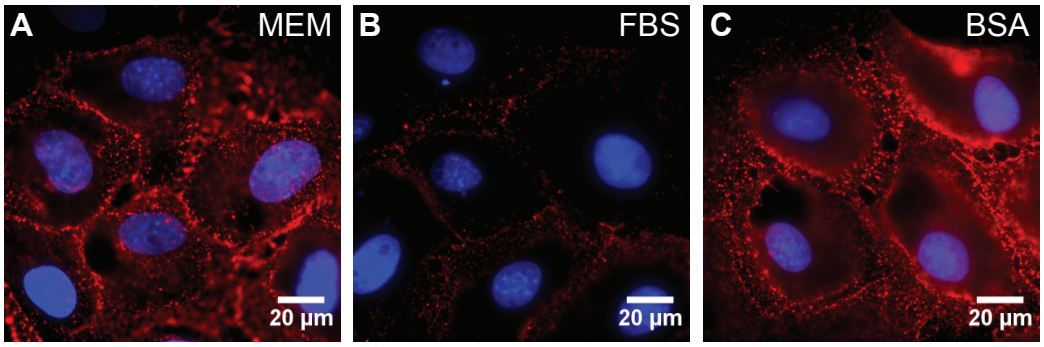

Figure 20: Fluorescence microscopy images of LDL fluorescently labeled with DiD (red) bound to BS-C-1 cells at 4 °C. Nuclei are stained with DAPI (blue). LDL-DiD was incubated with cells in (A) MEM, (B) MEM supplemented with FBS, and (C) MEM supplemented with BSA.

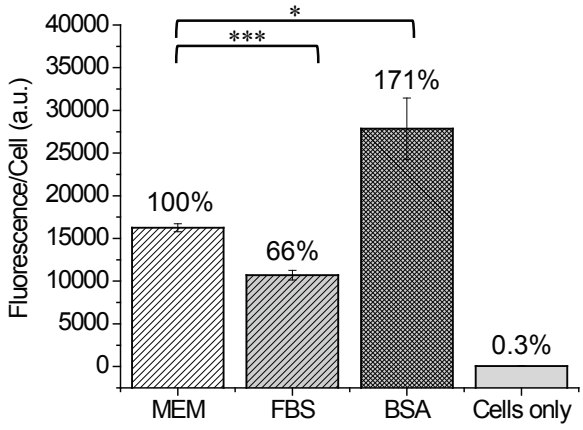

Figure 21: Cellular binding of LDL particles in MEM, MEM supplemented with FBS (FBS), and MEM supplemented with BSA (BSA) quantified with flow cytometry. Autofluorescence from cells in the absence of LDL (cells only) is shown for comparison. Binding was normalized to 100% in MEM. (Statistical p-values: *$p < 0.05$; ***$p < 0.001$)

polystyrene NPs.[3] While this list of NPs is not comprehensive, it demonstrates that cellular binding trends are consistent for a range of NPs with diverse surface modifications and compositions. In the case of QDs, the competition of QDs with BSA for cellular binding sites suggests that the protein-QD complexes utilize BSA receptors on the cell surface. This may also be true for gold NPs, although the competition is less extensive. We have explored different methods for studying the cellular binding of gold NPs, and the relative percent binding does appear to be dependent upon the method used, i.e. flow cytometry or UV-Vis absorption spectroscopy. For LDL, a low abundance protein within the FBS mixture is likely responsible for the inhibition of cellular binding. NPs used in biological and medical applications will encounter a complex environment of extracellular proteins. Our results show that anionic NPs will likely have inhibited cellular binding when proteins are present, possibly limiting their efficacy. These results further support the necessity of characterizing NP interactions with cells in a realistic, biological environment where the presence of extracellular proteins can greatly alter binding. The following chapter examines the underlying molecular basis for the differences in the cellular binding of protein-NP complexes as a function of the structure of adsorbed corona proteins.

4.4 References

[1] Lynch, I., Cedervall, T., Lundqvist, M., Cabaleiro-Lago, C., Linse, S., and Dawson, K. A., "The nanoparticle-protein complex as a biological entity; A complex fluids and surface science challenge for the 21st century." *Adv. Colloid Interface Sci.*, **2007**, *134-135*, 167–174.

[2] Walczyk, D., Bombelli, F. B., Monopoli, M. P., Lynch, I., and Dawson, K. A., "What the cell "sees" in bionanoscience." *J. Am. Chem. Soc.*, **2010**, *132*, 5761–5768.

[3] Fleischer, C. C. and Payne, C. K., "Nanoparticle surface charge mediates the cellular receptors used by protein-nanoparticle complexes." *J. Phys. Chem. B*, **2012**, *116*, 8901–8907.

[4] Fleischer, C. C., Kumar, U., and Payne, C. K., "Cellular binding of anionic nanoparticles is inhibited by serum proteins independent of nanoparticle composition." *Biomater. Sci.*, **2013**, *1*, 975–982.

[5] Alivisatos, A. P., Gu, W., and Larabell, C., "Quantum dots as cellular probes." *Annu. Rev. Biomed. Eng.*, **2005**, *7*, 55–76.

[6] Mattoussi, H., Palui, G., and Na, H. B., "Luminescent quantum dots as platforms for probing *in vitro* and *in vivo* biological processes." *Adv. Drug Delivery Rev.*, **2012**, *64*, 138–166.

[7] Michalet, X., Pinaud, F. F., Bentolila, L. A., Tsay, J. M., Doose, S., Li, J. J., Sundaresan, G., Wu, A. M., Gambhir, S. S., and Weiss, S., "Quantum dots for live cells, *in vivo* imaging, and diagnostics." *Science*, **2005**, *307*, 538–544.

[8] Giljohann, D., Seferos, D., Daniel, W., Massich, M., Patel, P., and Mirkin, C., "Gold nanoparticles for biology and medicine." *Angew. Chem., Int. Ed.*, **2010**, *49*, 3280–3294.

[9] Dreaden, E. C., Alkilany, A. M., Huang, X., Murphy, C. J., and El-Sayed, M. A., "The golden age: Gold nanoparticles for biomedicine." *Chem. Soc. Rev.*, **2012**, *41*, 2740–2779.

[10] Brown, M. S. and Goldstein, J. L., "A receptor-mediated pathway for cholesterol homeostasis." *Science*, **1986**, *232*, 34–47.

[11] Alberts, B., Bray, D., Lewis, J., Raff, M., Roberts, K., and Watson, J. D., *Molecular Biology of the Cell*. Garland Publishing Inc., New York, 3rd edn., **1994**.

[12] Cady, N. C., Strickland, A. D., and Batt, C. A., "Optimized linkage and quenching strategies for quantum dot molecular beacons." *Mol. Cell. Probes*, **2007**, *21*, 116–124.

[13] Freshney, R. I., *Culture of Animal Cells*. John Wiley and Sons, Inc., Hoboken, 5th edn., **2005**.

[14] Pieper, R., Gatlin, C. L., Makusky, A. J., Russo, P. S., Schatz, C. R., Miller, S. S., Su, Q., McGrath, A. M., Estock, M. A., Parmar, P. P., Zhao, M., Huang, S. T., Zhou, J., Wang, F., Esquer-Blasco, R., Anderson, N. L., Taylor, J., and Steiner, S., "The human serum proteome: Display of nearly 3700 chromatographically separated protein spots on two-dimensional electrophoresis gels and identification of 325 distinct proteins." *Proteomics*, **2003**, *3*, 1345–1364.

[15] Anderson, N. L. and Anderson, N. G., "The human plasma proteome: History, character, and diagnostic prospects." *Mol. Cell. Proteomics*, **2002**, *1*, 845–867.

[16] Adkins, J. N., Varnum, S. M., Auberry, K. J., Moore, R. J., Angell, N. H., Smith, R. D., Springer, D. L., and Pounds, J. G., "Toward a human blood serum proteome: Analysis by multidimensional separation coupled with mass spectrometry." *Mol. Cell. Proteomics*, **2002**, *1*, 947–955.

[17] Pastan, I. and Willingham, M., "Journey to the center of the cell: Role of the receptosome." *Science*, **1981**, *214*, 504–509.

[18] Szymanski, C. J., Yi, H., Liu, J. T., Wright, E. R., and Payne, C. K., "Imaging intracellular quantum dots: Fluorescence microscopy and transmission electron microscopy." *In* Rosenthal, S. J. and Wright, D. X., eds., "Nanobiotechnology Protocols," Humana Press, **2012**.

[19] Callaini, G., Dallai, R., and Riparbelli, M. G., "Microfilament distribution in cold-treated Drosophila embryos." *Exp. Cell Res.*, **1991**, *194*, 316–321.

[20] Watts, R. G. and Howard, T. H., "Evidence for a gelsolin-rich, labile F-actin pool in human polymorphonuclear leukocytes." *Cell Motil. Cytoskel.*, **1992**, *21*, 25–37.

[21] Goldenthal, K. L., Pastan, I., and Willingham, M. C., "Initial steps in receptor-mediated endocytosis - The influence of temperature on the shape and distribution of plasma-membrane clathrin-coated pits in cultured mammalian-cells." *Exp. Cell Res.*, **1984**, *152*, 558–564.

[22] Harding, C., Heuser, J., and Stahl, P., "Receptor-mediated endocytosis of transferrin and recycling of the transferrin receptor in rat reticulocytes." *J. Cell Biol.*, **1983**, *97*, 329–339.

[23] Röcker, C., Potzl, M., Zhang, F., Parak, W. J., and Nienhaus, G. U., "A quantitative fluorescence study of protein monolayer formation on colloidal nanoparticles." *Nat. Nanotechnol.*, **2009**, *4*, 577–580.

[24] Gessner, A., Lieske, A., Paulke, B.-R., and Müller, R. H., "Functional groups on polystyrene model nanoparticles: Influence on protein adsorption." *J. Biomed. Mater. Res., Part A*, **2003**, *65A*, 319–326.

[25] Jedlovszky-Hajdú, A., Bombelli, F. B., Monopoli, M. P., Tombácz, E., and Dawson, K. A., "Surface coatings shape the protein corona of SPIONs with relevance to their application *in vivo*." *Langmuir*, **2012**, *28*, 14983–14991.

[26] Casals, E., Pfaller, T., Duschl, A., Oostingh, G. J., and Puntes, V., "Time evolution of the nanoparticle protein corona." *ACS Nano*, **2010**, *4*, 3623–3632.

[27] Brewer, S. H., Glomm, W. R., Johnson, M. C., Knag, M. K., and Franzen, S., "Probing BSA binding to citrate-coated gold nanoparticles and surfaces." *Langmuir*, **2005**, *21*, 9303–9307.

[28] Zhu, Y., Li, W., Li, Q., Li, Y., Li, Y., Zhang, X., and Huang, Q., "Effects of serum proteins on intracellular uptake and cytotoxicity of carbon nanoparticles." *Carbon*, **2009**, *47*, 1351–1358.

[29] Shang, L., Dörlich, R. M., Trouillet, V., Bruns, M., and Nienhaus, G. U., "Ultrasmall fluorescent silver nanoclusters: Protein adsorption and its effects on cellular responses." *Nano Res.*, **2012**, *5*, 531–542.

[30] Dobrovolskaia, M. A., Patri, A. K., Zheng, J., Clogston, J. D., Ayub, N., Aggarwal, P., Neun, B. W., Hall, J. B., and McNeil, S. E., "Interaction of colloidal gold nanoparticles with human blood: Effects on particle size and analysis of plasma protein binding profiles." *Nanomed: Nanotechnol. Biol. Med.*, **2009**, *5*, 106–117.

[31] Dominguez-Medina, S., McDonough, S., Swanglap, P., Landes, C. F., and Link, S., "*In situ* measurement of bovine serum albumin interaction with gold nanospheres." *Langmuir*, **2012**, *28*, 9131–9139.

[32] Chakraborty, S., Joshi, P., Shanker, V., Ansari, Z. A., Singh, S. P., and Chakrabarti, P., "Contrasting effect of gold nanoparticles and nanorods with different surface modifications on the structure and activity of bovine serum albumin." *Langmuir*, **2011**, *27*, 7722–7731.

CHAPTER V

ROLE OF CORONA PROTEIN STRUCTURE ON THE BINDING OF PROTEIN-NANOPARTICLE COMPLEXES

5.1 Introduction

The protein corona controls the cellular interactions of nanoparticles (NPs) by determining the cell surface receptor used by the protein-NP complex.[1–4] In Chapter 3, for a model system of polystyrene NPs, we observed that protein-NP complexes formed with cationic NPs are directed to scavenger receptors while complexes formed with anionic NPs bind to native protein receptors.[1] These results were extended in Chapter 4 to anionic quantum dots, colloidal gold NPs, and low-density lipoprotein, a biological NP.[2] The cellular binding of each of these biomedically relevant NPs was inhibited by free serum proteins, observations consistent with experiments using polystyrene NPs. While we observed in Chapters 3 and 4 that charge is a dominating factor in the cellular binding of protein-NP complexes, the mechanism for these differences was unknown. In this chapter, we describe a comprehensive study that relates the structure of proteins adsorbed on the NP surface to the cellular receptors used by protein-NP complexes.

To advance the use of NPs for applications in biology and medicine, it is necessary to understand, on a molecular level, the interaction between adsorbed proteins, NPs, and cells. The interplay is dynamic as the adsorbed proteins determine the interactions of NPs with cells,[3–7] but the NP itself changes the structure and molecular properties of the proteins in the corona.[7–13] In order to unravel the relationship between the structure of the corona proteins and the cell surface receptors used by the protein-NP complex, we characterized a model system of anionic, carboxylate-modified and

cationic, amine-modified polystyrene NPs with similar diameters. Bovine serum albumin (BSA) adsorbs onto the surface of both anionic and cationic NPs resulting in nearly identical, net anionic, protein-NP complexes. Although the same protein forms the corona, these protein-NP complexes bind to different cellular receptors. BSA-NP complexes formed with anionic NPs bind to native protein receptors, while BSA-NP complexes formed with cationic NPs bind to scavenger receptors. Given that the same protein results in two different cellular outcomes, this provides an ideal system to probe the relationship between protein structure and the cell surface receptors. Using circular dichroism (CD) spectroscopy, we determined that the native structure of BSA is retained after binding to anionic NPs, while BSA structure is disrupted on cationic NPs. Isothermal titration calorimetry (ITC) was used to determine equilibrium association constants, enthalpy of adsorption, and binding stoichiometry of BSA on both anionic and cationic NPs. Fluorescence quenching experiments support the trends observed with ITC.

The use of NPs for biological and biomedical applications requires a detailed understanding of the protein corona.[14–16] As all NPs in a physiological environment are likely to acquire some extent of a protein corona, it is important to understand how the protein corona will control the interaction of the NP with the cell. This chapter illustrates the molecular-level relationship between serum protein secondary structure, NPs, and cell surface receptors, providing a foundation for rational targeting of diagnostic and therapeutic NPs.

5.2 Results

Experiments were carried out using polystyrene NPs in a range of diameters with either an anionic, carboxylate-modified or cationic, amine-modified surface. Anionic and cationic NPs used for comparison were matched as closely as possible in diameter. We used fluorescent NPs for fluorescence microscopy and flow cytometry experiments.

Dark, non-fluorescent NPs were used for experiments in which the NP fluorescence would interfere with the measurement. The hydrodynamic diameter (d_h) and zeta potential (ZP) of all NPs was measured in water (Table 4). The diameter supplied by the manufacturer, which can differ from the hydrodynamic diameter depending on characterization method, is used to denote the NP throughout the text. All values are reported as the mean and standard deviation of at least three experiments.

Table 4: Hydrodynamic diameter (d_h) and zeta potential (ZP) of the NPs used in the course of experiments

	NPs	d_h(nm)	ZP (mV)
Fluorescent	93 nm COOH	102.5 ± 1.6	-30.1 ± 5.4
	87 nm NH_2	152.7 ± 3.2	39.2 ± 3.6
	200 nm COOH	236.2 ± 3.3	-31.0 ± 1.6
	200 nm NH_2	270.1 ± 9.3	19.9 ± 3.4
Dark	60 nm COOH	64.1 ± 1.4	-39.8 ± 3.9
	58 nm NH_2	63.4 ± 1.2	40.3 ± 4.0

The transmission electron microscopy (TEM) diameter of the fluorescent NPs is reported in Chapter 3, but was not provided by the manufacturer for the dark NPs. TEM images of both 60 nm carboxylate-modified and 58 nm amine-modified NPs were acquired under our experimental conditions with the help of Yusuf Uddin in the lab of Professor Ingeborg Schmidt-Krey. Images were acquired of unwashed (140 nM, Figure 22) and washed (14 nM, Figure 23) NPs in Minimum Essential Medium (MEM) and MEM supplemented with 10 mg·mL^{-1} BSA. The Feret, or longest, diameter was measured from the TEM images. The mean TEM diameter of the unwashed NPs in MEM was 54.6 ± 7.6 for the 60 nm NPs (n = 101 NPs) and 53.6 ± 7.6 for the 58 nm NPs (n = 107 NPs). Histograms show the size distribution of the NPs fit to a Gaussian distribution (Figure 24). Protein was visible on the unwashed NPs

after incubation in MEM supplemented with BSA (Figure 22, MEM + BSA). The protein layer was not evenly distributed over the surface of either NP. We observed an increase in diameter of ∼7-8 nm on both the 60 nm and 58 nm NPs after BSA adsorption.

The diameters of washed 60 nm and 58 nm NPs after incubation in MEM were 51.9 ± 5.3 (n = 41 NPs) and 52.7 ± 6.1 (n = 37 NPs), respectively. After washing the NPs in MEM twice via centrifugation, the diameter was unchanged relative to the diameter of the unwashed NPs in MEM, demonstrating that the wash steps do not alter the NP size. Following incubation in MEM supplemented with 10 mg·mL^{-1} BSA and four wash steps via centrifugation, the diameters of the 60 nm and 58 nm NPs were 50.2 ± 6.2 nm (n = 84 NPs) and 51.6 ± 6.3 nm (n = 66 NPs), respectively. It is difficult to observe a protein layer on either NP surface after washing.

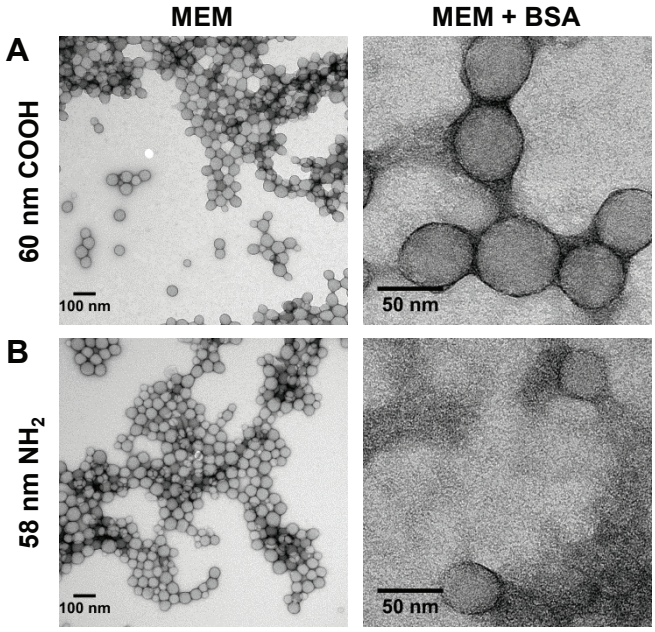

Figure 22: TEM images of unwashed 60 nm carboxylate-modified (60 nm COOH) and 58 nm amine-modified (58 nm NH_2) NPs in MEM and MEM supplemented with BSA.

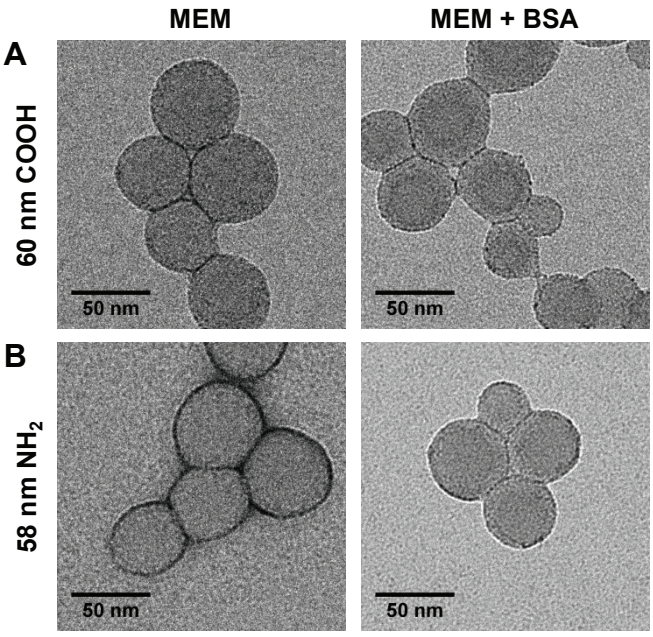

Figure 23: TEM images of washed 60 nm carboxylate-modified (60 nm COOH) and 58 nm amine-modified (58 nm NH_2) NPs in MEM and MEM supplemented with BSA.

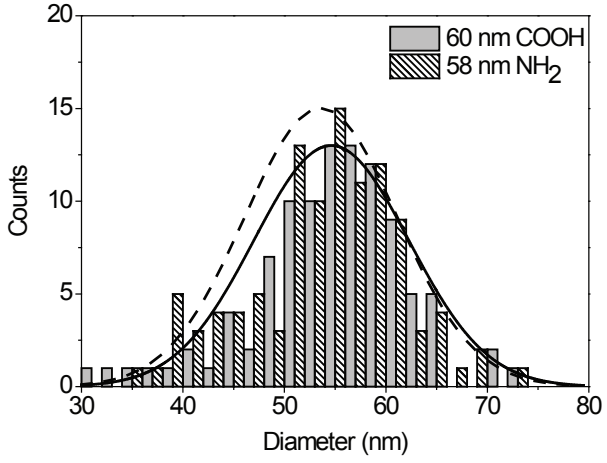

Figure 24: TEM diameters of 60 nm carboxylate-modified (60 nm COOH) and 58 nm amine-modified (58 nm NH_2) NPs. Histograms are fit to a Gaussian distribution.

5.2.1 Protein Corona Formation

The TEM images demonstrate that protein is present on both anionic and cationic NPs. However, the TEM images are taken of dried NPs, and NPs used in biological systems will be in an aqueous solution. To confirm that BSA forms a protein corona on both anionic and cationic NPs in a representative biological environment, 60 nm carboxylate-modified (14 nM) and 58 nm amine-modified (0.4 nM) NPs were incubated in MEM supplemented with 10 mg·mL^{-1} BSA for 10 minutes at 4 °C. These conditions are identical to those used in cellular binding experiments. Free BSA was removed from solution with four wash steps consisting of centrifugation, removal of supernatant, and resuspension in water. This method has been shown to remove unbound protein from solution.[1] After the final wash, the pellet was resuspended in a buffer containing 6% (w/v) sodium dodecyl sulfate (SDS), a detergent that removes bound BSA,[1] and the supernatant was loaded onto a polyacrylamide gel (4-20% gradient). For both anionic and cationic NPs, a protein band is present at ∼66 kDa, the molecular weight of BSA (Figure 25). NPs resuspended in H_2O rather than SDS leads to the absence of a protein band on the gel (Figure 25). The protein observed following treatment with SDS is the corona.

Dynamic light scattering was used to monitor the hydrodynamic diameter, polydispersity index (PDI), and zeta potential of the NPs in response to the presence of BSA (Figure 26). For the 60 nm anionic, carboxylate-modified NPs, increasing concentrations of BSA led to an increase in hydrodynamic diameter (64.1 ± 1.4 in water to 69.8 ± 3.4 in 10 mg·mL^{-1} BSA) and slight aggregation of the NPs, indicated by the increasing PDI (Figure 26A). For the 58 nm cationic, amine-modified NPs, the addition of BSA led to a significantly larger increase in both hydrodynamic diameter and PDI (Figure 26B). At relatively low protein concentrations (0.01 - 0.1 mg·mL^{-1} BSA), adsorption of negatively charged proteins cause the initially cationic NPs to become nearly neutral (Figure 26D). The reduction in surface charge is responsible

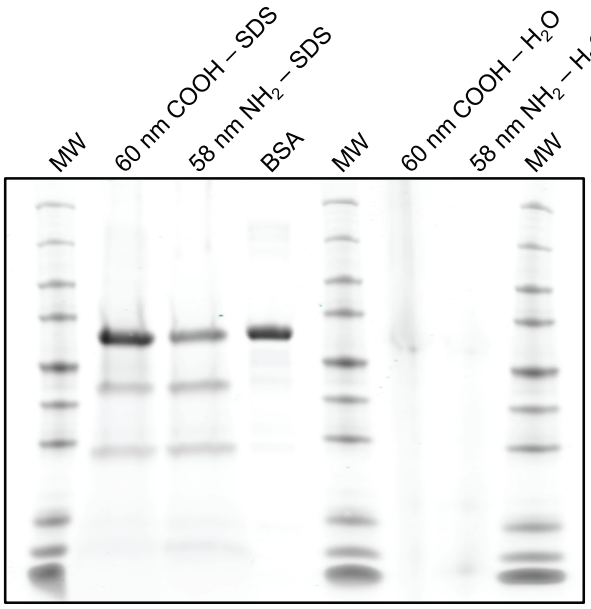

Figure 25: Gel electrophoresis of 60 nm carboxylate-modified (60 nm COOH) and 58 nm amine-modified (58 nm NH_2) NPs following incubation in MEM supplemented with BSA confirms the presence of a protein corona. SDS was used to remove the protein corona from the NP surface. Incubation of NPs in H_2O, rather than SDS, led to no visible protein. BSA, in the absence of NPs, is shown for reference. Molecular weight (MW) marker shows 225, 150, 100, 75, 50, 35, 25, 15, 10, and 5 kDa.

for the observed aggregation of the cationic NPs. These large aggregates are not observed in cell experiments as they are likely removed, along with unbound NPs, during the wash steps prior to analysis. The initial zeta potential of the anionic NPs in water is -39.8 ± 3.9 mV (Figure 26C). In the presence of 10 mg·mL^{-1} BSA, the zeta potential increases to -18.5 ± 1.0 mV, similar to the zeta potential of BSA alone (-22 mV). The cationic NPs, with an initial effective surface charge of 40.3 ± 4.0 in water, become anionic following incubation with BSA, with a final effective surface charge of -19.0 ± 2.2 in the presence of 10 mg·mL^{-1} BSA (Figure 26D). The increased diameter and change in zeta potential support the gel electrophoresis experiments (Figure 25) demonstrating the formation of a BSA corona on both anionic and cationic NPs.

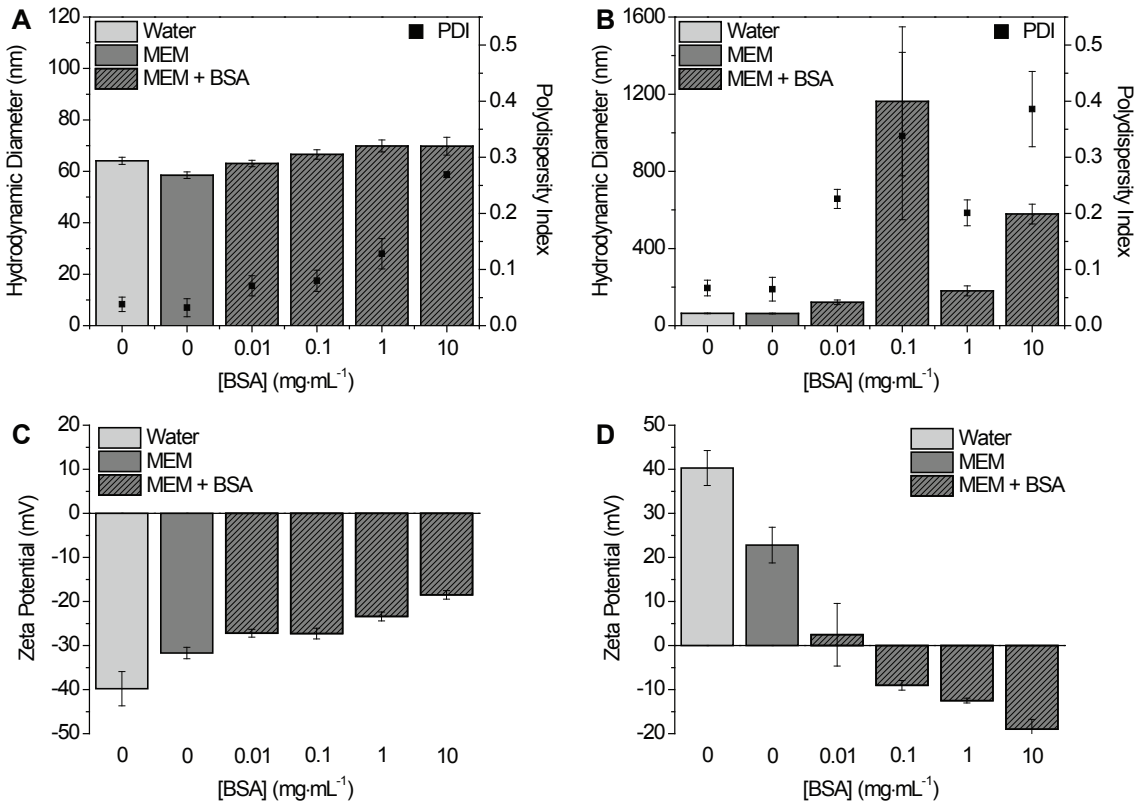

Figure 26: Dynamic light scattering and zeta potential measurements of 60 nm carboxylate-modified and 58 nm amine-modified NPs in the presence of increasing concentrations of BSA. Hydrodynamic diameter and polydispersity index of (A) 60 nm carboxylate-modified and (B) 58 nm amine-modified NPs. Zeta potential of (C) 60 nm carboxylate-modified and (D) 58 nm amine-modified NPs.

Serum, the protein component of whole blood, contains thousands of unique proteins.[17–19] Serum albumin is the most abundant protein in the blood stream,[17,18] and the bovine and human versions are very similar in structure and function.[20,21] We repeated the gel electrophoresis and dynamic light scattering measurements on protein-NP complexes formed with fetal bovine serum (FBS), the complete mixture of serum proteins. Gel electrophoresis shows a band at ∼66 kDa (Figure 27) suggesting that for FBS, the main protein present in the corona of both anionic and cationic NPs is likely BSA. We observe a similar increase in hydrodynamic diameter for FBS-NP complexes (Figure 28A), along with the formation of net negatively charged protein-NP complexes with both anionic and cationic NPs (Figure 28B). NPs incubated in FBS are larger than NPs incubated in BSA (Figure 26), suggesting that other proteins and components in FBS contribute to an increased hydrodynamic diameter.

5.2.2 Cellular Binding of BSA-NP Complexes

The cellular binding of anionic and cationic NPs in the presence of BSA was studied with fluorescence microscopy. Cells are commonly cultured in a buffered solution such as MEM containing inorganic salts, amino acids, and vitamins. The medium is supplemented with serum proteins, typically FBS.[22] Since our goal was to isolate molecular level protein-NP-cell interactions, we used the isolated BSA protein for the majority of experiments.

Fluorescent NPs, either 93 nm anionic, carboxylate-modified or 87 nm cationic, amine-modified, were incubated with monkey kidney epithelial (BS-C-1) cells in MEM or in MEM supplemented with 10 mg·mL^{-1} BSA. This concentration of BSA is approximately equal to the total protein concentration used in typical cell culture (Chapter 2.3). Cellular binding studies were carried out at 4 °C, which allows NP binding to the cell surface but blocks cellular internalization of the NPs.[23–28] For the anionic, carboxylate-modified NPs, we observed NP binding in MEM (Figure 29A).

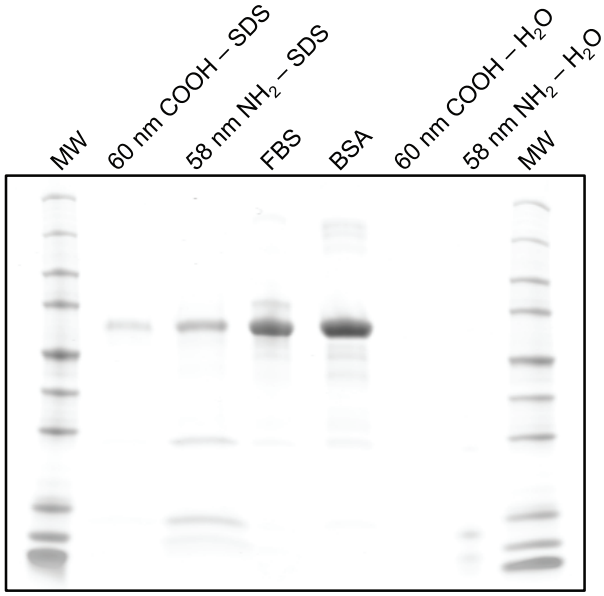

Figure 27: Gel electrophoresis of 60 nm carboxylate-modified (60 nm COOH) and 58 nm amine-modified (58 nm NH_2) NPs following incubation in MEM supplemented with FBS confirms the presence of a protein corona composed primarily of BSA. SDS was used to remove the protein corona from the NP surface. Incubation of NPs in H_2O, rather than SDS, led to no visible protein. FBS and BSA, in the absence of NPs, are shown for reference. Molecular weight (MW) marker shows 225, 150, 100, 75, 50, 35, 25, 15, 10, and 5 kDa.

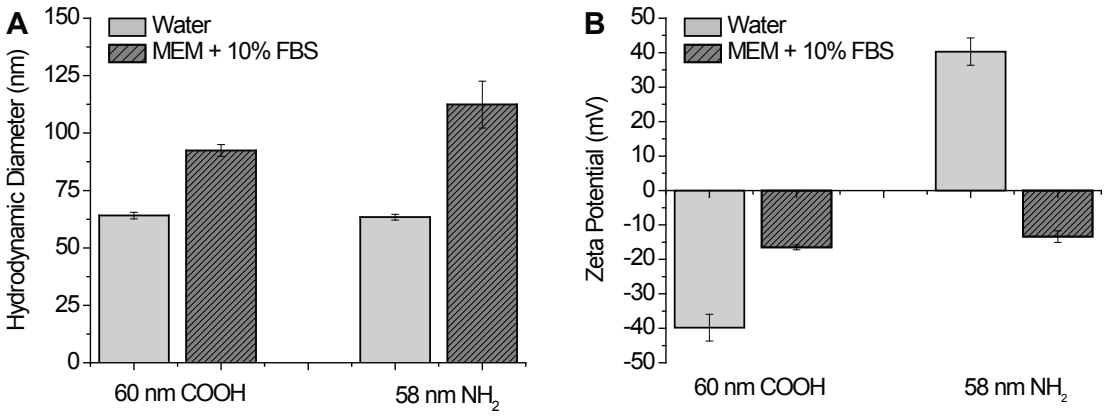

Figure 28: Dynamic light scattering measurements of 60 nm carboxylate-modified (60 nm COOH) and 58 nm amine-modified (58 nm NH_2) NPs in water and in MEM supplemented with FBS. (A) Hydrodynamic diameter. (B) Zeta potential.

The addition of BSA significantly inhibited NP binding. Interestingly, we observe the opposite trend for the cationic, amine-modified NPs. Minimal cellular binding was observed in MEM while the addition of BSA enhances cationic NP binding (Figure 29B). Similar results were observed for Chinese hamster ovary (CHO) cells (Figure 30). CHO cells are also cultured in a different cell culture medium (Ham's F-12) indicating that this trend is not cell type-dependent, nor is it dependent upon the specific formulation of cell culture medium.

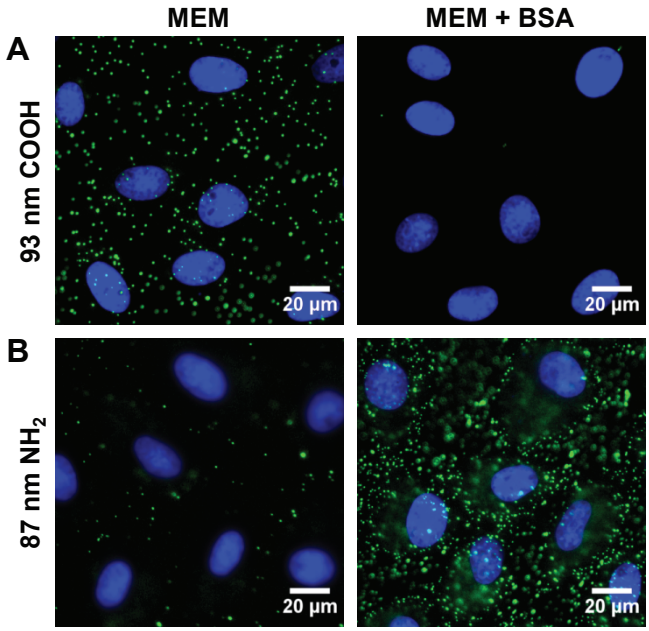

Figure 29: Fluorescence microscopy images show cellular binding of NPs (green) to BS-C-1 cells at 4 °C in MEM and MEM supplemented with BSA (MEM + BSA). (A) 93 nm carboxylate-modified NPs. (B) 87 nm amine-modified NPs. Nuclei are stained with DAPI (blue).

5.2.3 Cellular Receptors used by BSA-NP Complexes

As the cellular binding trends for NPs of similar diameter, but opposite initial surface charge were different (Figure 29), we sought to identify the cellular receptors used by

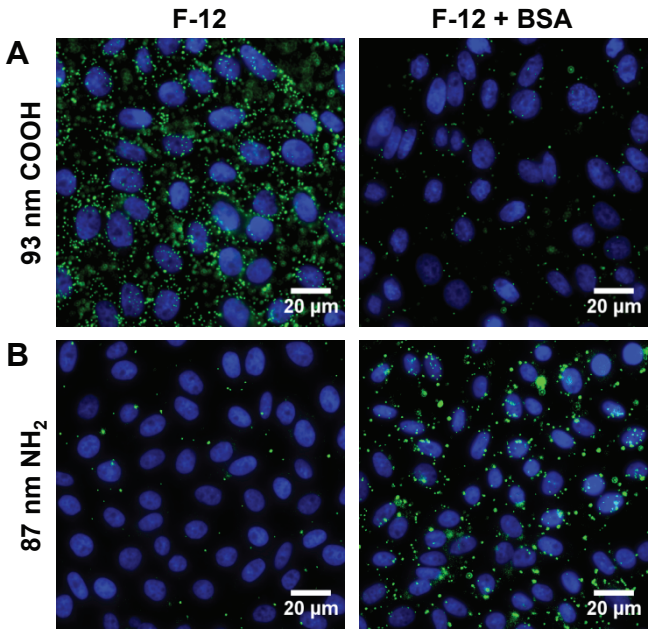

Figure 30: Fluorescence microscopy images show cellular binding of NPs (green) to CHO cells at 4 °C in F-12 and F-12 supplemented with BSA (F-12 + BSA). (A) 93 nm carboxylate-modified NPs. (B) 87 nm amine-modified NPs. Nuclei are stained with DAPI (blue).

the NPs. Albumin has a dedicated receptor on the cell surface as it is an essential blood serum protein.[29–33] Cellular binding of the anionic, carboxylate-modified NPs was inhibited by BSA, suggesting that BSA-NP complexes formed from anionic NPs compete with BSA for binding to the native albumin receptor. To test this hypothesis, we carried out cellular binding competition studies in the presence of increasing concentrations of BSA. If BSA-NP complexes bind to native albumin receptors, we expect increasing concentrations of BSA will lead to a decrease in cellular binding of BSA-NPs. Using flow cytometry as a high-throughput, quantitative measure of cellular binding, we observe decreased BSA-NP binding in the presence of increasing concentrations of BSA (Figure 31A). At a BSA concentration of 10 $mg{\cdot}mL^{-1}$, similar to the concentration used in cell culture, BSA-NP binding was reduced to 32% relative to 100% in the absence of BSA. This supports the hypothesis that BSA-NPs

formed from anionic NPs bind to the native albumin receptors on the cell surface.

Since BSA-NP complexes formed from cationic NPs bind to cells in the presence of excess BSA (Figure 29B), these complexes do not bind to albumin receptors. Previous studies have shown that some NPs and protein-NP complexes bind to scavenger receptors,[1,34–36] specifically scavenger receptors with an affinity for modified albumins.[37–39] To determine if the BSA-NPs formed from cationic NPs bind to scavenger receptors, we carried out competition studies in the presence of both fucoidan (Figure 31B) and polyinosinic acid (Figure 31C), known competitors for scavenger receptors.[38] Competition studies with cationic NPs were carried out in MEM supplemented with 10 $mg{\cdot}mL^{-1}$ BSA. Increasing concentrations of fucoidan and polyinosinic acid both led to decreased cellular binding of the BSA-NP complexes, although fucoidan was a stronger competitor (11% binding at 2500 $\mu g{\cdot}mL^{-1}$ compared to 25%). As a control, we measured cellular binding of BSA-NPs formed from cationic NPs in the presence of polyadenylic acid (Figure 31D). Polyadenylic acid has a similar structure to polyinosinic acid, but is not a competitor for scavenger receptors.[40] We did not observe competition in the presence of polyadenylic acid (polyA, 88% binding compared to a control normalized to 100%). The contribution from cellular autofluorescence is 9% (cells only). The error bar is present but too small to see on the respective scale.

5.2.4 Protein Secondary Structure in the Presence of NPs

Our fluorescence microscopy and flow cytometry experiments show that BSA-NP complexes formed from anionic NPs bind to native protein receptors, while BSA-NP complexes formed from cationic NPs bind to scavenger receptors (Figures 29 and 31). The same protein binding to different cell surface receptors suggests a structural difference in BSA following adsorption on the anionic and cationic NPs. To test this hypothesis, we used circular dichroism (CD) spectroscopy to probe the structure of BSA following incubation with dark, non-fluorescent, polystyrene NPs. For isolated

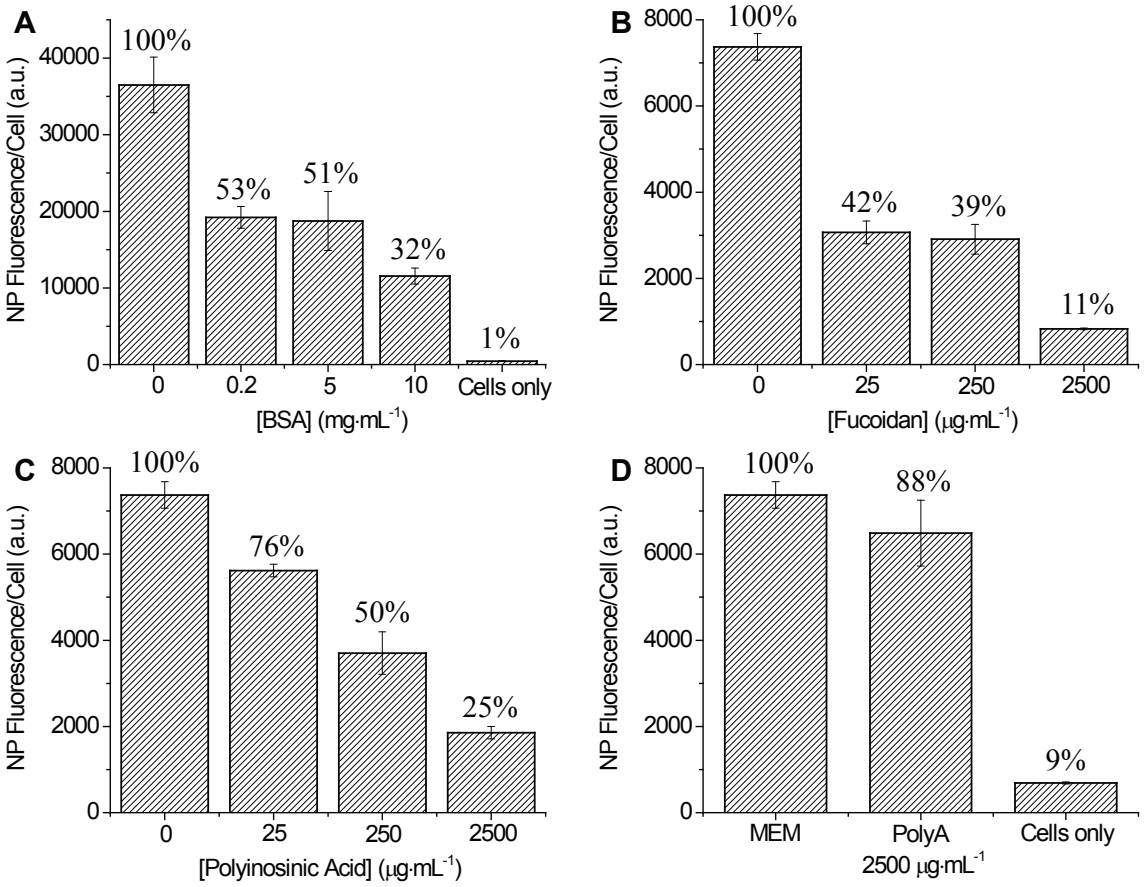

Figure 31: Identification of cell surface receptors using cellular binding competition assays measured with flow cytometry. (A) Cellular binding of 93 nm anionic, carboxylate-modified NPs in MEM with increasing concentrations of BSA. (B) Cellular binding of 87 nm cationic, amine-modified NPs in MEM supplemented with BSA in the presence of increasing concentrations of fucoidan and (C) polyinosinic acid. (D) Control experiments show binding of 87 nm amine-modified NPs in the presence of polyadenylic acid (polyA) and the autofluorescence from cells in the absence of NPs (cells only).

BSA, a primarily α-helical protein, the far-UV CD spectrum contains a positive band at 195 nm and two negative bands at 208 and 222 nm (Figure 32A), in good agreement with previous CD measurements.[41,42] Spectra are in units of mean residue ellipticity (MRE) and each spectrum is the average of 10 consecutive scans.

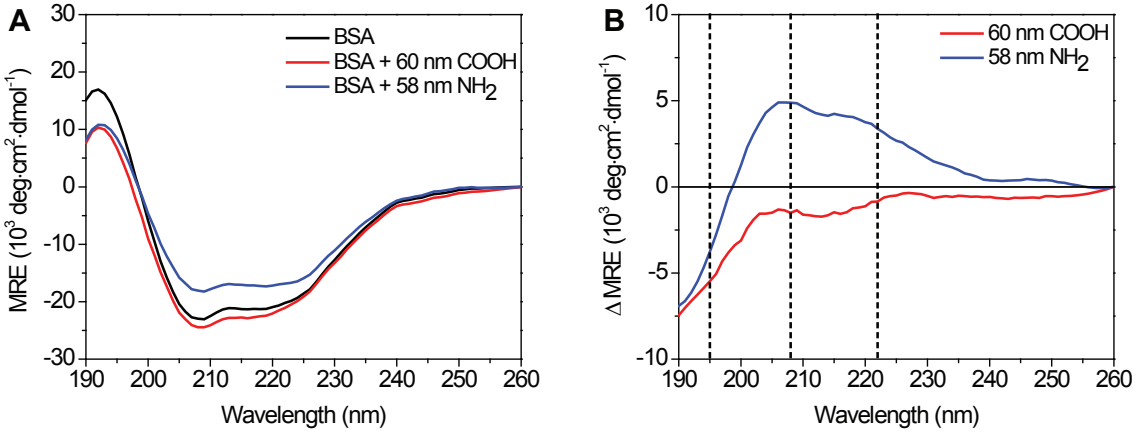

Figure 32: Circular dichroism spectra of BSA in the presence of 60 nm carboxylate-modified NPs (red), 58 nm amine-modified NPs (blue), and in the absence of NPs (black). (A) Raw circular dichroism spectra. (B) Circular dichroism difference spectra were calculated by subtracting the spectrum of BSA from BSA in the presence of 60 nm carboxylate-modified (red) or 58 nm amine-modified NPs (blue). Black dashed lines correspond to spectral peaks at 195, 208, and 222 nm.

Incubation with 60 nm anionic, carboxylate-modified NPs shows little change in the CD spectrum (Figure 32A). In comparison, incubation with 58 nm cationic, amine-modified NPs results in more positive mean residue ellipticity (MRE) values, indicating a loss in protein secondary structure (Figure 32A). CD difference spectra were calculated by subtracting the spectrum of BSA alone from the spectrum of BSA in the presence of NPs (Figure 32B). The difference spectra reveal a larger change in BSA secondary structure in the presence of cationic, compared to anionic, NPs. We observe similar results for BSA in the presence of 200 nm NPs (Figure 33). The

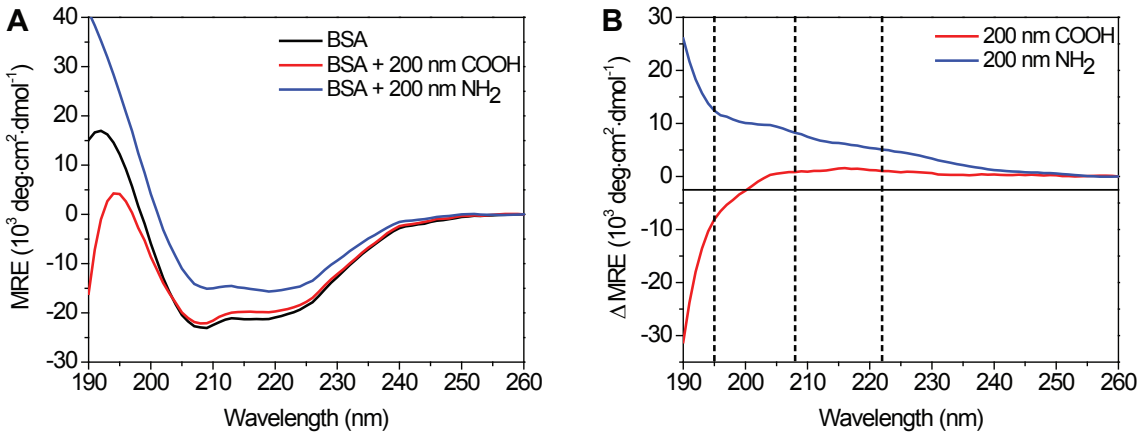

Figure 33: Circular dichroism spectra of BSA in the presence of 200 nm carboxylate-modified NPs (red), 200 nm amine-modified NPs (blue), and in the absence of NPs (black). (A) Raw circular dichroism spectra. (B) Circular dichroism difference spectra were calculated by subtracting the spectrum of BSA from BSA in the presence of 200 nm carboxylate-modified (red) or 200 nm amine-modified NPs (blue). Black dashed lines correspond to spectral peaks at 195, 208, and 222 nm.

percent α-helicity was calculated using the CD peak at 208 nm (Table 5). The α-helicity of BSA alone was 65%, consistent with previous reports.[43,44] For BSA in the presence of the 58 nm and 200 nm cationic, amine-modified NPs, a loss in α-helicity was observed (48% and 37%, respectively), demonstrating that cationic NPs disrupt the secondary structure of BSA. For BSA in the presence of 60 nm anionic, carboxylate-modified NPs, a slight increase in α-helicity to 71% was observed. In the presence of 200 nm carboxylate-modified NPs, there was little change (63%).

Table 5: Percent α-helicity of BSA as a function of NP size and charge

	BSA	COOH NPs		NH_2 NPs	
		60 nm	**200 nm**	**58 nm**	**200 nm**
% α-helix	65	71	63	48	37

In the case of BSA, we observe that adsorption on cationic NPs disrupts the secondary structure of the protein while adsorption on anionic NPs does not affect BSA structure (Figure 32). To determine if this trend was general, we examined the structure of transferrin, an iron-transporting serum protein,[28,45] in the presence of 60 nm carboxylate-modified and 58 nm amine-modified NPs (Figure 34). For transferrin, a loss in secondary structure was observed in the presence of the 60 nm anionic, carboxylate-modified NPs, but not the 58 nm cationic, amine-modified NPs.

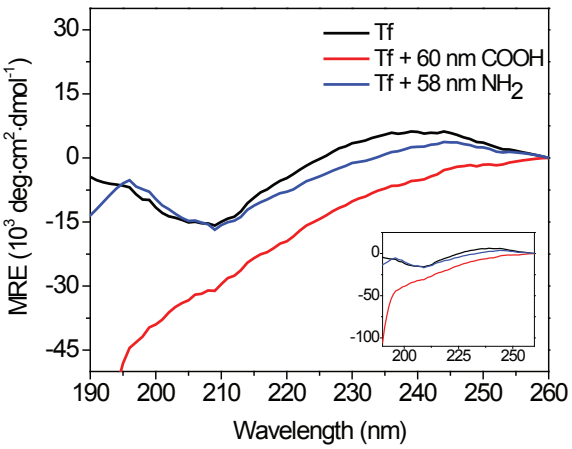

Figure 34: Circular dichroism spectra of transferrin (Tf) in the presence of 60 nm carboxylate-modified NPs (red), 58 nm amine-modified NPs (blue), and in the absence of NPs (black). Inset shows full-scale spectra.

5.2.5 Thermodynamic Parameters of BSA Adsorption on NPs using Isothermal Titration Calorimetry

The equilibrium association constant, enthalpy, and binding stoichiometry of BSA adsorbed on 60 nm anionic, carboxylate-modified NPs and 58 nm cationic, amine-modified NPs was determined using isothermal titration calorimetry (ITC) (Figure 35). The NP concentration was optimized for each individual NP solution so that BSA saturation on the NP surface was achieved. The heat of dilution of BSA into

buffer was subtracted from the titration curve of BSA into the NP solution (Figure 36). As the plots of differential power in Figure 35 have been corrected for BSA dilution, the raw differential power plots were also plotted using the TA Instruments software, NanoAnalyze (Figure 37, top plots). The titration curves are more evident in the bottom plots of integrated heat values, as the enthalpy of BSA dilution has been subtracted from the titration.

An independent site model was used to fit the integrated titration curves and extract thermodynamic parameters (Table 6).[46] The association constant was nearly an order of magnitude higher for BSA adsorbed on anionic NPs with K_a values of 2.4 $\pm$ 0.9 x 10^5 M^{-1} and 4.0 $\pm$ 0.5 x 10^4 M^{-1} for 60 nm anionic, carboxylate-modified and 58 nm cationic, amine-modified NPs, respectively. The enthalpy of BSA binding to the 60 nm carboxylate-modified (-1.4 $\pm$ 0.4 x 10^4 kJ·mol^{-1}) and 58 nm amine-modified (-1.4 $\pm$ 0.7 x 10^4 kJ·mol^{-1}) NPs was almost identical. A significantly greater number of BSA molecules adsorbed onto the surface of the 60 nm NPs (871 $\pm$ 21 proteins per NP) compared to the 58 nm NPs (27 $\pm$ 8 proteins per NP). The percent coverage, relative to a monolayer coverage of 100%, was calculated assuming BSA binds end-on, maximizing the number of BSA molecules in a monolayer.[47,48] The coverage of BSA on the 60 nm carboxylate-modified NPs was 230 $\pm$ 6%, compared with significantly less than a monolayer on the 58 nm amine-modified NPs (8 $\pm$ 2%).

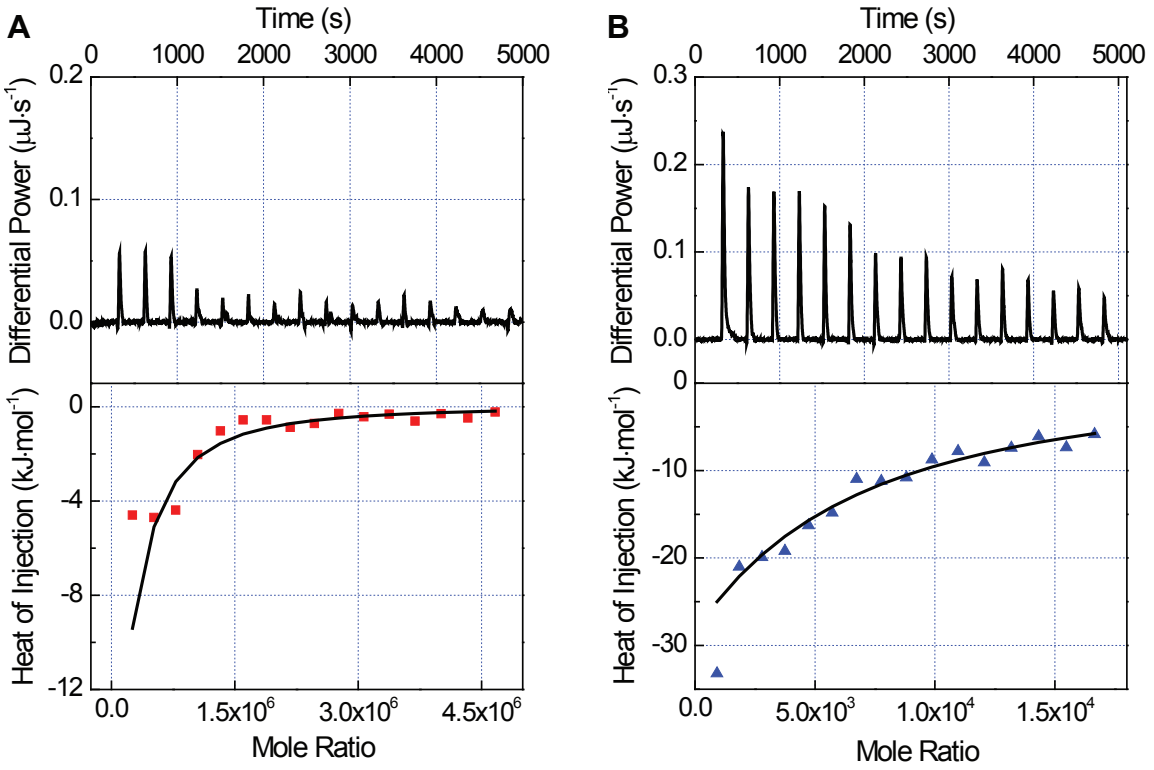

Figure 35: Isothermal titration calorimetry plots of differential power throughout the titration (top) and the integrated heat of injection as a function of the mole ratio of BSA adsorbed onto NPs (bottom). (A) BSA titrated into a solution of 60 nm carboxylate-modified NPs. (B) BSA titrated into a solution of 58 nm amine-modified NPs.

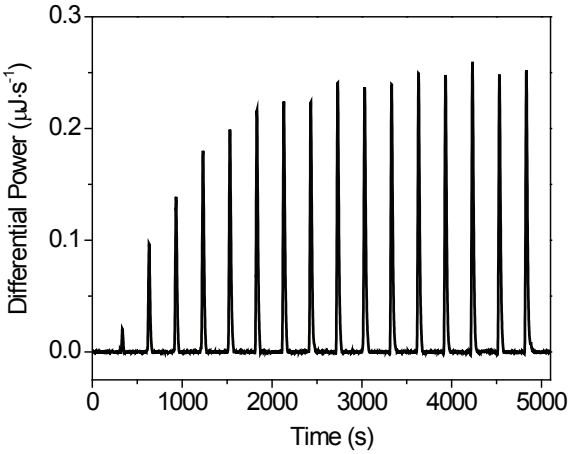

Figure 36: Isothermal titration calorimetry plot of BSA titrated into buffer in the absence of NPs. Peaks were subtracted injection-by-injection from the titration of BSA into a solution containing NPs.

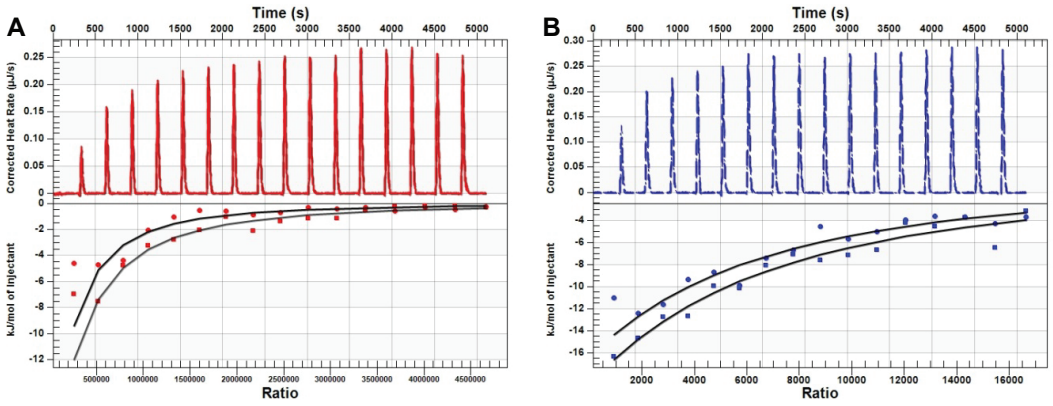

Figure 37: Isothermal titration calorimetry plots of differential power throughout the titration (top) and the integrated heat of injection as a function of the mole ratio of BSA adsorbed onto NPs (bottom) displayed using the TA Instruments software, NanoAnalyze. (A) BSA titrated into a solution of 60 nm carboxylate-modified NPs. (B) BSA titrated into a solution of 58 nm amine-modified NPs. The titration curve is more evident in the bottom plot of integrated heat values as the enthalpy of BSA dilution into buffer has been subtracted from the titration of BSA into NPs.

Table 6: Thermodynamic parameters of BSA adsorption to NPs

NP	K_a (10^5 M^{-1})	ΔH (10^4 kJ·mol^{-1})	Proteins/NP	% Coverage
60 nm COOH	2.4 ± 0.9	-1.4 ± 0.4	871 ± 21	230 ± 6%
58 nm NH_2	0.40 ± 0.05	-1.4 ± 0.7	27 ± 8	8 ± 2%

5.2.6 Fluorescence Spectroscopy of BSA in the Presence of NPs

Fluorescence spectroscopy was used as a complementary technique to measure equilibrium association constants by monitoring the quenching of tryptophan at ∼340 nm (Figure 38A).[49–51] The spectra were corrected by subtracting the contribution from NPs alone and buffer. The intensity at λ_{max} was calculated for each experiment. The ratio of fluorescence intensities in the absence and presence of NPs was plotted versus NP concentration in a Stern-Volmer plot (Figure 38B). As the plots were non-linear at higher NP concentrations, the first four points were used for a linear fit to extract an effective Stern-Volmer equilibrium constant (K_{SV}, Chapter 2.7.2). The effective K_{SV} is approximately equal to the effective K_a.[51] For BSA in the presence of 60 nm carboxylate-modified NPs, the effective K_a is 1.8 ± 0.1 x 10^9 M^{-1}, compared to the 58 nm amine-modified NPs with an effective K_a of 7.7 ± 0.1 x 10^8 M^{-1}. These values are several orders of magnitude higher than the K_a values calculated from ITC data (Table 6).

The normalized fluorescence spectra of BSA in the presence of increasing NP concentrations used to generate the Stern-Volmer plot are shown in Figure 39. The maximum fluorescence emission wavelengths are reported in Table 7. The peak wavelength of BSA in the presence of 58 nm amine-modified NPs was slightly more blue shifted (329 ± 3 nm) at the highest NP concentration of 0.53 nM compared to the 60 nm carboxylate-modified NPs (332 ± 0 nm) relative to BSA in the absence of NPs (339 ± 0.6 nm).

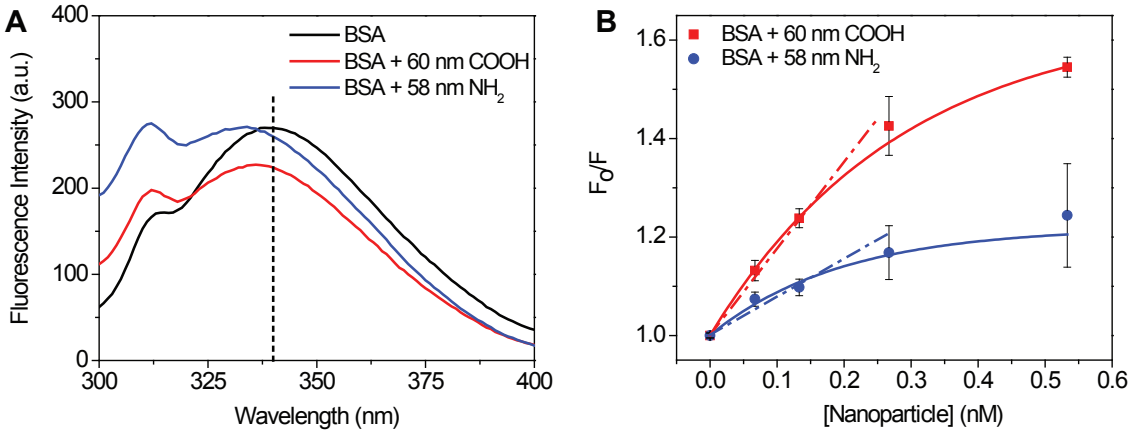

Figure 38: Fluorescence quenching of BSA in the presence of NPs. (A) Raw fluorescence spectra of BSA in the presence of 60 nm carboxylate-modified NPs (red), 58 nm amine-modified NPs (blue), and in the absence of NPs (black). The black dashed line at 340 nm corresponds to the emission from tryptophan residues in BSA. (B) Stern-Volmer plot of BSA quenching in the presence of increasing concentrations of NPs. The contribution from NPs alone and buffer were subtracted from the raw spectra. The solid lines correspond to an exponential fit of the raw data. Dashed lines are the initial slope used to calculate an effective equilibrium constant (Equation 3).

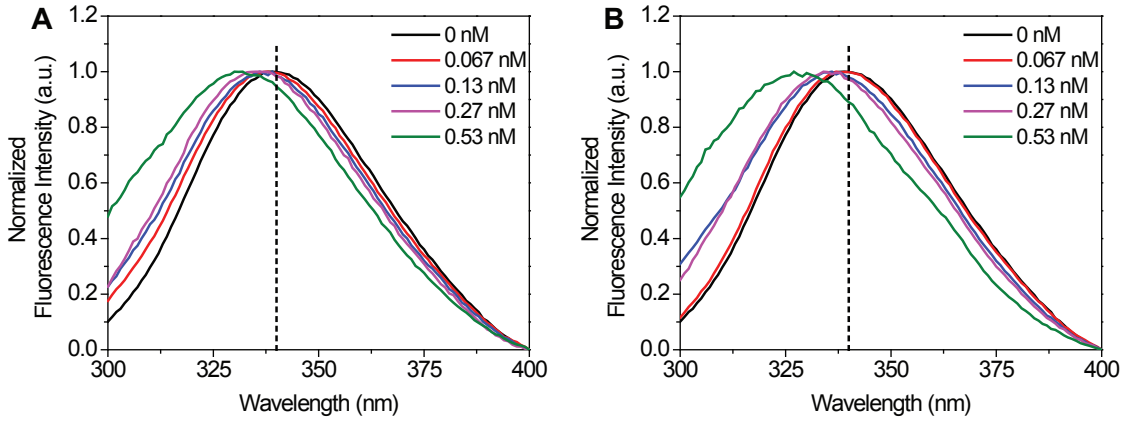

Figure 39: Normalized fluorescence spectra of BSA in the presence of increasing concentrations of (A) 60 nm carboxylate-modified NPs and (B) 58 nm amine-modified NPs.

Table 7: Maximum fluorescence emission wavelengths for BSA in the presence of carboxylate-modified (60 nm COOH) and amine-modified (58 nm NH_2) NPs

NP	0 nM	0.067 nM	0.13 nM	0.27 nM	0.53 nM
60 nm COOH	339 ± 0.6	338 ± 0.6	338 ± 1	335 ± 2	332 ± 0
58 nm NH_2	339 ± 0.6	339 ± 2	336 ± 1	335 ± 2	329 ± 3

5.3 Discussion

5.3.1 Formation of BSA-NP complexes

NPs used in any biological application are exposed to a complex mixture of extracellular proteins that form a protein corona on the NP surface.[3,17–19,47,52–57] Although polyethylene glycol can reduce corona formation, complete inhibition remains a challenge.[58–62] We have characterized the changes in protein secondary structure that result from adsorption to the NP surface and then relate these structural changes to the cell surface receptor used by the protein-NP complex. BSA adsorbs onto both anionic and cationic NPs to form a BSA-NP complex (Figures 25 and 26). Adsorption of proteins onto both anionic and cationic NPs has been observed previously by our group and others.[1–3,5,6,47,55–57,63] Our results confirm that a BSA-NP complex is formed under the conditions used in subsequent experiments. Incubating NPs in the complete mixture of serum proteins present in FBS, rather than isolated BSA, shows that BSA is the only protein detected in the corona (Figure 27), confirming that BSA is a good representative serum protein. Similar results were obtained for gold NPs between 10 and 200 nm.[2,64,65]

We also characterized the 60 nm carboxylate-modified and 58 nm amine-modified NPs using TEM. While TEM is not a solution-based measurement, the TEM diameter provides detailed information about the size distribution of NPs present in experiments (Figure 24). The Feret, or longest, diameter was measured from the TEM images. As the calculated circularity was approximately 1 for both NPs, the

Feret diameter is a good approximation of the NP diameter.

The thickness of the protein layer was measured from the TEM images of unwashed NPs incubated in MEM supplemented with 10 mg·mL^{-1} BSA (Figure 22). The increase in diameter of the NPs in the presence of BSA was ∼7-8 nm. This is consistent with previous reports that a 7 nm increase in diameter was observed on gold NPs coated with BSA.[66] We also observe a high number of protein aggregates in the images of 58 nm amine-modified NPs in the presence of BSA (Figure 22B). The protein aggregates appear as dark patches in the background, suggesting that the presence of amine-modified NPs can cause a structural change to proteins, even proteins not directly adsorbed to the NP surface.

While BSA has an isoelectric point of 4.7 and is net negatively charged at physiological pH,[67] it contains both positive and negative residues.[68,69] Adsorption of BSA onto the surface of anionic, carboxylate-modified NPs results in a slight increase in NP diameter and effective surface charge (Figures 26A and 26C), although the protein-NP complexes remain negatively charged (-18.5 ± 1.0 mV). At higher concentrations of BSA, some aggregation of NPs is observed by an increase in PDI (Figure 26A). The aggregates were removed during wash steps prior to cellular binding and competition assays. Cationic, amine-modified NPs are more sensitive to the addition of BSA. Low concentrations (0.01-0.1 mg·mL^{-1}) of BSA result in a nearly neutral NP that readily aggregates in solution (Figures 26B and 26D). At the BSA concentrations used in these experiments (10 mg·mL^{-1}), the initially cationic NPs become negatively charged (-19.0 ± 2.2 mV). In the presence of 10 mg·mL^{-1} BSA, both anionic and cationic NPs are net anionic, forming BSA-NP complexes that are nearly identical based on dynamic light scattering and zeta potential measurements (Figure 26).

5.3.2 Cellular Binding Trends of BSA-NP Complexes

While BSA-NP complexes formed with anionic and cationic NPs have identical corona compositions and surface charges (-18.5 mV and -19.0 mV, respectively), the cellular binding trends are drastically different. Cellular binding of BSA-NP complexes formed with anionic NPs is inhibited by the presence of excess BSA (Figure 29A). In comparison, the cellular binding of complexes formed with cationic NPs is strongly enhanced by BSA (Figure 29B). This difference in binding is independent of cell type as similar results were obtained for CHO cells (Figure 30). The differences in cellular binding suggest that the BSA-NP complexes formed with anionic and cationic NPs bind to different receptors. In a series of cellular binding competition studies, we observe that protein-NP complexes formed from anionic NPs bind to native albumin receptors, as these complexes are inhibited by increasing concentrations of BSA (Figure 31A). This suggests that BSA on the NP surface is recognized by the native receptor. In comparison, BSA-NP complexes formed with initially cationic NPs bind to scavenger receptors (Figures 31B and 31C).

Scavenger receptors are a broad class of receptors that bind modified low-density lipoproteins, modified proteins, polysaccharides, and polyribonucleotides.[37–39,70,71] Several others have reported that scavenger receptors can bind NPs and protein-NP complexes.[34,35,37–39] Schnitzer *et al.* determined that chemically or structurally modified albumins, including albumin-gold NP complexes, bind preferentially to the glycoprotein (gp) scavenger receptors gp30 and gp18 rather than the general class of modified protein receptors.[37–39] Mirkin *et al.* have observed that oligonucleotide-conjugated gold NPs bind to scavenger receptors.[34,35] Previous results using a complete mixture of FBS showed identical binding trends,[1] demonstrating that this result is not specific to isolated BSA.

Interestingly, for the BSA-NP complexes formed from cationic NPs, we observed that fucoidan is a much stronger competitor than polyinosinic acid (Figures 31B and

31C). At the highest competitor concentration (2500 $\mu g \cdot mL^{-1}$), BSA-NP binding was 11% in the presence of fucoidan, compared to 25% in the presence of polyinosinic acid. It is important to note that the concentration of polyinosinic acid used in these studies was relatively high compared to previously reported concentrations for cellular binding competition,[1,35] further confirming that polyinosinic acid is a less efficient competitor. Polyinosinic acid is a competitor for both gp30 and gp18,[37–39] as well as the general class of modified protein receptors.[72] In comparison, fucoidan is only a competitor for the gp30 and gp18 receptors.[37–39] The same concentration of polyinosinic acid is then less efficient at competing for modified albumin receptor sites as some of the molecules will also bind to general modified protein receptors. We propose that BSA-NP complexes formed from cationic NPs only bind to the receptors for modified albumins, gp30 and gp18, and not the general receptors for modified proteins. As fucoidan is only blocking the gp30 and gp18 receptors, it is a more effective competitor for the BSA-NP complexes. For comparison, we observed that polyinosinic acid competes more with protein-NP complexes formed with a mixture of serum proteins compared with BSA-NP complexes,[1] presumably because the mixture of serum proteins can bind to both types of modified protein receptors. Although further studies are required to determine the exact binding mechanism to specific scavenger receptors, these results highlight subtle differences in molecular-level interactions of NPs with cellular receptors.

5.3.3 Structure of Corona Proteins

The opposite binding trends observed for BSA-NP complexes formed from anionic and cationic NPs provided an optimal model system to study the effect of protein structure on the cellular receptors used by BSA-NP complexes. We hypothesized that BSA adsorbed on anionic NPs retained its native structure allowing the BSA-NP complexes to be recognized by the native albumin receptor. In comparison, we predicted that

BSA adsorbed on cationic NPs was disrupted, likely partially denatured, such that it is no longer recognizable by the native protein receptor and is instead redirected to a scavenger receptor. CD spectra of BSA in the presence of 60 nm anionic NPs show that the secondary structure of BSA is retained (Figure 32). In comparison, there is a loss in α-helicity for BSA in the presence of 58 nm cationic NPs (65% to 48%, Table 5). Similar results were obtained for BSA in the presence of 200 nm NPs (Figure 33). The greater loss in α-helicity on the 200 nm NPs is attributed to more BSA adsorption on the larger NPs, as the spectra include contributions from both free BSA in solution and BSA in direct contact with the NP surface.

While the decrease in α-helicity appears modest, boiled BSA has a similar percentage of α-helices as BSA on carboxylate-modified NPs (71% α-helix, data not shown). This indicates both a significant change in α-helicity for BSA on cationic NPs, as well as a difference in secondary structure for BSA disrupted as a result of boiling versus bound to a cationic NP surface. Changes in protein secondary structure are generally accompanied by the exposure of new peptide sequences in the protein. However, changes in secondary structure precede epitope exposure and higher order structural changes, and ultimately determine the cellular receptors used by the protein.

Based on these results, it is tempting to generalize: proteins maintain their structure following adsorption onto an anionic NP, while cationic NPs will disrupt protein structure. However, individual proteins will interact differently with the NP surface making it difficult to predict structural changes. As an example, we also examined the secondary structure of transferrin, an iron-transporting serum protein.[28,45] Using CD spectroscopy, we found that transferrin was denatured following incubation with anionic, rather than cationic NPs (Figure 34). A possible reason for this difference is illustrated by electrostatic site maps (Figure 40). Like BSA (Figure 40A), transferrin has regions of both positive and negative charge. However many regions of the transferrin surface are nearly neutral suggesting that other interactions (i.e. hydrophobic)

may dominate (Figure 40B). Transferrin contains a mixture of both α-helices and β-sheets, compared to BSA which only contains α-helices. Differences in secondary structure composition also contribute to the overall interaction with charged NPs. The CD spectroscopy experiments demonstrate that changes in protein secondary structure are protein-specific and will likely need to determined experimentally for each protein of interest.

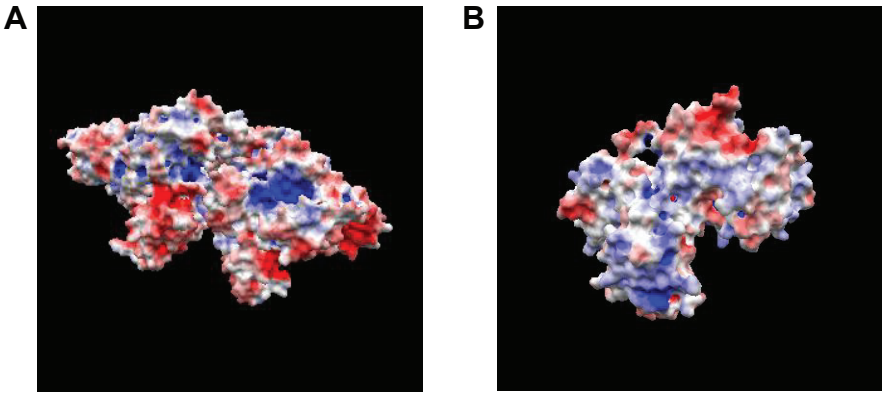

Figure 40: Electrostatic surface maps created with eF-surf. (A) BSA. (B) Transferrin. Red corresponds to negative (-0.1 V), white corresponds to neutral, and blue corresponds to positive (+0.1 V) electrostatic potential.

5.3.4 Thermodynamics of the Protein Corona

A change in protein secondary structure should be associated with changes in adsorption on the NP surface. Using ITC (Figure 35), we observe that fewer proteins adsorbed on the cationic, amine-modified NPs (27 $\pm$ 8 proteins per NP, compared to 871 $\pm$ 21 proteins per NP for anionic NPs). The coverage of BSA on the cationic NPs is likely an underestimate due to dimerization of these NPs during the titration. Similar results were obtained for sulfate-modified polystyrene NPs, which showed less than monolayer adsorption of BSA and disruption of BSA secondary structure.[44] The lower binding stoichiometry is likely due to the loss of BSA secondary structure.

When spread out on the NP surface, fewer BSA molecules can access the surface without an energy cost. This hypothesis is reinforced by the thermodynamic data (Table 6). The enthalpy of BSA binding to anionic and cationic NPs is identical (-1.4 ± 0.4 x 10^4 and -1.4 ± 0.7 x 10^4 kJ·mol^{-1}, respectively) which is surprising given that the maximum BSA adsorption to the surface of the 60 nm NPs is approximately 30-fold greater than on the 58 nm NPs. However, the association of BSA is much stronger on the anionic NP surface (2.4 ± 0.9 x 10^5 compared with 4.0 ± 0.5 x 10^4 M^{-1}), which we attribute to more energetically favorable packing of native BSA and possibly some degree of binding cooperativity. Previous ITC experiments have examined protein adsorption on NPs as a function of protein species and hydrophobicity.[54,63,73,74] Most similar to our measurements are experiments carried out by Baier *et al.* examining BSA adsorption onto ∼200 nm polystyrene NPs.[63] Equilibrium association constants and enthalpies are similar, considering the variability in ITC measurements. However, 27% protein coverage was observed for carboxylate-modified NPs and 63% coverage of amine-modified NPs,[63] compared to 230% and 8%, respectively, in our experiments (Table 6). This difference could be due to multiple factors, namely differences in NP diameter (200 nm versus 60 nm), pH, buffer, and surface modification. One reason for the difference in coverage as a function of NP surface charge is attributed to the magnitude of the surface charge. Baier *et al.* used cationic NPs with an initial zeta potential of +7 mV, compared to our experiments where cationic NPs had a zeta potential of +40 mV. As the number of charged surface groups on the NP has a large effect on electrostatic and hydrophobic interactions with proteins, this is one possibility for the observed difference in surface coverage. However, these prior experiments used BSA titrated into water as a control whereas we used BSA titrated into buffer. It is unclear what buffer was used for ITC experiments, and the enthalpy of ionization of the buffer greatly influences thermodynamic parameters. The differences between our results and previous studies with polystyrene NPs highlights the

difficulty of comparing ITC results under even slightly different conditions.

As a complementary method to ITC, fluorescence quenching was used to measure equilibrium association constants (Figure 38). The non-linear Stern-Volmer plot (Figure 38B) is indicative of a selective quenching mechanism.[50,51] At low NP concentrations, readily accessible tryptophan residues on BSA are quenched uniformly. In the presence of higher NP concentrations, the NP has limited access to BSA residues that can be quenched. Lower accessibility of the NP leads to selective quenching. The stronger association of BSA on 60 nm anionic compared to 58 nm cationic NPs was observed in both the ITC and fluorescence spectroscopy data, although the absolute values differ by several orders of magnitude (e.g. $K_a = 2.4 \pm 0.9$ x 10^5 M^{-1} with ITC versus 1.8 ± 0.1 x 10^9 M^{-1} from fluorescence spectroscopy for 60 nm anionic NPs). Thermodynamic parameters are highly sensitive to experimental conditions and, for our experiments, the buffers required to optimize ITC and fluorescence spectroscopy experiments were not identical. While ITC provides a better quantitative measure of the association constant as it is a direct, label-free measurement,[75] the use of multiple methods to confirm thermodynamic parameters is essential.[59] Fluorescence quenching has been used previously to study the adsorption of BSA on gold,[59,76] silver,[77] and silver-titanium dioxide NPs.[78] Equilibrium binding constants of 10^{10} to 10^{11} were reported for gold, 10^5 for silver-titanium dioxide, and 10^{10} to 10^{16} M^{-1} for silver depending on temperature. The high variability in reported equilibrium binding constants could be due to the fluorescence spectroscopy method itself, in addition to the fact that binding strength is highly sensitive to NP material, size, and surface modification. The exact mechanism by which the BSA fluorescence is quenched is unknown. Possible mechanisms include energy transfer from the protein to the high energy NP surface, absorption of BSA emission by the polystyrene, quenching of newly exposed residues by water molecules, or anisotropic fluorescence as a result of limited BSA rotation when bound to the NP.

In addition to the fluorescence quenching dynamics, the peak wavelength at the fluorescence maximum are also sensitive to the local environment. BSA contains phenylalanine, tyrosine, and tryptophan residues, all of which can contribute to the intrinsic protein fluorescence.[79,80] However, the quantum yield of phenylalanine is lower than both tyrosine and tryptophan, and as such contributes minimally to the fluorescence spectrum. All of these residues are subject to quenching by other residues and from exposure to the solvent, and BSA fluorescence is primarily due to the tryptophan residue at position 212.[79,81] This residue is located in a hydrophobic region of sub-domain IIA. In our experiments, we observe a blue shift in BSA fluorescence in the presence of both 60 nm anionic and 58 nm cationic NPs. We see a slightly larger wavelength shift for BSA in the presence of 0.53 nM 58 nm amine-modified NPs (329 ± 3 nm) compared with 0.53 nM 60 nm carboxylate-modified NPs (332 ± 0 nm) (Table 7). A blue-shift in fluorescence is indicative of a transition to a more hydrophobic local environment.[79] This suggests that the interaction of 58 nm amine-modified NPs with BSA creates a change in structure that exposes the tryptophan residue to either the hydrophobic surface of the NP itself or a hydrophobic residue in close proximity within the protein. While the changes in fluorescence peak wavelength are marginal, this data supports the CD data which showed a larger change in BSA structure on the surface of 58 nm amine-modified NPs compared with 60 nm carboxylate-modified NPs.

5.4 Conclusions

Using a model system, we demonstrate a molecular link between the structure of the proteins that comprise the corona and the cellular receptors used by the protein-NP complex. We observed that changes in protein structure upon adsorption to NPs determine the cell surface receptor used by the protein-NP complex. In the case of BSA, protein secondary structure is retained upon adsorption to anionic NPs allowing

the BSA-NP complex to bind to native albumin receptors. BSA is denatured following adsorption to cationic NPs, directing the BSA-NP complexes to bind to scavenger receptors. These results have important implications for the *in vivo* targeted delivery of NPs. Beyond merely confirming the presence of a protein corona, it is also critical to characterize the structure of the corona proteins. Composition, dynamics, and protein structure of the corona will all affect cellular and physiological outcomes. We anticipate these results will be useful in the design of NPs for use in physiological environments, ultimately paving the way for targeted, personalized nanomedicine.

5.5 References

[1] Fleischer, C. C. and Payne, C. K., "Nanoparticle surface charge mediates the cellular receptors used by protein-nanoparticle complexes." *J. Phys. Chem. B*, **2012**, *116*, 8901–8907.

[2] Fleischer, C. C., Kumar, U., and Payne, C. K., "Cellular binding of anionic nanoparticles is inhibited by serum proteins independent of nanoparticle composition." *Biomater. Sci.*, **2013**, *1*, 975–982.

[3] Doorley, G. W. and Payne, C. K., "Cellular binding of nanoparticles in the presence of serum proteins." *Chem. Commun.*, **2011**, *47*, 466–468.

[4] Monopoli, M. P., Åberg, C., Salvati, A., and Dawson, K. A., "Biomolecular coronas provide the biological identity of nanosized materials." *Nat. Nanotechnol.*, **2012**, *7*, 779–786.

[5] Doorley, G. W. and Payne, C. K., "Nanoparticles act as protein carriers during cellular internalization." *Chem. Commun.*, **2012**, *48*, 2961–2963.

[6] Lunov, O., Syrovets, T., Loos, C., Beil, J., Delecher, M., Tron, K., Nienhaus, G. U., Musyanovych, A., Mailaender, V., Landfester, K., and Simmet, T., "Differential uptake of functionalized polystyrene nanoparticles by human macrophages and a monocytic cell line." *ACS Nano*, **2011**, *5*, 1657–1669.

[7] Nel, A. E., Madler, L., Velegol, D., Xia, T., Hoek, E. M. V., Somasundaran, P., Klaessig, F., Castranova, V., and Thompson, M., "Understanding biophysicochemical interactions at the nano-bio interface." *Nat. Mater.*, **2009**, *8*, 543–557.

[8] Lacerda, S. H. D., Park, J. J., Meuse, C., Pristinski, D., Becker, M. L., Karim, A., and Douglas, J. F., "Interaction of gold nanoparticles with common human blood proteins." *ACS Nano*, **2010**, *4*, 365–379.

[9] You, C.-C., Verma, A., and Rotello, V. M., "Engineering the nanoparticle-biomacromolecule interface." *Soft Matter*, **2006**, *2*, 190–204.

[10] Slocik, J. M. and Naik, R. R., "Probing peptide-nanomaterial interactions." *Chem. Soc. Rev.*, **2010**, *39*, 3454–3463.

[11] Aubin-Tam, M. E. and Hamad-Schifferli, K., "Structure and function of nanoparticle-protein conjugates." *Biomed. Mater.*, **2008**, *3*, 034001.

[12] Shemetov, A. A., Nabiev, I., and Sukhanova, A., "Molecular interaction of proteins and peptides with nanoparticles." *ACS Nano*, **2012**, *6*, 4585–4602.

[13] Treuel, L., Malissek, M., Grass, S., Diendorf, J., Mahl, D., Meyer-Zaika, W., and Epple, M., "Quantifying the influence of polymer coatings on the serum albumin corona formation around silver and gold nanoparticles." *J. Nanopart. Res.*, **2012**, *14*, 1–12.

[14] Verma, A. and Stellacci, F., "Effect of surface properties on nanoparticle-cell interactions." *Small*, **2010**, *6*, 12–21.

[15] Gagner, J. E., Shrivastava, S., Qian, X., Dordick, J. S., and Siegel, R. W., "Engineering nanomaterials for biomedical applications requires understanding the nano-bio interface: A perspective." *J. Phys. Chem. Lett.*, **2012**, *3*, 3149–3158.

[16] Pelaz, B., Charron, G., Pfeiffer, C., Zhao, Y., de la Fuente, J. M., Liang, X.-J., Parak, W. J., and del Pino, P., "Interfacing engineered nanoparticles with biological systems: Anticipating adverse nano-bio interactions." *Small*, **2013**, *9*, 1573–1584.

[17] Pieper, R., Gatlin, C. L., Makusky, A. J., Russo, P. S., Schatz, C. R., Miller, S. S., Su, Q., McGrath, A. M., Estock, M. A., Parmar, P. P., Zhao, M., Huang, S. T., Zhou, J., Wang, F., Esquer-Blasco, R., Anderson, N. L., Taylor, J., and Steiner, S., "The human serum proteome: Display of nearly 3700 chromatographically separated protein spots on two-dimensional electrophoresis gels and identification of 325 distinct proteins." *Proteomics*, **2003**, *3*, 1345–1364.

[18] Adkins, J. N., Varnum, S. M., Auberry, K. J., Moore, R. J., Angell, N. H., Smith, R. D., Springer, D. L., and Pounds, J. G., "Toward a human blood serum proteome: Analysis by multidimensional separation coupled with mass spectrometry." *Mol. Cell. Proteomics*, **2002**, *1*, 947–955.

[19] Anderson, N. L. and Anderson, N. G., "The human plasma proteome: History, character, and diagnostic prospects." *Mol. Cell. Proteomics*, **2002**, *1*, 845–867.

[20] Huang, B. X., Kim, H.-Y., and Dass, C., "Probing three-dimensional structure of bovine serum albumin by chemical cross-linking and mass spectrometry." *J. Am. Soc. Mass. Spectrom.*, **2004**, *15*, 1237–1247.

[21] Sułkowska, A., "Interaction of drugs with bovine and human serum albumin." *J. Mol. Struct.*, **2002**, *614*, 227–232.

[22] Freshney, R. I., *Culture of Animal Cells*. John Wiley and Sons, Inc., Hoboken, 5th edn., **2005**.

[23] Pastan, I. and Willingham, M., "Journey to the center of the cell: Role of the receptosome." *Science*, **1981**, *214*, 504–509.

[24] Szymanski, C. J., Yi, H., Liu, J. T., Wright, E. R., and Payne, C. K., "Imaging intracellular quantum dots: Fluorescence microscopy and transmission electron microscopy." *In* Rosenthal, S. J. and Wright, D. X., eds., "Nanobiotechnology Protocols," Humana Press, **2012**.

[25] Callaini, G., Dallai, R., and Riparbelli, M. G., "Microfilament distribution in cold-treated Drosophila embryos." *Exp. Cell Res.*, **1991**, *194*, 316–321.

[26] Watts, R. G. and Howard, T. H., "Evidence for a gelsolin-rich, labile F-actin pool in human polymorphonuclear leukocytes." *Cell Motil. Cytoskel.*, **1992**, *21*, 25–37.

[27] Goldenthal, K. L., Pastan, I., and Willingham, M. C., "Initial steps in receptor-mediated endocytosis - The influence of temperature on the shape and distribution of plasma-membrane clathrin-coated pits in cultured mammalian-cells." *Exp. Cell Res.*, **1984**, *152*, 558–564.

[28] Harding, C., Heuser, J., and Stahl, P., "Receptor-mediated endocytosis of transferrin and recycling of the transferrin receptor in rat reticulocytes." *J. Cell Biol.*, **1983**, *97*, 329–339.

[29] Tiruppathi, C., Finnegan, A., and Malik, A. B., "Isolation and characterization of a cell surface albumin-binding protein from vascular endothelial cells." *Proc. Natl. Acad. Sci. U. S. A.*, **1996**, *93*, 250–254.

[30] Vogel, S. M., Minshall, R. D., Pilipovic, M., Tiruppathi, C., and Malik, A. B., "Albumin uptake and transcytosis in endothelial cells *in vivo* induced by albumin-binding protein." *Am. J Physiol. Lung Cell. Mol. Physiol.*, **2001**, *281*, L1512–L1522.

[31] Schnitzer, J. E., "gp60 is an albumin-binding glycoprotein expressed by continuous endothelium involved in albumin transcytosis." *Am. J. Physiol.-Heart C.*, **1992**, *262*, H246–H254.

[32] Schnitzer, J. E., Carley, W. W., and Palade, G. E., "Albumin interacts specifically with a 60-kDa microvascular endothelial glycoprotein." *Proc. Natl. Acad. Sci.*, **1988**, *85*, 6773–6777.

[33] Schnitzer, J. E., Carley, W. W., and Palade, G. E., "Specific albumin binding to microvascular endothelium in culture." *Am. J. Physiol.-Heart C.*, **1988**, *254*, H425–H437.

[34] Choi, C. H. J., Hao, L., Narayan, S. P., Auyeung, E., and Mirkin, C. A., "Mechanism for the endocytosis of spherical nucleic acid nanoparticle conjugates." *Proc. Natl. Acad. Sci. U. S. A.*, **2013**, *110*, 7625–7630.

[35] Patel, P. C., Giljohann, D. A., Daniel, W. L., Zheng, D., Prigodich, A. E., and Mirkin, C. A., "Scavenger receptors mediate cellular uptake of polyvalent oligonucleotide-functionalized gold nanoparticles." *Bioconjugate Chem.*, **2010**, *21*, 2250–2256.

[36] Giljohann, D. A., Seferos, D. S., Patel, P. C., Millstone, J. E., Rosi, N. L., and Mirkin, C. A., "Oligonucleotide loading determines cellular uptake of DNA-modified gold nanoparticles." *Nano Lett.*, **2007**, *7*, 3818–3821.

[37] Schnitzer, J. E., Sung, A., Horvat, R., and Bravo, J., "Preferential interaction of albumin-binding proteins, gp30 and gp18, with conformationally modified albumins. Presence in many cells and tissues with a possible role in catabolism." *J. Biol. Chem.*, **1992**, *267*, 24544–24553.

[38] Schnitzer, J. E. and Bravo, J., "High affinity binding, endocytosis, and degradation of conformationally modified albumins. Potential role of gp30 and gp18 as novel scavenger receptors." *J. Biol. Chem.*, **1993**, *268*, 7562–7570.

[39] Schnitzer, J. E. and Oh, P., "Albondin-mediated capillary permeability to albumin. Differential role of receptors in endothelial transcytosis and endocytosis of native and modified albumins." *J. Biol. Chem.*, **1994**, *269*, 6072–6082.

[40] Pearson, A. M., Rich, A., and Krieger, M., "Polynucleotide binding to macrophage scavenger receptors depends on the formation of base-quartet-stabilized four-stranded helices." *J. Biol. Chem.*, **1993**, *268*, 3546–3554.

[41] Greenfield, N. J., "Using circular dichroism spectra to estimate protein secondary structure." *Nat. Protoc.*, **2007**, *1*, 2876–2890.

[42] Holzwarth, G. and Doty, P., "The ultraviolet circular dichroism of polypeptides." *J. Am. Chem. Soc.*, **1965**, *87*, 218–228.

[43] Norde, W. and Favier, J. P., "Structure of adsorbed and desorbed proteins." *Colloids Surf.*, **1992**, *64*, 87–93.

[44] Norde, W. and Giacomelli, C. E., "BSA structural changes during homomolecular exchange between the adsorbed and the dissolved states." *J. Biotechnol.*, **2000**, *79*, 259–268.

[45] Irie, S. and Tavassoli, M., "Transferrin-mediated cellular iron uptake." *Am. J. Med. Sci.*, **1987**, *293*, 103–111.

[46] Freire, E., Mayorga, O. L., and Straume, M., "Isothermal titration calorimetry." *Anal. Chem.*, **1990**, *62*, 950A–959A.

[47] Brewer, S. H., Glomm, W. R., Johnson, M. C., Knag, M. K., and Franzen, S., "Probing BSA binding to citrate-coated gold nanoparticles and surfaces." *Langmuir*, **2005**, *21*, 9303–9307.

[48] Rezwan, K., Meier, L. P., Rezwan, M., Voros, J., Textor, M., and Gauckler, L. J., "Bovine serum albumin adsorption onto colloidal Al_2O_3 particles: A new model based on zeta potential and UV-Vis measurements." *Langmuir*, **2004**, *20*, 10055–10061.

[49] Walton, A. G. and Maenpa, F. C., "Application of fluorescence spectroscopy to the study of proteins at interfaces." *J. Colloid Interface Sci.*, **1979**, *72*, 265–278.

[50] Eftink, M. R. and Ghiron, C. A., "Exposure of tryptophanyl residues in proteins. Quantitative determination by fluorescence quenching studies." *Biochemistry*, **1976**, *15*, 672–680.

[51] Lakowicz, J. R., *Principles of Fluorescence Spectroscopy*. Springer, New York, 3rd edn., **2006**.

[52] Walczyk, D., Bombelli, F. B., Monopoli, M. P., Lynch, I., and Dawson, K. A., "What the cell "sees" in bionanoscience." *J. Am. Chem. Soc.*, **2010**, *132*, 5761–5768.

[53] Lynch, I., Cedervall, T., Lundqvist, M., Cabaleiro-Lago, C., Linse, S., and Dawson, K. A., "The nanoparticle-protein complex as a biological entity; A complex fluids and surface science challenge for the 21st century." *Adv. Colloid Interface Sci.*, **2007**, *134-135*, 167–174.

[54] Cedervall, T., Lynch, I., Lindman, S., Berggård, T., Thulin, E., Nilsson, H., Dawson, K. A., and Linse, S., "Understanding the nanoparticle-protein corona using methods to quantify exchange rates and affinities of proteins for nanoparticles." *Proc. Natl. Acad. Sci. U. S. A.*, **2007**, *104*, 2050–2055.

[55] Treuel, L. and Nienhaus, G. U., "Toward a molecular understanding of nanoparticle-protein interactions." *Biophys. Rev.*, **2012**, *4*, 137–147.

[56] Gessner, A., Lieske, A., Paulke, B.-R., and Müller, R. H., "Functional groups on polystyrene model nanoparticles: Influence on protein adsorption." *J. Biomed. Mater. Res., Part A*, **2003**, *65A*, 319–326.

[57] Alkilany, A. M., Nagaria, P. K., Hexel, C. R., Shaw, T. J., Murphy, C. J., and Wyatt, M. D., "Cellular uptake and cytotoxicity of gold nanorods: Molecular origin of cytotoxicity and surface effects." *Small*, **2009**, *5*, 701–708.

[58] Walkey, C. D. and Chan, W. C. W., "Understanding and controlling the interaction of nanomaterials with proteins in a physiological environment." *Chem. Soc. Rev.*, **2012**, *41*, 2780–2799.

[59] Boulos, S. P., Davis, T. A., Yang, J. A., Lohse, S. E., Alkilany, A. M., Holland, L. A., and Murphy, C. J., "Nanoparticle-protein interactions: A thermodynamic and kinetic study of the adsorption of bovine serum albumin to gold nanoparticle surfaces." *Langmuir*, **2013**, *29*, 14984–14996.

[60] Gref, R., Lück, M., Quellec, P., Marchand, M., Dellacherie, E., Harnisch, S., Blunk, T., and Müller, R. H., "'Stealth' corona-core nanoparticles surface modified by polyethylene glycol (PEG): Influences of the corona (PEG chain length and surface density) and of the core composition on phagocytic uptake and plasma protein adsorption." *Colloids Surf., B*, **2000**, *18*, 301–313.

[61] Gref, R., Domb, A., Quellec, P., Blunk, T., Müller, R. H., Verbavatz, J. M., and Langer, R., "The controlled intravenous delivery of drugs using PEG-coated sterically stabilized nanospheres." *Adv. Drug Delivery Rev.*, **1995**, *16*, 215–233.

[62] Ehrenberg, M. S., Friedman, A. E., Finkelstein, J. N., Oberdörster, G., and McGrath, J. L., "The influence of protein adsorption on nanoparticle association with cultured endothelial cells." *Biomaterials*, **2009**, *30*, 603–610.

[63] Baier, G., Costa, C., Zeller, A., Baumann, D., Sayer, C., Araujo, P. H. H., Mailaender, V., Musyanovych, A., and Landfester, K., "BSA adsorption on differently charged polystyrene nanoparticles using isothermal titration calorimetry and the influence on cellular uptake." *Macromol. Biosci.*, **2011**, *11*, 628–638.

[64] Benetti, F., Fedel, M., Minati, L., Speranza, G., and Migliaresi, C., "Gold nanoparticles: Role of size and surface chemistry on blood protein adsorption." *J. Nanopart. Res.*, **2013**, *15*, 1–9.

[65] Dobrovolskaia, M. A., Patri, A. K., Zheng, J., Clogston, J. D., Ayub, N., Aggarwal, P., Neun, B. W., Hall, J. B., and McNeil, S. E., "Interaction of colloidal gold nanoparticles with human blood: Effects on particle size and analysis of plasma protein binding profiles." *Nanomed: Nanotechnol. Biol. Med.*, **2009**, *5*, 106–117.

[66] Kohli, I., Alam, S., Patel, B., and Mukhopadhyay, A., "Interaction and diffusion of gold nanoparticles in bovine serum albumin solutions." *Appl. Phys. Lett.*, **2013**, *102*, 203705.

[67] Carter, D. C. and Ho, J. X., "Structure of serum albumin." *In* "Advances in Protein Chemistry," Academic Press, vol. 45, **1994**, 153–203.

[68] Böhme, U. and Scheler, U., "Effective charge of bovine serum albumin determined by electrophoresis NMR." *Chem. Phys. Lett.*, **2007**, *435*, 342–345.

[69] Hirayama, K., Akashi, S., Furuya, M., and Fukuhara, K.-I., "Rapid confirmation and revision of the primary structure of bovine serum albumin by ESIMS and Frit-FAB LC/MS." *Biochem. Biophys. Res. Commun.*, **1990**, *173*, 639–646.

[70] Krieger, M., Acton, S., Ashkenas, J., Pearson, A., Penman, M., and Resnick, D., "Molecular flypaper, host defense, and atherosclerosis. Structure, binding properties, and functions of macrophage scavenger receptors." *J. Biol. Chem.*, **1993**, *268*, 4569–4572.

[71] Brown, M. S., Basu, S. K., Falck, J. R., Ho, Y. K., and Goldstein, J. L., "The scavenger cell pathway for lipoprotein degradation: Specificity of the binding site that mediates the uptake of negatively-charged LDL by macrophages." *J. Supramol. Struct.*, **1980**, *13*, 67–81.

[72] Zhang, H., Yang, Y., and Steinbrecher, U. P., "Structural requirements for the binding of modified proteins to the scavenger receptor of macrophages." *J. Biol. Chem.*, **1993**, *268*, 5535–5542.

[73] De, M., You, C.-C., Srivastava, S., and Rotello, V. M., "Biomimetic interactions of proteins with functionalized nanoparticles: A thermodynamic study." *J. Am. Chem. Soc.*, **2007**, *129*, 10747–10753.

[74] Lindman, S., Lynch, I., Thulin, E., Nilsson, H., Dawson, K. A., and Linse, S., "Systematic investigation of the thermodynamics of HSA adsorption to N-iso-propylacrylamide/N-tert-butylacrylamide copolymer nanoparticles. Effects of particle size and hydrophobicity." *Nano Lett.*, **2007**, *7*, 914–920.

[75] Ladbury, J. E. and Chowdhry, B. Z., "Sensing the heat: The application of isothermal titration calorimetry to thermodynamic studies of biomolecular interactions." *Chem. Biol.*, **1996**, *3*, 791–801.

[76] Wangoo, N., Suri, C. R., and Shekhawat, G., "Interaction of gold nanoparticles with protein: A spectroscopic study to monitor protein conformational changes." *Appl. Phys. Lett.*, **2008**, *92*, 133104.

[77] Mariam, J., Dongre, P. M., and Kothari, D. C., "Study of interaction of silver nanoparticles with bovine serum albumin using fluorescence spectroscopy." *J. Fluoresc.*, **2011**, *21*, 2193–2199.

[78] Kathiravan, A., Renganathan, R., and Anandan, S., "Interaction of colloidal $AgTiO_2$ nanoparticles with bovine serum albumin." *Polyhedron*, **2009**, *28*, 157–161.

[79] Feldman, I., Young, D., and McGuire, R., "Static and dynamic quenching of protein fluorescence. I. Bovine serum albumin." *Biopolymers*, **1975**, *14*, 335–351.

[80] Chen, Y. and Barkley, M. D., "Toward understanding tryptophan fluorescence in proteins." *Biochemistry*, **1998**, *37*, 9976–9982.

[81] Togashi, D., Ryder, A., and O'Shaughnessy, D., "Monitoring local unfolding of bovine serum albumin during denaturation using steady-state and time-resolved fluorescence spectroscopy." *J. Fluoresc.*, **2010**, *20*, 441–452.

CHAPTER VI

CONCLUSIONS AND FUTURE WORK

6.1 Conclusions and Outlook

Characterizing fundamental interactions of NPs with cells is essential for the transition of NPs out of *in vitro* systems and into clinical applications. NP properties such as size, composition, and surface charge, combined with the extracellular proteins adsorbed to the NP surface all influence cellular interactions of the protein-NP complex. We observed the formation of a protein corona on the surface of a diverse range of NPs. Our studies have shown that initial NP surface charge dominates the cellular binding of NPs in the presence of serum proteins and determines the cellular receptors used for binding. These cellular binding trends are attributed to the molecular properties and structure of adsorbed proteins (Figure 41).

We focused primarily on a model system consisting of polystyrene NPs and the serum albumin protein. We further demonstrated that the effect of NP surface charge on cellular binding is a general trend. Consistent results were also observed for biomedically relevant NPs including quantum dots, colloidal gold NPs, and low-density lipoprotein. While we observed that initial NP surface charge modulates protein secondary structure for our model system, structure is dependent upon both the type of protein as well as the NP properties and will have to be characterized for each system of interest. The complexity in protein structural studies lies in the diverse number of proteins that can adsorb to the surface of individual NPs. This is further complicated by the dynamic composition of the corona, emphasizing the importance of characterizing fundamental interactions of NPs with cells in a biologically relevant environment.

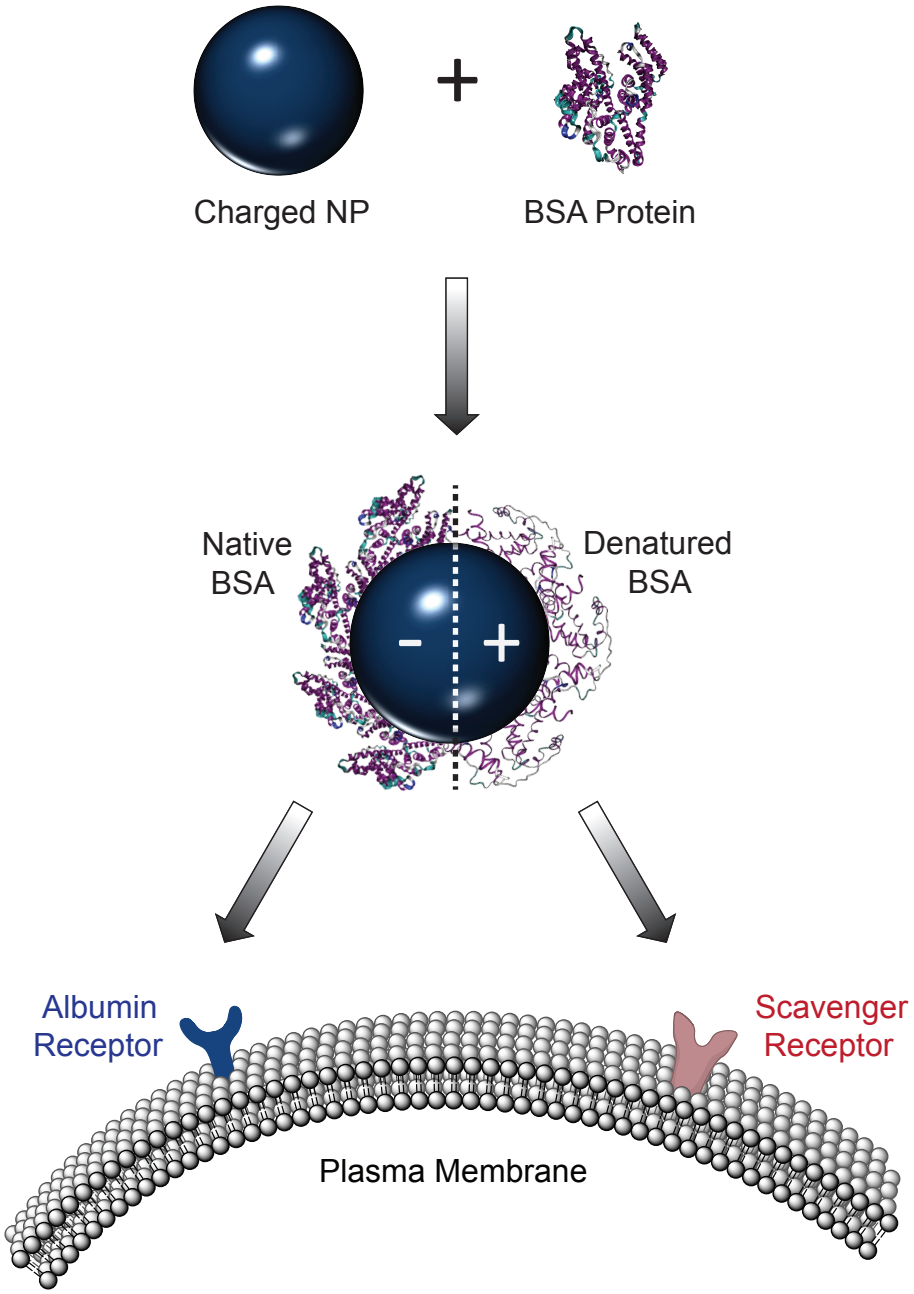

Figure 41: Cellular binding of protein-NP complexes. A corona composed primarily of BSA adsorbs onto the surface of both anionic and cationic NPs. The molecular properties of BSA differ based on the initial NP charge and subsequently determine the cellular receptors used for binding.

The presence of a protein corona will ultimately influence NP distribution, accumulation, and eventual clearance. NP clearance mechanisms from cells, tissues, and organs are not well understood and are further challenged by the lack of a good model system. Cellular experiments and mouse models work well for fundamental and proof of concept studies, but the dynamics of corona formation, circulation, and retention times will differ in humans.[1] Extrapolation from the cellular environment to realistic observations in clinical trials remains a significant hurdle.

This dissertation has focused on cellular binding as this is the first step in the course of most biomedical applications of NPs. However, the protein corona will also influence the internalization and transport pathways of the NP. Directing cellular binding, understanding mechanisms of cellular internalization, and characterizing transport dynamics of protein-NP complexes are future avenues for the research presented in this dissertation.

6.2 Future work

While we have characterized the effect of NP charge and protein structure on the cellular binding of protein-NP complexes, these fundamental studies must be expanded to understand the complete mechanistic details of NP interactions with cells. Two primary areas of future research are included here with accompanying preliminary data.

6.2.1 Cellular Binding

We have observed that initial NP surface charge determines both the structure of adsorbed proteins along with the cellular receptor used by the protein-NP complex. Specifically, we observed that the protein structure of BSA is retained on anionic NPs, allowing complexes formed with anionic NPs to bind to native albumin receptors. To further verify this result, we have attempted to steer anionic NPs away from native BSA receptors by incubating the anionic NPs with denatured proteins prior to cellular

binding studies. We expect that the protein-NP complex formed with anionic NPs will no longer be recognized by the native BSA receptor, which is the trend we observed for cationic NPs. However, these steering experiments have proven to be extremely challenging, as we have used BSA that was boiled, modified with H_2CO, and denatured with guanidine salts, all to no avail. In all cases, anionic NPs were still blocked by free BSA indicating that the protein-NP complex can access and be recognized by native BSA receptors.

However, we observed that using BSA labeled with AlexaFluor647 (AF647) leads to mixed competition (Figure 42). Incubation with MEM supplemented with 10 $mg{\cdot}mL^{-1}$ BSA leads to a decrease in binding (68% relative to 100% cellular binding in MEM). The presence of 250 $\mu g{\cdot}mL^{-1}$ polyinosinic acid also leads to a decrease in binding (63%), and the presence of both BSA and polyinosinic acid leads to nearly complete inhibition (48%) relative to the cell background. The autofluorescence from cells alone is 43%. These results demonstrate that fluorescently labeled BSA competes both with free BSA as well as a molecule that binds to scavenger receptors. Fluorescently labeling BSA likely leads to a distribution of protein structures (and exposed epitopes) that allows a subset to bind to native receptors and another subset to bind to scavenger receptors. We anticipate a similar effect is occuring after adsorption of BSA to the NP surface. We also expect that the disrupted structure of BSA on cationic NPs is not the same as BSA denatured by other methods, and molecular differences in protein structure are responsible for the challenges in steering anionic NPs away from native protein receptors. Future experiments will need to determine the degree and type of denaturation that causes BSA to no longer be recognized by the native receptor. An additional control would be to find or produce a cell line that does not have an albumin receptor and repeat binding experiments with anionic NPs coated with albumin. We would expect that the albumin-NP complex would either not bind, or reduced binding would be observed to these cells.

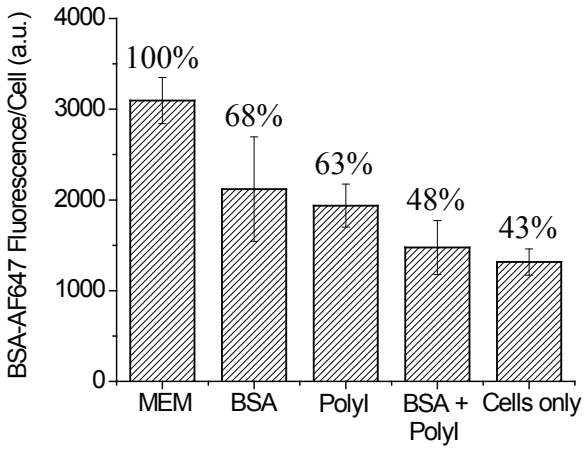

Figure 42: Cellular binding competition studies of BSA-AF647 in MEM, MEM supplemented with BSA (BSA), MEM supplemented with polyinosinic acid (polyI), and MEM supplemented with both BSA and polyinosinic acid (BSA + polyI). Control experiment shows autofluorescence from cells in the absence of BSA-AF647 (cells only).

6.2.2 Cellular Internalization and Transport

While our experiments have focused primarily on cellular binding, the effect of the protein corona on NP cellular internalization is also key to understanding NP efficacy. Previous research in our group demonstrated that protein stays bound to the NP as protein-NP complexes bind to and cross the plasma membrane.[2,3] This suggests that NP internalization and transport is at least partially dependent upon the protein adsorbed onto the surface.

In order to probe the differences in intracellular transport of free BSA and BSA bound to a NP, BS-C-1 cells were incubated with either BSA-NP complexes or BSA-AF647 at 37 °C. Incubation at 37 °C allows both cellular binding and internalization to occur. Complexes were formed with 87 nm amine-modified, green fluorescent NPs (34 pM) incubated with 6 μM BSA for 20 minutes before adding to cells. The lysosome was used as a terminal vesicle for endocytic transport, and the fluoresently

labeled lysosome-associated membrane protein-1 (LAMP1) was used to image lysosomes. For studies with BSA-AF647, BS-C-1 cells stably expressing LAMP1 labeled with enhanced yellow fluorescent protein (EYFP) were used. For BSA-NP internalization studies, the LAMP1 protein was immunofluorescently labeled with red Cy5 (Chapter 2.4.2).

The transport of BSA-NP complexes and BSA-AF647 was visualized as a function of time using confocal fluorescence microscopy, and colocalization with lysosomes via the LAMP1 protein was calculated (Figure 43). After 10 minutes, $10 \pm 9\%$ of BSA-NP complexes were found in lysosomes compared to $51 \pm 21\%$ of BSA-AF647, suggesting a slightly slower accumulation of BSA-NP complexes into lysosomal vesicles. The accumulation is dependent on a number of factors including, but not limited to the amount of NPs or proteins that can be contained in a single vesicle, rate of transport to the lysosome, as well as the limits of visualization inherent to fluorescence microscopy. We expect that some of the observed difference is due to the fact that BSA-AF647 cannot be visualized below an accumulation threshold. After 18 hours, the majority of BSA-NP complexes and BSA-AF647 are found in lysosomes ($78 \pm 20\%$ and $90 \pm 7\%$, respectively). Overlay images demonstrate colocalization after incubation for 18 hours (Figures 43A and 43B). The colocalization signal appears yellow in the images. Individual images used to form overlays are shown in Figure 44. While this strongly suggests that both BSA and BSA-NP complexes are transported via the endocytic pathway, the exact internalization mechanism is unknown. For anionic NPs, the process should be similar to that of the BSA protein, as anionic NPs bind to native albumin receptors on the cell surface. Future work should focus on determining differences in internalization of BSA-NP complexes as a function of NP charge, and identify the mechanism as either clathrin- or caveolin-dependent. We anticipate that differences in the rate or internalization mechanism are due to the receptor used by the protein-NP complex, combined with differences in adsorbed protein structure.

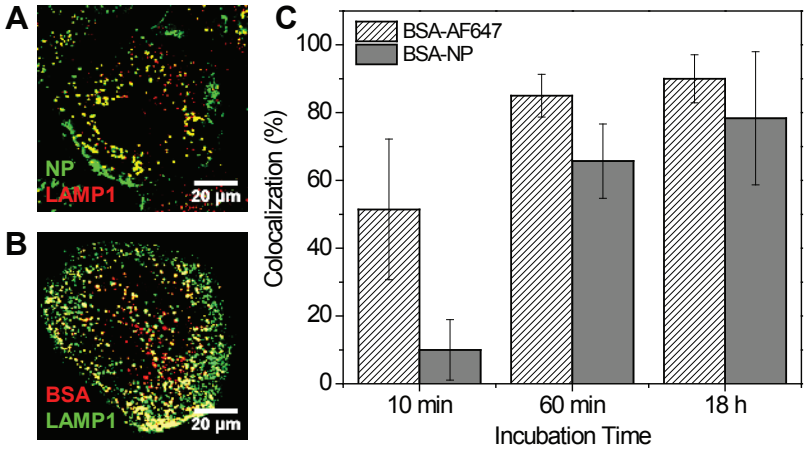

Figure 43: Transport studies of BSA-NP complexes and BSA-AF647 in BS-C-1 cells as a function of incubation time at 37 °C. The LAMP1 protein was used as an endpoint for transport. Merged images show colocalization after an 18 hour incubation. (A) BSA-NP complexes (green) in cells labeled with LAMP1-Cy5 (red). (B) BSA-AF647 (red) in cells expressing LAMP1-EYFP (green). (C) Colocalization of BSA-NP complexes and BSA-AF647 with LAMP1 as a function of incubation time.

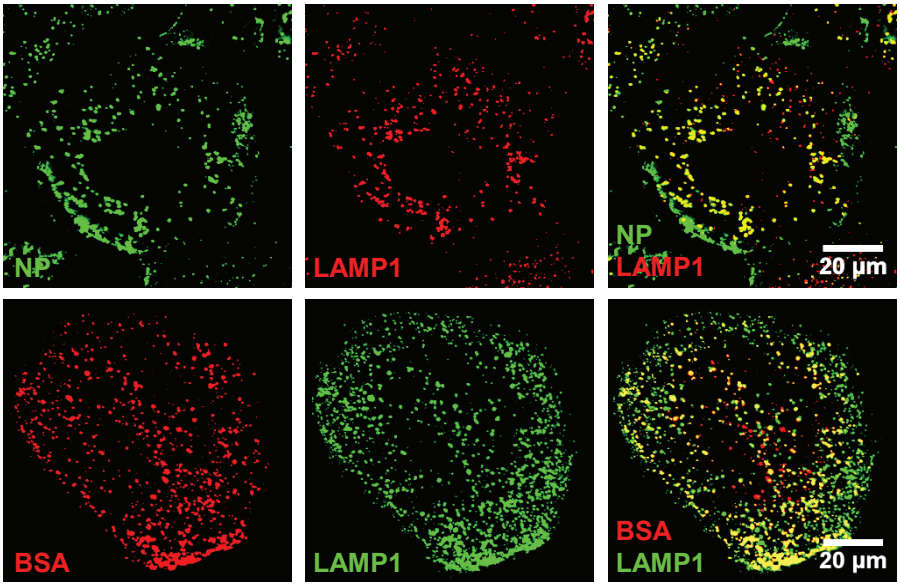

Figure 44: Individual images from transport studies of BSA-NP and BSA-AF647 to LAMP1 positive vesicles used to construct merged images shown in Figure 43.

While we examined cellular transport using accumulation at single time points, the dynamics of transport may also differ as a function of NP charge as a result of the complexes formed with anionic and cationic NPs using different cellular receptors. Single particle tracking experiments have been initiated, but no differences were observed between transport kinetics of vesicles containing BSA or BSA-NP complexes. Transport experiments are challenging as vesicles transport multiple types of cargo simultaneously, including many intracellular proteins. It is difficult to deduce the effect the type of molecule contained within the vesicle has on the overall transport dynamics. Future experiments will need to characterize vesicle transport *in vitro* to first understand an isolated system, followed by intracellular studies of the dynamics of transporting proteins versus protein-NP complexes. This will require the use of multi-color particle tracking, perhaps in conjunction with sub-diffraction limited imaging.

6.3 References

[1] Riviere, J. E., "Of mice, men and nanoparticle biocoronas: Are *in vitro* to *in vivo* correlations and interspecies extrapolations realistic?" *Nanomedicine*, **2013**, *8*, 1357–1359.

[2] Doorley, G. W. and Payne, C. K., "Cellular binding of nanoparticles in the presence of serum proteins." *Chem. Commun.*, **2011**, *47*, 466–468.

[3] Doorley, G. W. and Payne, C. K., "Nanoparticles act as protein carriers during cellular internalization." *Chem. Commun.*, **2012**, *48*, 2961–2963.

CHAPTER VII

APPENDIX

The following appendix describes methods in expanded detail and includes suggestions for experimental design and optimization.

7.1 Cell Experiments

Cell health, the pH of the cell culture medium, and passage number all influence the outcome of cellular binding and internalization experiments. All experiments should be repeated with cells from multiple passage numbers to control for heterogeneity in phenotype often observed in cultured cells. For cellular binding, medium with a pH of 7.2 for MEM and 7.4 for MEM supplemented with 10% (v/v) FBS was used. Difficulties repeating cellular binding experiments can often be traced to a change in the pH of the medium over time.

Cellular binding experiments were always performed in culture dishes or well plates incubated on a bed of ice covered with aluminum foil. Incubation in a 4 °C fridge is another method for cold binding studies. However, the cells and the medium equilibrate much slower using this method and the temperature is maintained more homogeneously on ice.

7.2 Microscopy

7.2.1 Wide Field Fluorescence

Wide field fluorescence microscopy has the advantage of faster acquisition time over confocal microscopy, but multiple images cannot be recorded simultaneously. When acquiring images from multiple fluorophores in a single spatial region, the focus (or z position) of the microscope should be kept constant between images, ensuring that

overlaid images accurately reflect the spatial location of the fluorophores. Time course recordings are also possible with the wide field microscope, however, there is a slight drift in the z position over time (x and y positions are relatively constant). Re-centering the illumination from the xenon lamp often improves image quality. The aperture iris condenser can also be aligned, however this will only improve the bright field image quality and will have no effect on the final image acquired on the CCD camera. Changing the xenon bulb is also required after 1000 - 2000 hours of use, and care should be taken to ensure that the new bulb is aligned properly (see Olympus Manual).

Calibration of the microscope (i.e. determining the distance in nm per pixel) should be done regularly. This is achieved by acquiring an image of a calibration slide at the same magnification used in experiments. The image should contain a calibration ruler with 10 lines spaced 10 nm apart, and the pixels in the image are then counted as a function of distance using ImageJ. For all images used in this thesis, the calibration was calculated for multiple widths along the calibration ruler and averaged to acquire a final value. Experimental calibration values can be corroborated with the calculated value using the pixel size of the CCD and objective magnification.

7.2.2 Confocal Fluorescence

For static imaging, the confocal imaging system should be turned on 30 minutes to 1 hour prior to use. For live cell imaging, allowing the system to warm up over several hours is required to eliminate axial drift and equilibrate laser emission. The emission pinhole should be set to a size of 1 airy unit for best resolution. The pinhole can opened beyond this size to simulate 'wide field' imaging, but doing so allows more background and out-of-focus light to reach the detector without increasing the excitation volume.

Images used for comparison, including control samples, must be acquired with

the same dwell time, PMT voltage, pinhole size, and laser power. It is important to ensure that the PMT detectors are not oversaturated during imaging using the hi-lo look-up tables in the FluoView software. The calibration that is exported with the images is accurate and has been checked with external calibration.

7.2.3 Dark Field

Dark field microscopy was used to image the cellular binding of gold NPs and is shown in Figure 45. NPs down to ∼30 nm in diameter can be visualized with dark field microscopy. Samples were prepared for dark field measurements by sealing the cells adhered to a circular cover slip between a clean, rectangular cover slip (Figure 45A). A small amount of glycerol is placed between the cover slips, and the edges are sealed with either nail polish or epoxy to prevent from drying. Samples prepared in this manner can be kept for up to one week at room temperature.

The dark field microscopy setup in our lab was assembled using an upright Olympus microscope. A dark field condenser with a numerical aperture (N.A.) greater than that of the objective is used to focus a narrow beam of light, or a hollow illumination cone, onto the sample. An iris objective with a variable N.A. is used to collect scattered, but not transmitted, photons (Figure 45B). While the objective and condenser are shown at a distance above and below the sample to demonstrate the optical path, both are oil objectives and require direct contact with the cover slips.

A Nikon D200 DSLR is used to acquire images. The camera is attached to the top port of the microscope and is directly connected to the computer via USB. Open source micro-manager software (www.micro-manager.org, version 1.4) is used for viewing images. The NK Remote software (version 2.7) interfaces micro-manager with the Nikon D200. While we have purchased a one year license, this software can be used indefinitely. The NK Remote software requires a 32-bit version of micro-manager.

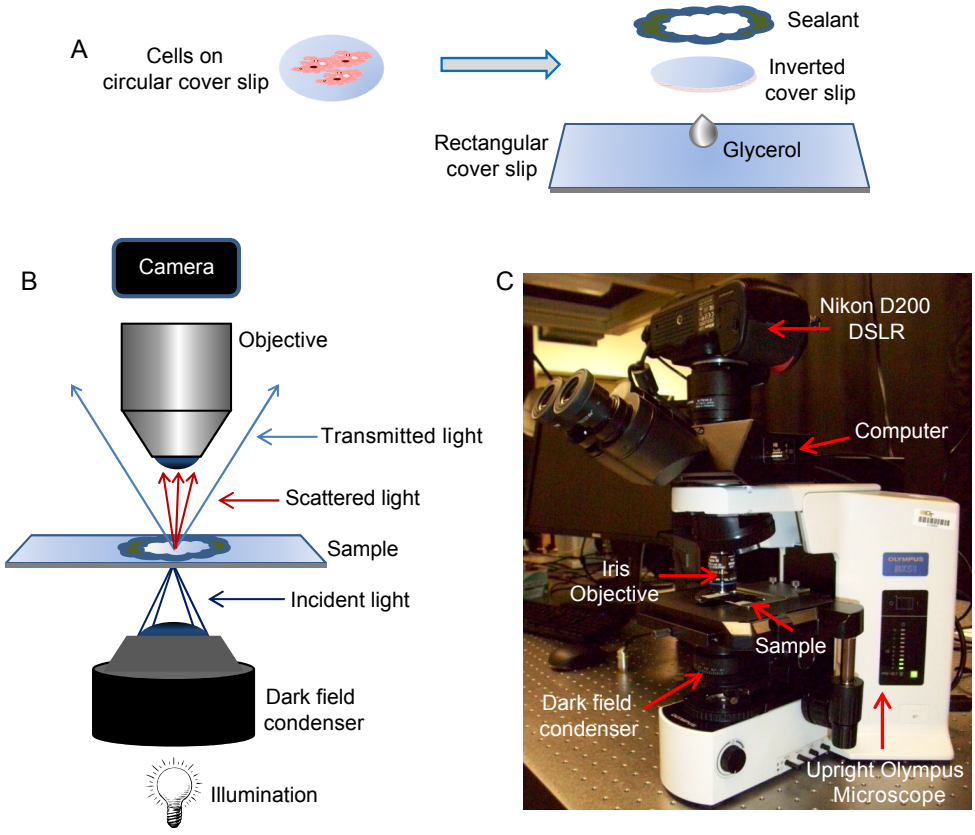

Figure 45: Dark field microscopy instrumentation. (A) Schematic of sample preparation. (B) Optical path in dark field microscopy. (C) Photo of dark field imaging system.

7.3 Spectroscopy

General experimental challenges for fluorescence and absorption spectroscopy include interference in the UV region by strong absorbers (e.g. chloride, polystyrene), inner filter effects at high concentrations, and scattering. Contributions to the inner filter effect should be characterized for each experiment, especially for strongly absorbing or strongly scattering molecules and particles.

For circular dichroism spectroscopy, the concentration of the sample is one of the most important parameters. While higher sample concentration can increase sample absorption, an increase in absorption also results in fewer photons reaching the PMTs. This in turn leads to higher PMT voltage (and often a longer integration time) and a decrease in the signal-to-noise ratio. Optimization of concentration and buffer are essential for accurate and reproducible spectra. There is also considerable baseline drift over time. The baseline should be checked frequently by acquiring another spectrum of buffer alone with the baseline correction applied. A spectrum that is flat within ±1 millidegree (instrument noise range) is acceptable. Baseline drift should only be subtracted if first verified by measuring the baseline and sample at similar times, using a region of the sample spectrum where the signal should be zero. If magnitude of the baseline drift from the buffer and the sample is the same, then a change in baseline can be attributed to instrument, rather than sample, fluctuations. Spectra are generally reported in units of molar ellipticity or mean residue ellipticity. If a spectrum is smoothed, a difference spectrum should be calculated for the raw and smoothed spectra. If there are no features greater than the instrument noise (±1 millidegree), then the spectrum has not been oversmoothed.

7.4 Isothermal Titration Calorimetry

A general isothermal titration calorimetry (ITC) experiment consists of ligand loaded into the titration syringe and substrate loaded into the cell at a concentration of 10:1

ligand to substrate, assuming one-to-one binding. Accurate ligand concentration is required to obtain reliable thermodynamic parameters. For weak binding, the concentrations should be at least as large as the K_d. The reference cell should always be filled with water, regardless of the buffer loaded into the sample cell, and the reference and sample cells must be filled accurately to the same volume. Either distilled or deionized water can be used for the reference cell and for cleaning. Nanopure water is not required and should not be used for washing as large volumes of water are needed to clean the instrument thoroughly. The ligand and substrate buffer must be matched within 0.1 pH units, or pH effects will be visible in the titration curves and are difficult to subtract out. Water is generally never used as the solvent in an ITC experiment for this reason. A control titration of ligand into buffer alone must always be completed and subtracted from the experiment titration. Under optimal conditions, the integrated peaks will be 4-5 times larger for the experiment compared with the control, but this is not always possible for weak binding systems.

Optimal settings range from 250-350 rpm for stirring, 16-25 injections, and 1-4 μL injections. Both the syringe and cell should be washed with water followed by buffer prior to loading each with sample. The titration syringe must be completely dry before filling and void of bubbles after filling. The first injection should be discarded during data analysis as some of the volume will diffuse out of the injection syringe prior to the first injection.

A clean instrument, proper controls, and unbiased fitting of the data are critical for acquiring accurate thermodynamic parameters. Optimization of ligand and substrate concentration, buffer, equilibration time, and temperature will be required for every experiment. Final thermodynamic values are highly dependent upon buffer, chemical composition, and temperature. Reproducibility is key.

An instrument quality control check, which should be done on a weekly basis if the instrument is in frequent use, is to run a water-water titration. With water in both the

titration syringe and in the cell, twenty 2.5 μL titrations should give consistent peaks of 5 μJ each. Deviations in the water-water run, a noisy baseline, and inconsistent peaks are all indicators that the instrument is not clean. A solution of 20% (v/v) contrad solution can be used for rigorous cleaning. However, the contrad itself is very difficult to remove completely and should be used sparingly. Yearly maintenance should include soaking the cell with contrad at 60 °C (avoiding inhalation of any contrad fumes), greasing the o-rings in the buret handle, and running instrument gain calibration. There are many tutorials available on TA Instrument's website for further details and visual explanations.

VITA

Candace C. Fleischer was raised in Washington state. She graduated from Western Washington University with both B.S. and M.S. degrees in chemistry. Her master's thesis work focused on the development of a surface-enhanced Raman scattering probe for chemical imaging under the advisement of Dr. Steven R. Emory. After several years teaching at the university level and abroad, she began the graduate program in physical chemistry at the Georgia Institute of Technology. She currently resides in Atlanta, GA with her husband.